Dear Prof. Jian Wang,

We would like to express our great appreciation to you and the reviewers for the valuable comments and suggestions. We have addressed the comments raised by the reviewers, and the amendments are highlighted in red in the revised manuscript. The main corrections in the paper and the responses to the reviewers' comments are in the following. We hope that the revision is acceptable.

Thank you and looking forward to hearing from you soon.

Best regards,

Shengzhen Zhou, PhD

Jun Zhao, PhD

Response to the referee's comments

We would like to thank the reviewer for valuable comments and suggestions. We have addressed all raised issues in the revision accordingly. Please kindly find our following point-by-point responses. The reviewer's comments in black and our responses in blue. Any amendments in the revised manuscript are highlighted in red.

***Response to Reviewer #1*:**

This manuscript investigated the aerosol composition and sources in Guangzhou, China, with a focus on ACSM measurements and subsequent PMF analysis. Routine analysis and plots were made. The conclusions are solid, but not exciting. However, latter part of the manuscript brought advance to the knowledge base by investigating the SOA sources and formation mechanisms from the perspective of RO2 chemistry. It is found that SOA has moderate correlation with RO2* in non-pollution days, but not in polluted episodes. Some conclusions are inferred by this analysis and I will discuss more later in the comment. This analysis distinguishes this manuscript from previous studies. I would like note that this type of novel analysis is missing from most of previous studies in China that are based on AMS+PMF analysis. Overall, I recommend publication with major revisions.

***[A]*:** We would like to thank the reviewer for valuable comments and suggestions. Please find below our point-by-point responses.

Major Comment

1. Even though the analysis on the relationship between SOA and RO_2 is novel, some discussions can be improved and I hope the authors will consider the following comments to make the manuscript hopefully more impactful. The major issue in this analysis is that SOA and RO_2 have dramatically different lifetime (days vs seconds). From this point of view, I find the moderate correlation between SOA and RO_2 in figure 10a and b intriguing, but hard to explain. My hypothesis for this correlation is that both SOA and RO2 are controlled by the amount of oxidants available. Another hypothesis is that they have similar diurnal variation (as shown in figure 5). It would be helpful to de-trend the SOA and RO_2 and then make the correlation analysis. For example, correlating SOA and RO_2 for data points at the same hour of day. In addition, the lifetime issue is especially important in polluted days when the air is more stagnant, SOA lingers for a long time, but RO_2 lifetime is short due to enhanced NOx concentration. This is likely the

main reason for the lack of correlation between SOA and RO_2 in polluted days (i.e., figure 10c and d, Page 17 Line 495). Overall, the different lifetimes of SOA and RO_2 should be kept in mind when interpreting any results.

***[A]*:** We thank the reviewer for raising the important points on the correlations between SOA and RO_2*. We agree with the reviewer that lifetimes between SOA and RO_2^* are dramatically different. However, following the reviewer's suggestions, we further analyze the measurement data and find that the lifetime effects probably play a minor role in poor correlations between SOA and RO_2^* during pollution periods. Our results further confirm that gas-phase oxidation and gas-phase oxidation in combination with heterogenous reactions are respectively the main reasons for moderate correlations between SOA and RO_2^* during non-pollution periods and poor correlations during pollution periods.

(1) We believe that moderate correlations between SOA and RO_2^* in non-pollution period are due to gas-phase oxidation of VOCs that leads to formation of both RO_2^* and SOA (Details can be found in 147-159 in the revision). Thus, excluding heterogeneous reactions, intense gas phase oxidation (not only related to the amount of oxidants but VOCs) is expected to enhance the whole system of RO_2*+SOA. Otherwise, both RO_2* and SOA concentrations will decrease under weak gas phase oxidation. This is where the correlation between SOA and RO_2* comes from.

According to the reviewer's suggestions, for the non-pollution period, we de-trended the correlations between the two species by plotting the dependence of SOA on RO_2* concentration for the same short period (every 2 hours, to ensure enough points) of every day during non-pollution period in Fig. S13 (see it in supplementary or below). Like Figs. 10a and b in the manuscript, moderate correlations are seen from the de-trending plots. The results suggest the relationship between SOA and RO_2^*, especially the upward trend of SOA with increasing RO_2^*, is convincing. Thus, similar diurnal variations between SOA and RO_2^* in non-pollution period are the result of shared influence from gas phase oxidation of VOCs.

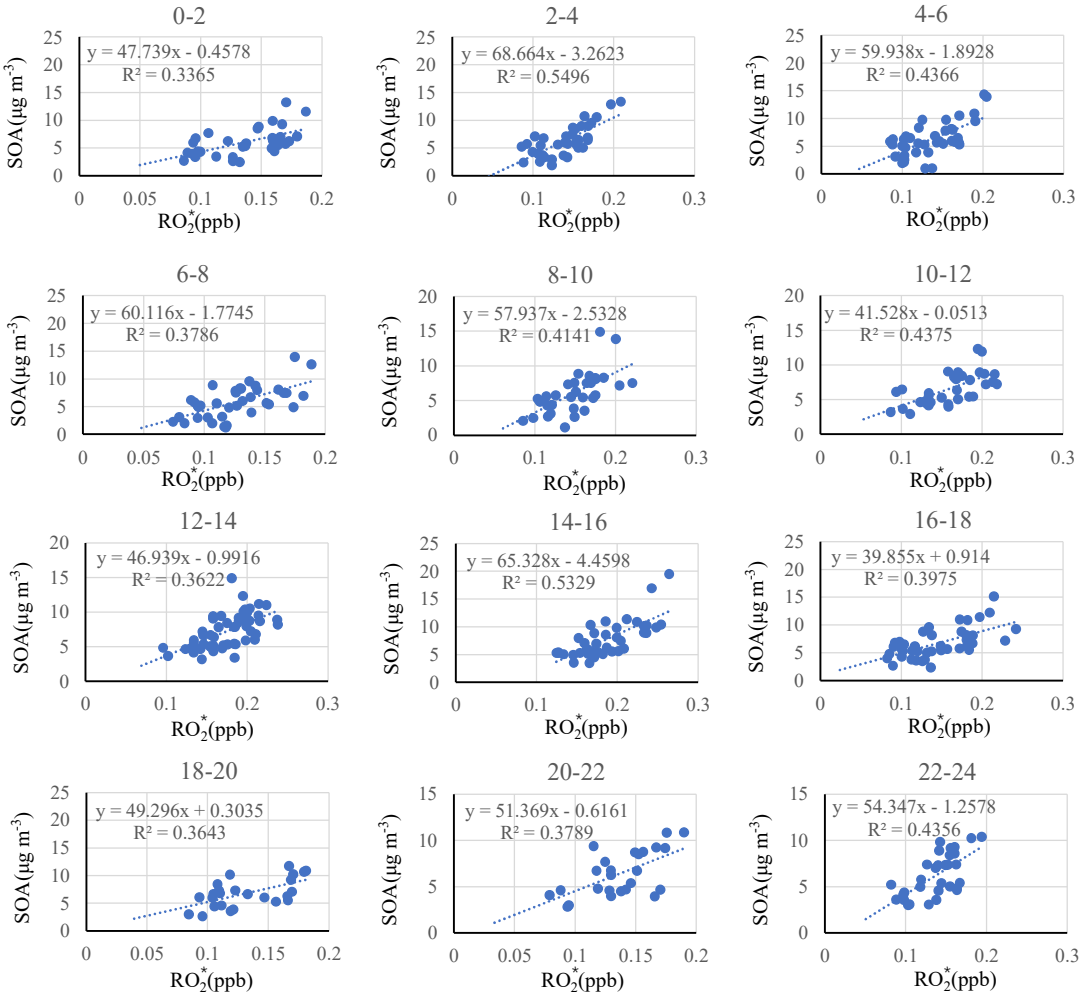

Figure S13. Dependence of SOA on RO_2* concentration for the same short period of every day (i.e., every 2 hours) during non-pollution periods. Note that all the correlations are statistically significant (p-value < 0.01).

(2) During pollution periods, however, the correlations between SOA and RO_2* become a little more complicated than those during non-pollution periods. We agree with the reviewer that lifetimes between SOA and RO_2* are dramatically different (days vs seconds). However, here we show that the dramatic differences of lifetimes between the two species are not likely the main reasons which lead to poor correlations between them. As we mentioned in the paper, the odd oxygen (O_x =O_3 + NO_2) can be used as a robust photochemical indicator, which has a lifetime of about one day, a similar magnitude to that of SOA (Schaub et al., 2007; Lamsal et al., 2010; Valin et al., 2013). Here we present daytime relationship of O_x with SOA and RO_2* during non-pollution and pollution EPs respectively (Fig. S14, see it in supplementary or below). Reasonably good correlations were found between RO_2^* and O_x during both non-pollution and pollution EPs. However, only reasonably good correlation between SOA and O_x was found during non-pollution periods, while no correlation at all was found during pollution EPs, neither

was found for the correlation between SOA and RO_2* during pollution EPs (Fig. 10c in the revision). If the dramatic difference of lifetime was to play an important role in the correlation as the reviewer hypothesizes, the reasonably good correlation between RO_2* and O_x in non-pollution period shouldn't exist during pollution EPs, just like what happen to RO_2* and SOA. Besides, when we discuss the relationship between SOA and O_x (similar life time), the same pattern as that for SOA and RO_2* (Fig. S15 c and d) is revealed. Hence, we believe that the lifetime effects probably play an insignificant role in the poor correlation between SOA and RO_2* during pollution EPs. We think that no correlations between SOA and RO_2*/Ox during pollution EPs implied dramatical changing of SOA formation mechanisms.

As the reviewer pointed out, the enhanced NO_x during polluted days would influence the lifetime of RO_2*. As NO_x concentration increases, more RO_2* was consumed. Then the correlation between RO_2^* and O_x (also SOA) may become worse with significantly enhanced NO_x levels. However, this influence is probably not significant in this study because a good correlation was still found between RO_2^* and O_x during pollution EPs (Fig. S15b).

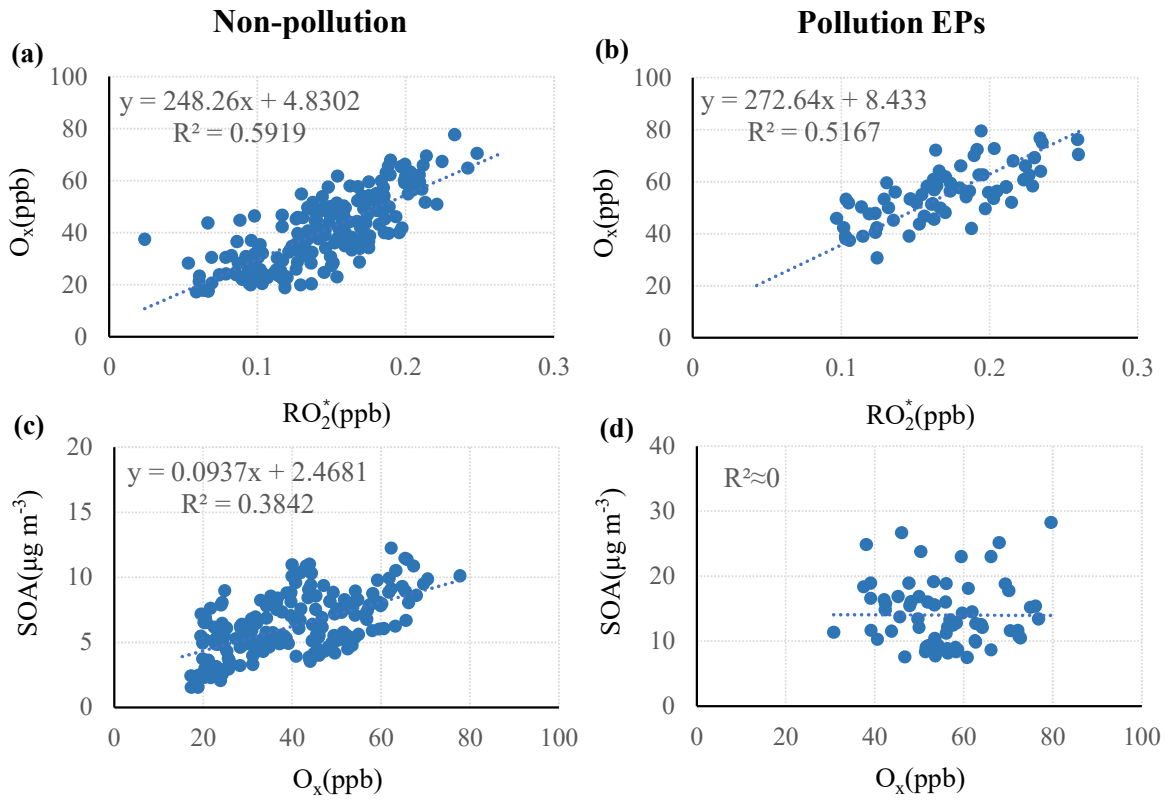

Figure S14. Daytime dependence of O_x on RO_2* (a, b) and dependence of SOA on O_x (c, d) for pollution EPs and non-pollution period.

（3）We further confirm the distinctly different mechanisms for SOA formation between non-pollution and pollution EPs by plotting estimated H/C ratio as a function of O/C ratio in the Van Krevelen

diagram. The O/C and H/C ratios were estimated from f_{43} and f_{44}, which were proposed by Aiken et al. (2008) and Ng et al. (2011) respectively. Similar diagrams based on ACSM unit mass resolution data were reported in previous studies (Brito et al., 2014; Reece et al., 2017; Saha et al., 2018). The area enclosed by the two red boundary lines was defined for ambient OOA components in Ng et al. (2011). Our data points were slightly outside of this area and were further shifted to the upper right corner of the plot. Similar differences from other ambient or laboratory measurements were also reported in previous studies (Budisulistiorini et al., 2018; Saha et al., 2018), which were attributed to different precursors emitted or aging processes. As is shown in Fig. 11a (see it in revision or below), the H/C ratio is linearly correlated with the O/C ratio and is confined into a narrow belt during non-pollution periods, indicating the precursors, mechanism, and chemical components of SOA are likely similar (Ng et al. 2010, 2011). Although the H/C ratio follows similar trends with O/C ratio during pollution periods, the shape is much broader with respect to the H/C ratio especially in the middle portion of the O/C ratio, strongly indicating that more diverse components in SOA are present surrounding the measurement site in Guangzhou. A wider range of H/C ratio during pollution EPs imply more diverse precursor sources and (or) different mechanisms which lead to formation of SOA components with highly variable H/C ratios (Ng et al. 2010, 2011). Although we cannot totally rule out the possibility of dramatic changes in the emission sources, it is unlikely for those changes to occur within a month of the measurement period. Besides, it is unreasonable that these changes only coincidently happened in pollution EPs. Hence it is more likely that the formation mechanisms during non-pollution and pollution periods are distinctly different. Here we propose two most possible different mechanisms of SOA formation during pollution EPs: (1) gas-phase oxidation under enhanced NO_x concentration which leads to dramatically different SOA components from these under lower NO_x concentration (Ziemann et al., 2012); (2) other mechanisms such as additional heterogeneous/multiphase reactions from dramatic increases of PM mass loading and hence more available particle surfaces or volumes for reactions. We replot estimated H/C ratio vs estimated O/C ratio in the Van Krevelen diagram with an overlapped NO_x concentration range during the two periods to remove the enhanced NO_x effects (Fig. 11b). Similar patterns were obtained, highlighting the high possibility of significant heterogeneous/multiphase reactions in pollution EPs. A new Figure 11 and relevant content were added in the revised manuscript (lines 496-523, page 17).

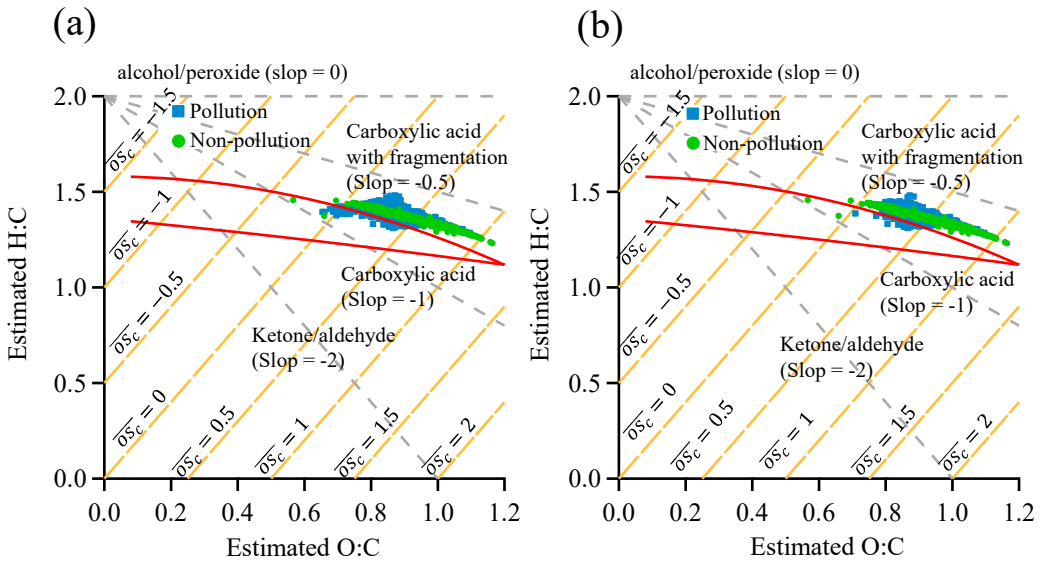

Figure 11. Plot of estimated H/C ratio as a funciton of estimated O/C ratio in the Van Krevelen diagram: (a) Non-pollution vs. pollution EPs; (b) Non-pollution vs. pollution EPs with an overlaped NO_x concentration range during the two periods. The area enclosed by the two red boundary lines was defined for ambient OOA components in Ng et al. (2011).

"We further investigate the distinctly different mechanisms for SOA formation between non-pollution and pollution EPs by plotting estimated H/C ratio as a function of O/C ratio in the Van Krevelen diagram (Fig.11). The O/C and H/C ratios were estimated from f_{43} and f_{44}, which were proposed by Aiken et al. (2008) and Ng et al. (2011) respectively. Similar diagrams based on ACSM unit mass resolution data were reported in previous studies (Brito et al., 2014; Reece et al., 2017; Saha et al., 2018). The area enclosed by the two red boundary lines was defined for ambient OOA components in Ng et al. (2011). Our data points were slightly outside of this area and were further shifted to the upper right corner of the plot. Similar differences from other ambient or laboratory measurements were also reported in previous studies (Budisulistiorini et al., 2018; Saha et al., 2018), which were attributed to different precursors emitted or aging processes. As shown in Fig. 11 a, the H/C ratio is linearly correlated with the O/C ratio and is confined into a narrow belt during non-pollution periods, indicating the precursors, mechanism, and chemical components of SOA are likely similar (Ng et al. 2010, 2011). Although the H/C ratio follows similar trends with O/C ratio during pollution periods, the shape is much broader with respect to the H/C ratio especially in the middle portion of the O/C ratio, strongly indicating that more diverse components in SOA are present surrounding the measurement site in Guangzhou. A wider range of H/C ratio during pollution EPs imply more diverse precursor sources and (or) different mechanisms which lead to

formation of SOA components with highly variable H/C ratios (Ng et al. 2010, 2011). Although we cannot totally rule out the possibility of dramatic changes in the emission sources, it is unlikely for those changes to occur within a month of the measurement period. Hence it is more likely that the formation mechanisms during non-pollution and pollution periods are distinctly different. Here we propose two most possible different mechanisms of SOA formation during pollution EPs: (1) gas-phase oxidation under enhanced NOx concentration which leads to dramatically different SOA components from these under lower NOx concentration (Ziemann et al., 2012); (2) other mechanisms such as additional heterogeneous/multiphase reactions from dramatic increases of PM mass loading and hence more available particle surfaces or volumes for reactions. We replot estimated H/C ratio vs estimated O/C ratio in the Van Krevelen diagram with an overlapped NOx concentration range during the two periods to remove the enhanced NOx effects (Fig. 11b). Similar patterns were obtained, highlighting the possibility of significant heterogeneous/multiphase reactions in the pollution EPs."

2. Correlation between RO_2 and O_3. Assume RO_2 is at steady-state, then we can approximate d[RO2]/dt=k[O3][VOC]-k[RO2][NO]=0 [RO2]â´ L˙I ([O_3][VOC])/([NO]) If the [VOC]/[NO] ratio doesn't change much, a correlation between RO_2 and O_3 may be expected. The equation here is over-simplified, but my point is that many discussions may start from or be explained by this type of simple mathematical derivation.

***[A]*:** We thank the reviewer for valuable suggestions. According to recent measurements in Guangzhou, about 67%, 17% and 16% of VOCs are alkanes, alkenes and aromatic hydrocarbons respectively (Zou et al., 2015). Hence during daytime, it is likely that the predominant sources of RO_2* are from OH-initiated hydrocarbon oxidation, complicated by a probably minor contribution from ozone- alkene/aromatic hydrocarbon oxidation. In fact, based on previous VOCs (Zou et al., 2015) and OH (Rohrer et al., 2014) measurement data in Guangzhou, along with O_3 concentration in this study and rate constants reported in Atkinson et al. (2003), the OH contribution to RO_2* is estimated 100 times larger than O_3 contribution. During nighttime, however, since it is likely that the predominant sources of RO_2* are from NO_3-initiated hydrocarbon oxidation, along with a minor contribution from ozone-alkene/aromatic hydrocarbon oxidation (Volkamer et al., 2010; Stone et al., 2014). In either case, the relationship between RO_2* and ozone is not straightforward. Hence it is unlikely to connect them with a simple and explicit mathematical form.

In fact, in this paper, we employ O_x (O_x=O_3+NO_2) instead of ozone itself as a proxy when discussing the effects of photochemistry on SOA formation (Herndon et al., 2008). Here NO_2 is used to compensate O_3 consumption. Here we plot O_x concentration as a function of RO_2* concentration for different scenarios (non-pollution daytime, non-pollution nighttime, pollution daytime and pollution night time) (Fig. S4 a-d, see it in supplementary or below). The results show that good correlations between O_x and RO_2^* were only seen during daytime when photochemistry occurs while poor or no correlations at all were observed during nighttime when photochemistry is shut off. Interestingly, when we plot ozone concentration as a function of RO_2* concentration for the four scenarios, good correlations between ozone and RO_2^* were all seen during regardless of daytime or nighttime (Fig. S4 e-h). As mentioned above, good correlation between RO_2* and O_3 should come from shared photochemistry during daytime. In contrast, RO_2* is mainly contributed by NO_3/O_3-initiated VOCs oxidation during nighttime. Previous studies have proved that nocturnal NO_3 radicals mainly comes from NO_2 oxidation by O_3, i.e., NO_2+O_3= NO_3+O_2 (Volkamer et al., 2010; Stone et al., 2014). Thus, RO_2* is always related to O_3 concentration at night, likely explaining their good nocturnal correlations.

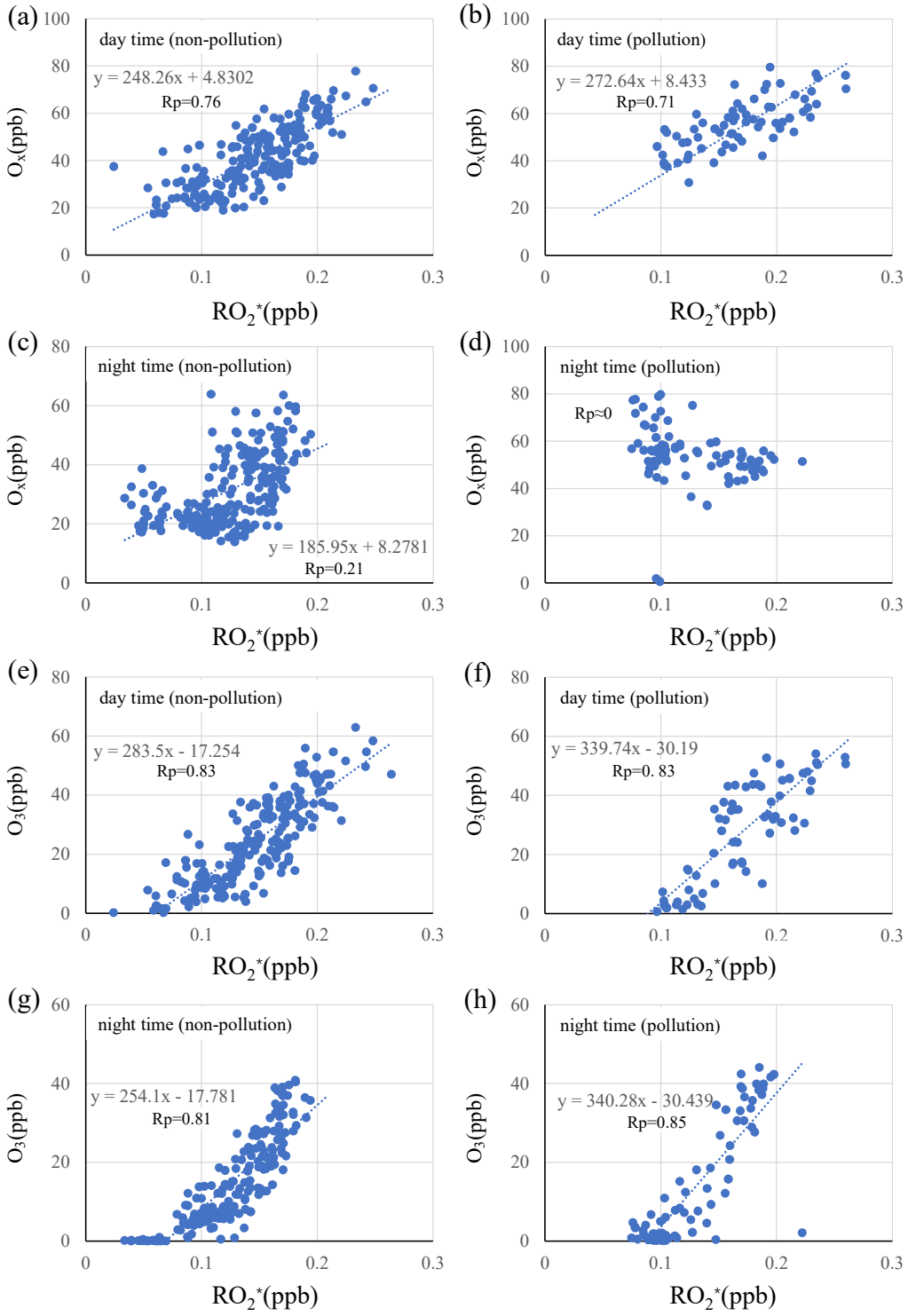

Figure S4. Dependence of O_x and O_3 on RO_2* for different scenarios (non-pollution daytime period, pollution daytime EPs, non-pollution nighttime period, and pollution nighttime EPs). All the regressions are orthogonally linear.

3. In figure S4, the correlation between RO_2 and O_3 for the whole campaign is shown. I suggest the authors also categorize all data points into sub-groups (non-pollution vs polluted, day vs night, as figure 10) and show correlation relationship. The reason I suggest this is that based on figure 10c, polluted days only

account for a small fraction of all data points. Thus, the relationship between RO2 and O3 for polluted days are not clearly shown in the assembly of all data points.

***[A]*:** According to the reviewer's suggestions, we have adjusted Figure S4 and showed the correlation between RO_2 and O_3 with subgroups. Please refer to answer #2.

4. Figure 11 and Page 17 Line 505. By eyeballing, the correlation between RO2 and SOA at each sub-group is very week. The p-value for linear regression must be included.

***[A]*:** We included the p-values into Figure 11 in the original version (now Figure 12 in the revision).We also added a sentence to the caption of the figure, "all correlations of the concentration segments were statistically significant (p-value < 0.01, see detailed statistical information in Table S3)." Additionally, a table (Table S3) with detailed statistic information was added into the supplementary.

We agree with the reviewer that the correlations between SOA and RO_2* during pollution periods are not as strong as those during non-pollution periods probably due to fewer points. Nevertheless, we show that a more viable dependence trend of SOA on RO_2* in pollution EPs can be seen by dividing samples into 6 sub-groups based on different PM_1 mass intervals (Figure 12).

Table S3. P-value, T-value, number of points (n), and Pearson Correlations between SOA and RO_2* for different NR-PM_1 concentration intervals.

NR-PM_1 ($\mu g\ m^{-3}$)	r	n	T	p
< 30	0.31	47	5.07	<0.001
30-40	0.50	60	4.40	<0.001
40-50	0.53	35	3.56	0.0012
50-60	0.49	41	3.51	0.0011
60-70	0.62	40	4.93	<0.001
>70	0.59	30	3.85	<0.001

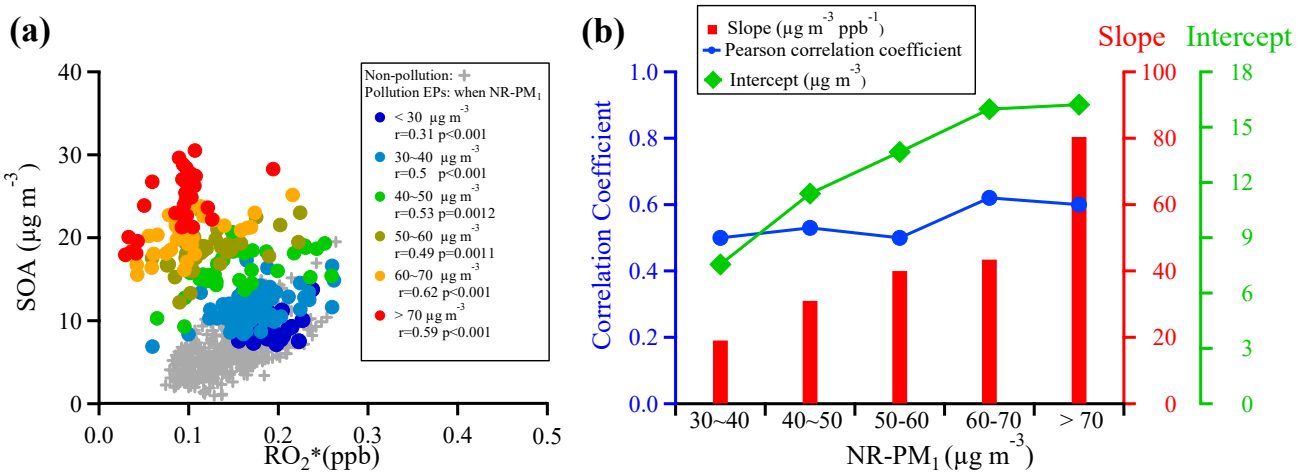

Figure 12. (a) Scatter plots of SOA and RO_2* during pollution EPs at different NR-PM_1 mass concentration segments, and (b) Correlation coefficients, slopes, and intercepts of linear regressions between SOA and RO_2* for NR-PM_1 mass concentration segments ranging from 30-40 to > 70 μg m^{-3}. The regressions are orthogonally linear, and all correlations of the concentration segments were statistically significant (p-value < 0.01, see detailed statistical information in Table S3).

5. Page 2 Line 62 and Page 17 Line 518. It is not clear why the intercept represents the extent of other SOA formation mechanisms. I think the related conclusions are overblown.

***[A]*:** We thank the reviewer for pointing this out. As we show in answer #1 that that gas-phase oxidation and gas-phase oxidation in combination with heterogenous reactions are respectively the main reasons for moderate correlations between SOA and RO_2^* during non-pollution periods and poor correlations during pollution periods. As also mentioned in the above answer, although the correlations between SOA and RO_2* during pollution periods are not as strong as those during non-pollution periods, the extrapolation of these regressions, that is, the intercepts might imply mechanisms of SOA formation as more SOA is formed with increasing PM concentrations. In addition, the intercept from the regressions between SOA and RO_2^* during non-pollution periods is essentially close to zero, leading us to believe that the intercepts likely correspond to the amount of SOA formed from other mechanisms (i.e., heterogenous reactions) other than gas-phase oxidation.

6.Page 17 Line 513: RO_2 concentration can not represent the amount of gas phase oxidation products

***[A]*:** We agree with the reviewer and have removed the relevant sentence.

~~"We assume that RO2* can roughly represent the amount of gas phase oxidation products of VOCs which seems to be reasonable."~~

7. Figure 8. Please include all data points in this plot, in addition to the binned-average.

***[A]*:** We thank the reviewer for the suggestion. We have modified Figure 8 in revision by including all data points and separating it into several panels. We have hence changed the caption of Figure 8 as shown below.

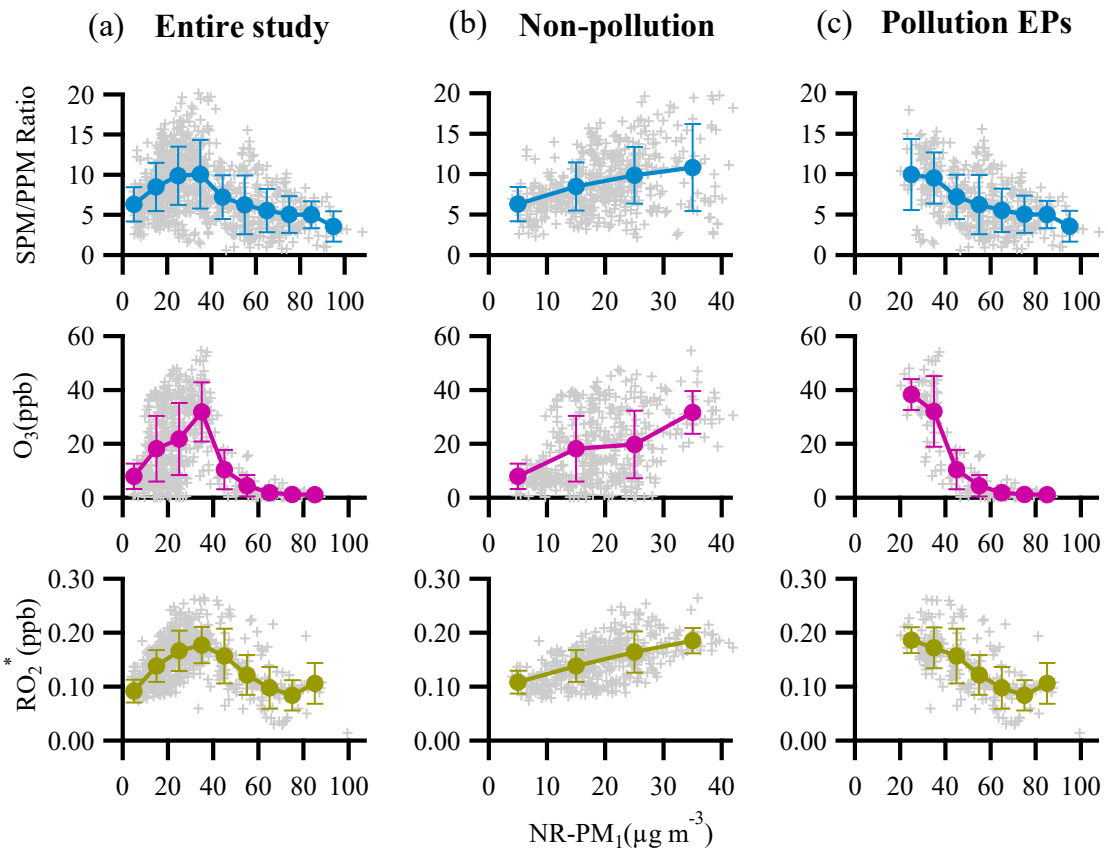

Figure 8. Dependences of SPM/PPM ratio, concentrations of the atmospheric oxidants (O_3 and RO_2*) on NR-PM_1 mass loading for (a) entire study, (b) non-pollution period and (c) pollution EPs. The binned data are also presented as solid circles with an interval of 10 μg m^{-3} NR-PM_1. The error bars are standard deviations.

8. Figure 10 and 11 and S4. Please use orthogonal linear regression, which considers the measurement uncertainty in both x- and y-axis.

***[A]*:** Per the reviewer's suggestions, we have replaced Figure 10, Figure 11 (now Figure 12 in the revision), and Figure S4 using orthogonal linear regressions (Minitab 2019, www.minitab.com). The renewed figures don't change our original conclusions. We also mentioned this in captions of these figures.

Minor Comments

1. Page 4 Line 102: I believe the authors mean "inevitable", instead of "evitable".

***[A]*:** Corrected (line 103, page 4).

2. Page 6 Line 175: Even though the measurement details of RO2* have been described in previous studies, it is still beneficial to briefly mention how the measurements were done.

***[A]*:** Agree, we have added several sentences to describe the measurement details of RO_2* in the revision (lines 194-200, page 7).

"The concentrations of the total peroxy radicals (RO_2* = $\Sigma RO_2^{\cdot}$+HO_2) were measured with a dual-channel PERCA (Peroxy Radical Chemical Amplification) instrument (Yang et al., 2018; Yang et al., 2019). In this instrument, ambient mixing ratios of RO_2* radicals were converted to a larger amount of NO_2 by reacting with NO and CO. The amplified NO_2 concentrations were then measured with a portable broadband cavity enhanced spectrometer (BBCES) with a precision of 40 pptv (1σ, with 21 s data acquisition time) (Fang, et al., 2017). The total uncertainty of the PERCA instrument was about 10% with a precision of about 0.4 pptv (1σ, 21 s)."

3. Page 9 Line 254: The selection of a-value should be justified.

***[A]*:** We thank the reviewer for pointing this out. We have now added several sentences in supplementary in the method section, "The results showed that an unreasonably high proportion of m/z 44 were presented in COA profiles for solutions with a-values of 0.5 and 0.7. We hence adopt 4 factors and an a-value of 0.3 as the optimal solution. The results from ME-2 are shown in Figures S5-S11".

In addition, we have also added one sentence in the revision (lines 278-279, page 9), "Detailed selection of a-value can be found in supplementary (method section)."

4. Page 9 Line 274: Even in non-pollution period, rush hour peaks in HOA are expected. Thus, the lack of diurnal variation in HOA in this study is alarming. It may be due to the low resolution of ACSM.

***[A]*:** We agree with the reviewer that the resolution of ACSM is low compared to regular AMS. The HOA concentration during non-pollution periods after ME-2 factorization is low (< 1 μg m^{-3}), close to an estimated detection limit of 0.7 μg m^{-3} for OA, leading to lack of diurnal variations in HOA. However, it is unlikely to affect other organic factors since the concentrations of other organic components are much higher than the estimated detection limit for OA.

For clarification, we have added several sentences in the revision (lines 299-302, page 10), "In comparison, the HOA concentration showed almost no variations during non-pollution period (even

during rush hours), which likely arose from its extremely low value (< 1 μg m^{-3} which was close to an estimated detection limit of 0.7 μg m^{-3} for OA with the ToF-ACSM)."

5. Page 10 Line 307: Replace "high volatility" with "semi-volatile".

***[A]*:** We have corrected it (line 333, page 11).

6. Page 16 Line 490: the trend between f44 and SOA concentration is not clear in figure 10. Regarding the claimed conclusion that f44 of SOA decreases with increase of SOA concentration, I suggest the authors to check if there is any "contamination" in PMF analysis. In other words, in polluted days, is some POA apportioned into SOA by PMF analysis? This can be done by either run PMF on non-pollution and polluted days separately and see if the fraction of SOA changed, or check the residual of POA characteristic ions during polluted days. The former approach is more reliable.

***[A]*:** According to the reviewer's suggestions, we plotted the dependence of SOA concentration on f44 for different scenarios (non-pollution daytime, non-pollution nighttime, pollution daytime and pollution night time) as is shown in Fig. S16 (see it in supplementary or below). The trends between SOA and f44 are clear: SOA concentrations increase with increasing f44 during non-pollution periods while opposite trends are observed during pollution periods. In addition, we ran Me-2 separately for non-pollution periods and pollution EPs (Fig. S17, see it in supplementary or below). The results from those additional runs show similar fractions and concentrations of SOA, confirming reliability of our original results.

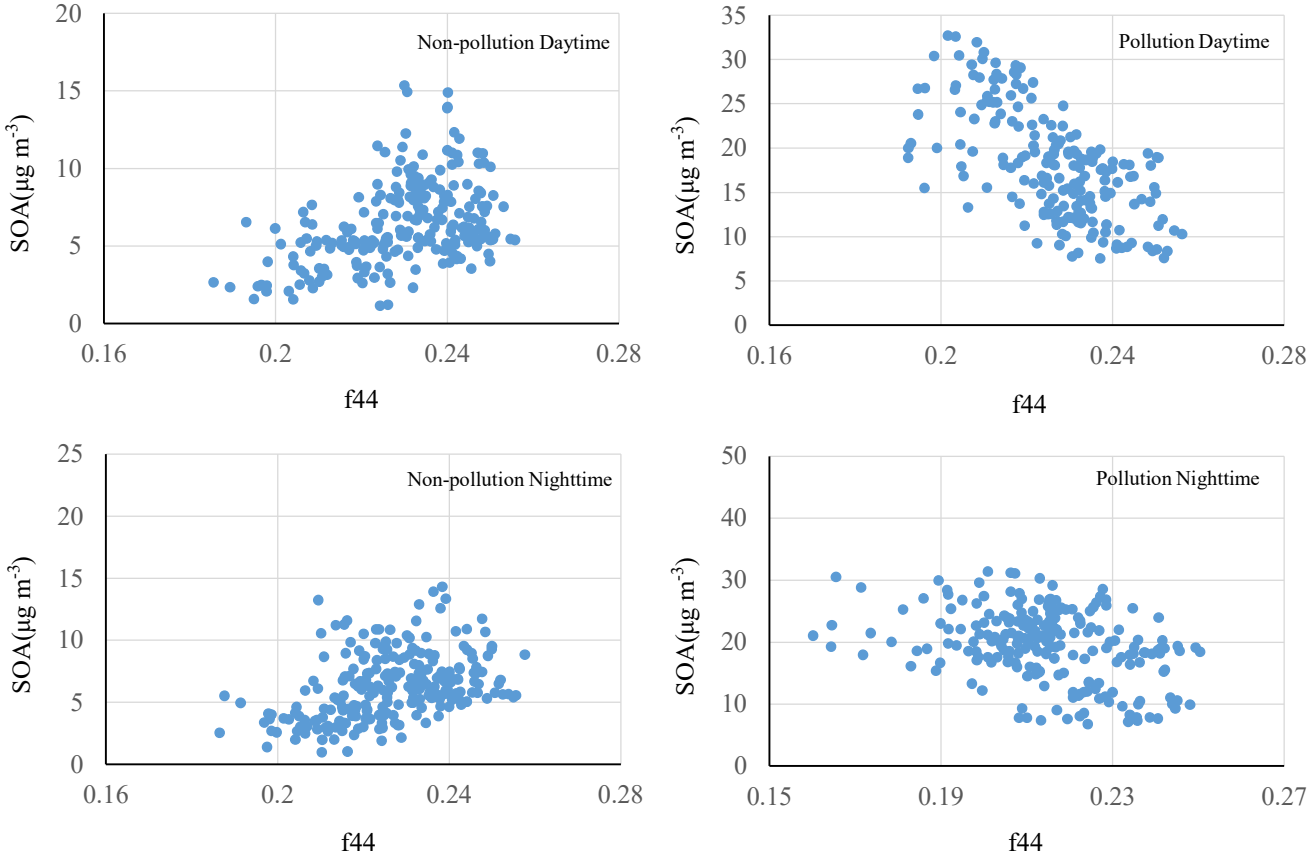

Figure S16. Scatter plots between SOA and f44 for different scenarios (non-pollution daytime, non-pollution nighttime, pollution daytime and pollution night time).

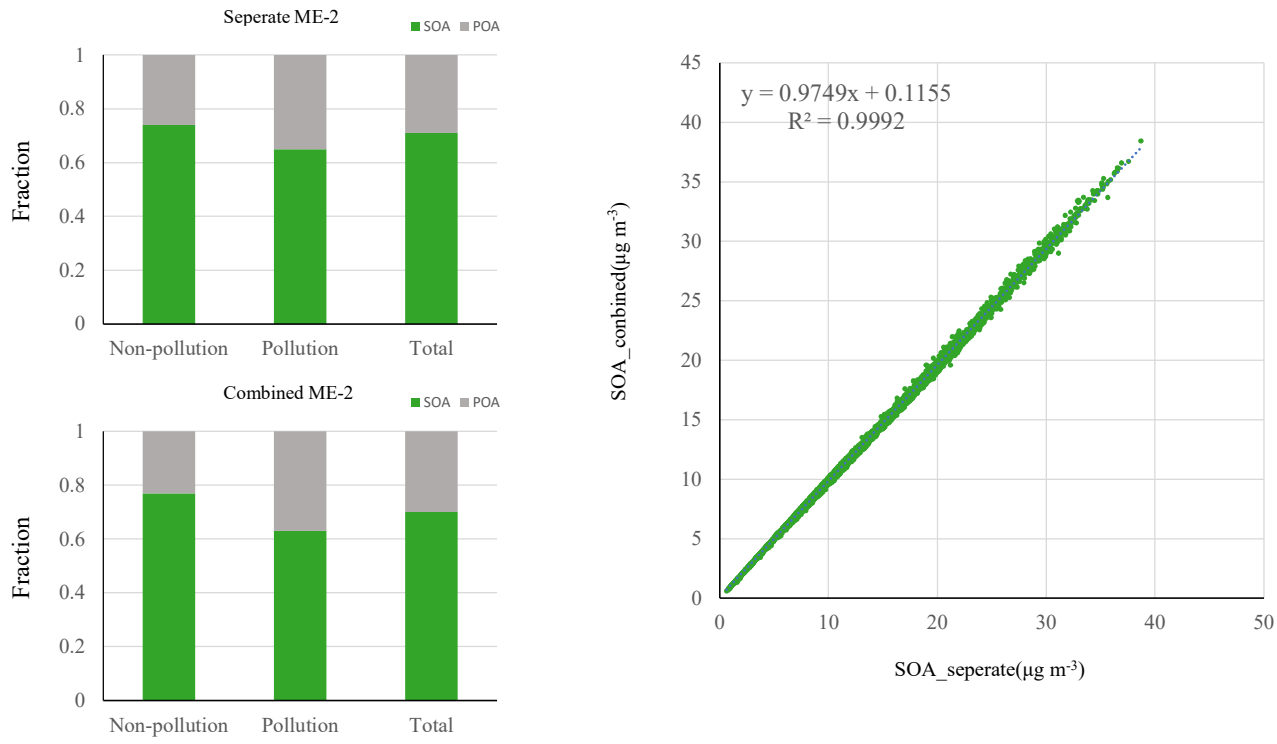

Figure S17. Comparison between combined ME-2 and separate ME-2, along with their correlations.

References

Aiken, A. C., DeCarlo, P. F., Kroll, J. H., Worsnop, D. R., Huffman, J. A., Docherty, K. S., Ulbrich, I. M., Mohr, C., Kimmel, J. R., Sueper, D., Sun, Y., Zhang, Q., Trimborn, A., Northway, M., Ziemann, P. J., Canagaratna, M. R., Onasch, T. B., Alfarra, M. R., Prevot, A. S. H., Dommen, J., Duplissy, J., Metzger, A., Baltensperger, U., and Jimenez, J. L.: O/C and OM/OC ratios of primary, secondary, and ambient organic aerosols with high-resolution time-of-flight aerosol mass spectrometry, Environ. Sci. Technol., 42, 4478–4485, 2008.

Atkinson, R. and Arey, J.: Atmospheric degradation of volatile organic compounds, Chem. Rev., 103, 4605–4638, 2003.

Brito, J., Rizzo, L. V., Morgan, W. T., Coe, H., Johnson, B., Haywood, J., Longo, K., Freitas, S., Andreae, M. O., and Artaxo, P.: Ground-based aerosol characterization during the South American Biomass Burning Analysis (SAMBBA) field experiment, Atmos. Chem. Phys., 14, 12069-12083, 10.5194/acp-14-12069-2014, 2014.

Budisulistiorini, S. H., Riva, M., Williams, M., Miyakawa, T., Chen, J., Itoh, M., Surratt, J. D., and Kuwata, M.: Dominant contribution of oxygenated organic aerosol to haze particles from real-time observation in Singapore during an Indonesian wildfire event in 2015, Atmos. Chem. Phys., 18, 16481-16498, 10.5194/acp-18-16481-2018, 2018.

Herndon, S. C., Onasch, T. B., Wood, E. C., Kroll, J. H., Canagaratna, M. R., Jayne, J. T., Zavala, M. A., Knighton, W. B., Mazzoleni, C., Dubey, M. K., Ulbrich, I. M., Jimenez, J. L., Seila, R., de Gouw, J. A., de Foy, B., Fast, J., Molina, L. T., Kolb, C. E., and Worsnop, D. R.: Correlation of secondary organic aerosol with odd oxygen in Mexico City, Geophys. Res. Lett., 35, 10.1029/2008gl034058, 2008.

Fang, B., Zhao, W.X.*, Xu, X.Z., Zhou, J.C, Ma, X., Wang, S., Zhang, W.J.*, Dean S. Venables, Chen, W.D. Portable broadband cavity-enhanced spectrometer utilizing Kalman filtering: application to real-time, in situ monitoring of glyoxal and nitrogen dioxide, Optics Express, 2017, 25, 26910-26922.

Lamsal, R. Martin, A. Van Donkelaar, E. Celarier, E. Bucsela, K. Boersma, R. Dirksen, C. Luo, Y. Wang: Indirect validation of tropospheric nitrogen dioxide retrieved from the OMI satellite instrument: insight into the seasonal variation of nitrogen oxides at northern midlatitudes, J. Geophys. Res. Atmos., 115 (2010), p. D05302

Valin, A. Russell, R. Cohen: Variations of OH radical in an urban plume inferred from NO2 column measurements, Geophys. Res. Lett., 40 (2013), pp. 1856-1860.

Ng, N. L., Canagaratna, M. R., Zhang, Q., Jimenez, J. L., Tian, J., Ulbrich, I. M., Kroll, J. H., Docherty, K. S., Chhabra, P. S., Bahreini, R., Murphy, S. M., Seinfeld, J. H., Hildebrandt, L., Donahue, N. M.,

DeCarlo, P. F., Lanz, V. A., Prévôt, A. S. H., Dinar, E., Rudich, Y., and Worsnop, D. R.: Organic aerosol components observed in Northern Hemispheric datasets from Aerosol Mass Spectrometry, Atmos. Chem. Phys., 10, 4625-4641, 10.5194/acp-10-4625-2010, 2010.

Ng, N. L., Canagaratna, M. R., Jimenez, J. L., Chhabra, P. S., Seinfeld, J. H., and Worsnop, D. R.: Changes in organic aerosol composition with aging inferred from aerosol mass spectra, Atmos. Chem. Phys., 11, 6465-6474, 10.5194/acp-11-6465-2011, 2011.

Reece, S. M., Sinha, A., and Grieshop, A. P.: Primary and Photochemically Aged Aerosol Emissions from Biomass Cookstoves: Chemical and Physical Characterization, Environ. Sci. Technol., 51, 9379-9390, 10.1021/acs.est.7b01881, 2017.

Rohrer, F., Lu, K., Hofzumahaus, A., Bohn, B., Brauers, T., Chang, C.-C., Fuchs, H., Häseler, R., Holland, F., Hu, M., Kita, K., Kondo, Y., Li, X., Lou, S., Oebel, A., Shao, M., Zeng, L., Zhu, T., Zhang, Y., and Wahner, A.: Maximum efficiency in the hydroxyl-radical-based self-cleansing of the troposphere, Nature Geosci., 7, 559-563, 10.1038/ngeo2199, 2014.

Saha, P. K., Reece, S. M., and Grieshop, A. P.: Seasonally Varying Secondary Organic Aerosol Formation From In-Situ Oxidation of Near-Highway Air, Environ. Sci. Technol., 52, 7192-7202, 10.1021/acs.est.8b01134, 2018.

Schaub, D., Brunner, D., Boersma, K. F., Keller, J., Folini, D., Buchmann, B., Berresheim, H., and Staehelin, J.: SCIAMACHY tropospheric NO_2 over Switzerland: estimates of NO_x lifetimes and impact of the complex Alpine topography on the retrieval, Atmos. Chem. Phys., 7, 5971–5987, https://doi.org/10.5194/acp-7-5971-2007, 2007.

Stone, D., Evans, M. J., Walker, H., Ingham, T., Vaughan, S., Ouyang, B., Kennedy, O. J., McLeod, M. W., Jones, R. L., Hopkins, J., Punjabi, S., Lidster, R., Hamilton, J. F., Lee, J. D., Lewis, A. C., Carpenter, L. J., Forster, G., Oram, D. E., Reeves, C. E., Bauguitte, S., Morgan, W., Coe, H., Aruffo, E., Dari-Salisburgo, C., Giammaria, F., Di Carlo, P., and Heard, D. E.: Radical chemistry at night: comparisons between observed and modelled HOx, NO3 and N2O5 during the RONOCO project, Atmos. Chem. Phys., 14, 1299-1321, 10.5194/acp-14-1299-2014, 2014.

Volkamer, R., Sheehy, P., Molina, L. T., and Molina, M. J.: Oxidative capacity of the Mexico City atmosphere – Part 1: A radical source perspective, Atmos. Chem. Phys., 10, 6969-6991, 10.5194/acp-10-6969-2010, 2010.

Yang, C., Zhao, W., Fang, B., Xu, X., Zhang, Y., Gai, Y., Zhang, W., Venables, D. S., and Chen, W.: Removing Water Vapor Interference in Peroxy Radical Chemical Amplification with a Large Diameter Nafion Dryer, Anal. Chem., 90, 3307-3312, 10.1021/acs.analchem.7b04830, 2018.

Yang, C., Zhao, W., Fang, B., Yu, H., Xu, X., Zhang, Y., Gai, Y., Zhang, W., Chen, W., and Fittschen, C.: Improved Chemical Amplification Instrument by Using a Nafion Dryer as an Amplification Reactor for Quantifying Atmospheric Peroxy Radicals under Ambient Conditions, Anal. Chem., 91, 776-779, 10.1021/acs.analchem.8b04907, 2019.

Ziemann, P. J., and Atkinson, R.: Kinetics, products, and mechanisms of secondary organic aerosol formation, Chem. Soc. Rev., 41, 6582-6605, 10.1039/c2cs35122f, 2012.

Zou, Y.; Deng, X. J.; Zhu, D.; Gong, D. C.; Wang, H.; Li, F.; Tan, H. B.; Deng, T.; Mai, B. R.; Liu, X. T.; Wang, B. G., Characteristics of 1 year of observational data of VOCs, NOx and O3 at a suburban site in Guangzhou, China. Atmos. Chem. Phys. 2015, 15, (12), 6625-6636.

Response to the referee's comments

We would like to thank the reviewer for valuable comments and suggestions. We have addressed all raised issues in the revision accordingly. Please kindly find our following point-by-point responses. The reviewer's comments in black and our responses in blue. Any amendments in the revised manuscript are highlighted in red.

Response to Reviewer #2

This manuscript reports a ToF-ACSM measurement study of sub-micron particles conducted during winter time in Guangzhou, South China. PMF with ME-2 algorithm was applied on the dataset to identify the major sources of organic aerosols (OA). Discussions are made on concentrations, compositions, and sources ambient PM1, highlighting the important roles of SOA. Additionally, the relationship with SOA and peroxy radicals was examined to reveal the different mechanisms responsible for SOA formation between non-pollution period and pollution Eps. The manuscript is well written and provides some interesting results for understanding ambient primary and secondary organic aerosol sources and processes. I would recommend the publication of this manuscript in Atmospheric Chemistry and Physics after the authors address the following comments.

***[A]*:** Thank you for the comments and valuable suggestions. We have changed accordingly. Please find our point-by-point responses below.

Comments:

1. The resolution and font sizes need to be improved? (e.g., Fig. 1, Fig. 4b and Fig. 5).

***[A]*:** We have increased the resolution and font sizes of the figures.

2. Please check the subscript in the texts and figures.

***[A]*:** We have doubly checked the entire manuscript to ensure no typos with the subscript.

3. Page 7, Line 191-194: It would be good to add a more accurate discussion of the calculated composition dependent CE values (e.g., range, highest frequency and uncertainty of CE values).

***[A]*:** We have added several sentences to discuss the calculated composition dependent CE values in the revision (lines 217-220, pages 7-8):

"The results showed that only about 1% of samples (78 of 6623) had CE values larger than 0.45 (others are 0.45), with the largest value being 0.578. Hence the influence induced by fluctuation of the CE values is negligible and we chose a CE value of 0.45 for the ACSM measurements in this study."

4. Page 8, Line 237-241: Recently, a large number of AMS/ACSM studies have been conducted in China in recent years. Is it possible to add more references and discuss with more results?

***[A]*:** We thank the reviewer for updating us on this information. We have included 11 additional publications, with a comprehensive summary being added in the revision (Table 1, in the revised manuscript or below). In addition, we have also modified in Figure 3 by including more measurement data for Beijing and Lanzhou in the revision.

Here we only compare measurements during winter season, corresponding to our measurement periods. Our survey shows that SOA formation is significantly influenced under different underlying surfaces (urban, suburban, and country). Nevertheless, additional survey adds more measurement data into the NR-PM_1 pool. However, our original conclusion of increasing the fraction of SOA in OA from north to south still holds. We have modified the paragraph that describes NR-PM_1 measurements in China in the revision (line 267-269, page 9). "Furthermore, Table 1 shows that the SOA fraction is generally enhanced from winter to summer for a specific site in China. In addition, Table 1 also revealed that SOA formation is significantly influenced under different underlying surfaces (urban, suburban, and country)."

5. Page 15, Line 455-477: I suggest the authors put these parts in introduction and highlight the differences of your results from previous ones.

***[A]*:** We thank the reviewer for valuable suggestions. We have made some modifications and moved these sentences to introduction section in the revision (lines 140-159, page 5).

In addition, we have added one sentence to highlight differences of our results from previous studies in the revision (lines 177-178, page 6).

"Possible mechanisms for wintertime SOA formation were explored through introducing RO_2^* as a proxy for gas-phase oxidation capacity during both daytime and nighttime."

6. Page 28, Fig. 4: The factors of HOA and COA were resolved using the constrain mode (a-value), but SVOOA and LVOOA were identified using the PMF free mode. So, to be more directly clear for readers,

the authors may consider adding the corresponding label in each mass spectrum of POA factors (e.g., constrained or a specific a-value) and SOA factors (e.g., unconstrained or free).

***[A]*:** According to the reviewer's suggestions, we have added the corresponding labels in Figure 4.

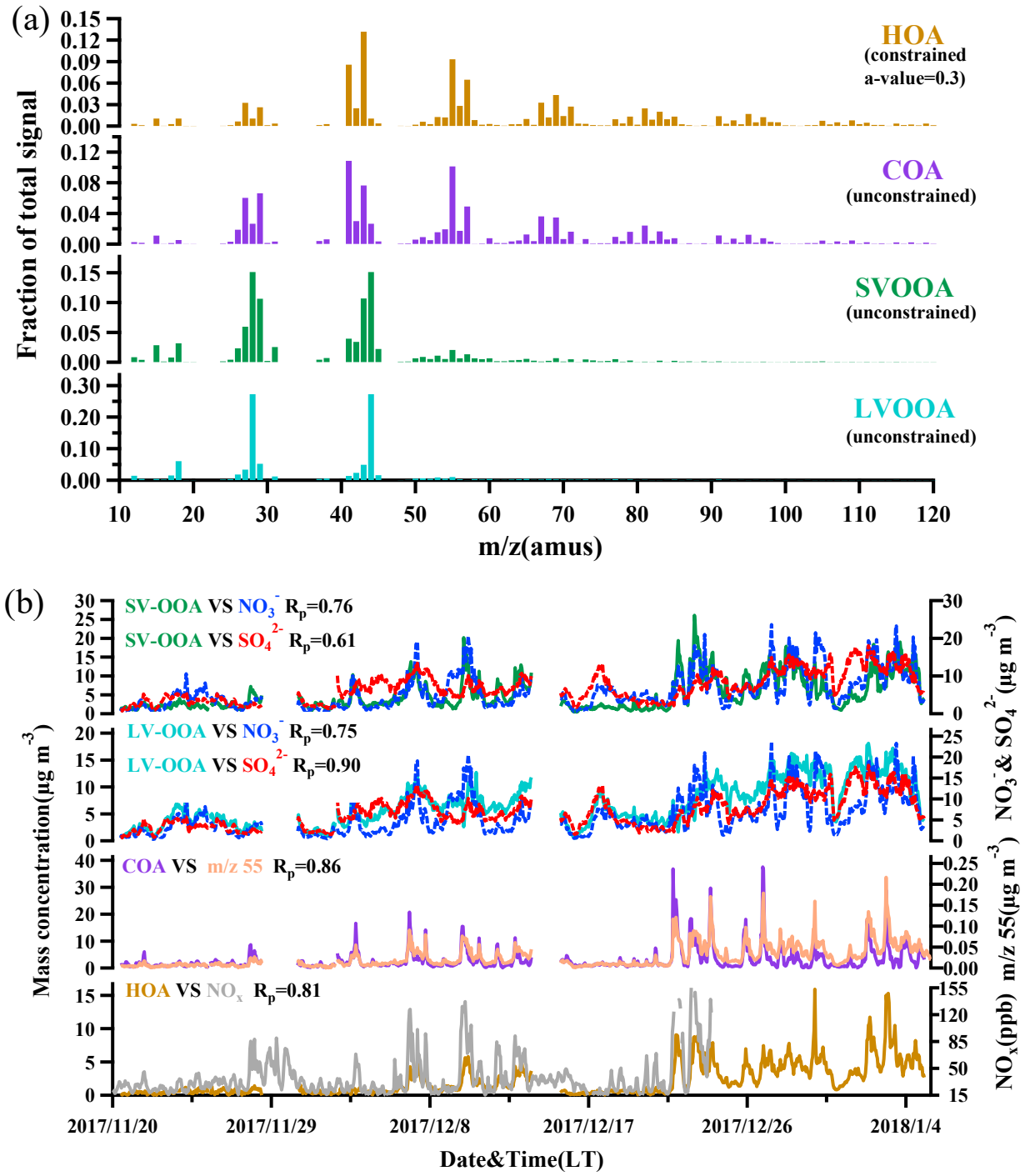

Figure 4. The mass spectra and time series of the four OA components (HOA, COA, SVOOA, and LVOOA).

7. Page 29, Fig. 5: The diurnal profile of NOx appears to be bi-modal, yet no morning traffic feature is visible in the HOA diurnal plot during pollution Eps. Have the authors looked for the variation of HOA mass fraction during early rush hour? More explanation about the diurnal profile of HOA would be good.

***[A]*:** We thank the reviewer for pointing this out. Though it is small, there was a small HOA peak at about 8:00 in Fig. 5 in the manuscript. In fact, strong traffic emissions from heavy duty vehicles during midnight to 6:00 in the early morning weaken the morning rush hour peak. Similar features were frequently reported in previous studies (Sun et al., 2013; Qin et al., 2017; Huang et al., 2019). The rapidly rising boundary layer after 7:00 would be possibly another reason for diluting PM accumulation from rush hour traffic. Besides, if we discuss the variation of HOA mass fraction, a clear morning peak was observed (Fig. S12, see it in supplementary or below). Thus, the diurnal feature of HOA during pollution Eps is reasonable. We have added a sentence in the revision for clarification (lines 298-299, page 10): "Besides, effects of emissions from heavy duty vehicles and the rapidly rising boundary layer after 7:00 would also account for the insignificant peak of HOA during morning rush hour."

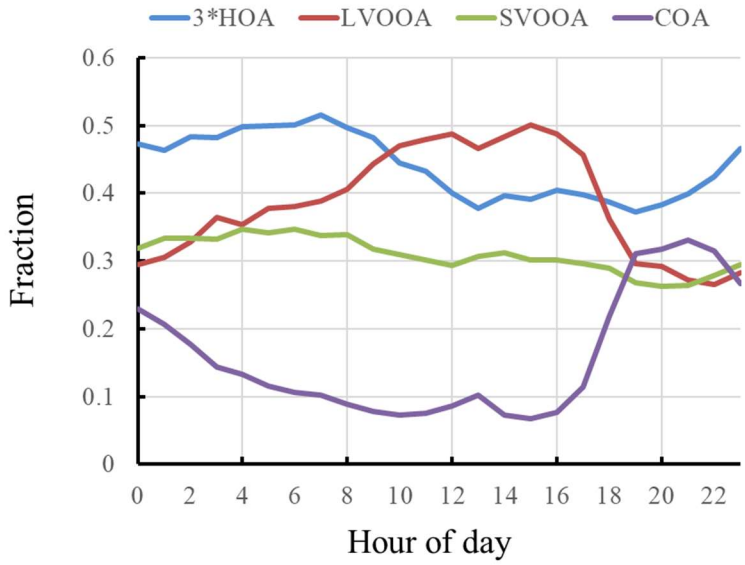

Figure S12. The diurnal variations of 4 OA components mass fractions for pollution EPs.

8. Section 3.5.2: It would be interesting to see how the SOA changes during different conditions. The authors may consider adding the correlations between SVOOA and LVOOA with RO2*, perhaps in the supplement.

***[A]*:** We have plotted dependence of SVOOA/LVOOA concentrations on RO_2* concentration during non-pollution periods and pollution periods in Figure S15 (see it in supplementary or below). It is shown that better correlations between LVOOA and RO_2* than between SVOOA and RO_2*. In addition, the slope from LVOOA vs RO_2* is higher than that from SVOOA vs RO_2*, implying transformation of SVOOA to LVOOA. In contrast, neither LVOOA nor SVOOA were well correlated to RO_2*, possibly due to strong heterogeneous/multiphase reactions during pollution EPs as discussed in the text.

We have added several sentences in the revision to reflect the correlations between SVOOA/LVOOA concentrations and RO_2* concentration (lines 491-495, page 17).

"In addition, correlations between SVOOA/LVOOA and RO_2 were explored by plotting dependence of SVOOA/LVOOA concentrations on RO_2* concentration during non-pollution periods and pollution periods (Fig. S15). The results show that better correlations and larger slope for LVOOA vs RO_2* than for SVOOA vs RO_2* during non-pollution periods. In contrast, neither LVOOA nor SVOOA were correlated to RO_2* during pollution EPs."

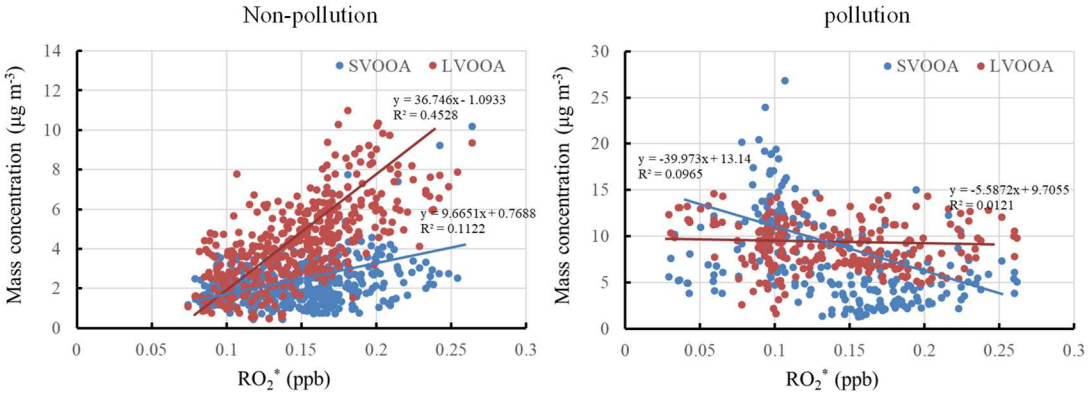

Figure S15. Scatter plots between RO_2* and SVOOA/LVOOA for non-pollution periods and pollution EPs.

Table 1. Summary of reported NR-PM_1 measurements in China.

Location	Date	Region	NR-PM_1 (μg m^{-3})	OA (%)	SOA/OA (%)	Ref.
Guangzhou	Winter, 2017	Pearl River Delta region	35.3	49	70	This study
Panyu	Winter, 2014	Pearl River Delta region	55.4	50.5	61	Qin et al., 2017
Shenzhen	Winter, 2009	Pearl River Delta region	44.5	46.2	46.6	He et al., 2011
Kaiping	Winter, 2008	Pearl River Delta region	33.1	36.3	75.4	Huang et al. 2011
Nanjing	Winter, 2015	Yangtze River Delta region	32.5	36	66	Zhang et al., 2017
Nanjing	Summer, 2013	Yangtze River Delta region	36.8	42	72	Zhang et al., 2015
Shanghai	Summer, 2010	Yangtze River Delta region	27	31	78	Huang et al., 2012
Beijing[1]	Winter	Beijing-Tianjin-Hebei region	70	52	43	**[1]**
Beijing	Summer, 2011	Beijing-Tianjin-Hebei region	80	32	65	Hu et al., 2016a
Shijiazhuang	Winter, 2014	Beijing-Tianjin-Hebei region	178	50	22	Huang et al. 2019
Handan	Winter, 2015	Beijing-Tianjin-Hebei region	178	47	17	Li et al., 2017
Lanzhou	Winter, 2014	Northwest of China	57.3	55	37	Xu et al., 2016
Lanzhou	Summer, 2012	Northwest of China	24	53	59	Xu et al., 2014
Hong Kong	Winter	South of China	20.7	45.5	69	Sun et al., 2016
Hong Kong	Summer, 2011	South of China	15.6	26	82	Li et al., 2015
Ziyang	Winter, 2012	Southwest of China	60	40	71.2	Hu et al., 2016

[1]: The three quantities for winter Beijing are the averaged values over six studies (Sun et al., 2013; Sun et al., 2014; Jiang et al., 2015; Wang et al., 2015; Hu et al., 2016a; Sun et al., 2016).

References

He, L. Y., Huang, X. F., Xue, L., Hu, M., Lin, Y., Zheng, J., Zhang, R., and Zhang, Y. H.: Submicron aerosol analysis and organic source apportionment in an urban atmosphere in Pearl River Delta of China using high-resolution aerosol mass spectrometry, J. Geophys. Res., 116, 10.1029/2010jd014566, 2011.

Hu, W., Hu, M., Hu, W.-W., Niu, H., Zheng, J., Wu, Y., Chen, W., Chen, C., Li, L., Shao, M., Xie, S., and Zhang, Y.: Characterization of submicron aerosols influenced by biomass burning at a site in the Sichuan Basin, southwestern China, Atmos. Chem. Phys., 16, 13213–13230, https://doi.org/10.5194/acp-16-13213-2016, 2016.

Hu, W., Hu, M., Hu, W., Jimenez, J. L., Yuan, B., Chen, W., Wang, M., Wu, Y., Chen, C., Wang, Z., Peng, J., Zeng, L., and Shao, M.: Chemical composition, sources and aging process of submicron aerosols in Beijing: contrast between summer and winter, J. Geophys. Res., 121, 1955–1977, https://doi.org/10.1002/2015JD024020, 2016a.

Huang, X. F., He, L. Y., Hu, M., Canagaratna, M. R., Kroll, J. H., Ng, N. L., Zhang, Y. H., Lin, Y., Xue, L., Sun, T. L., Liu, X. G., Shao, M., Jayne, J. T., and Worsnop, D. R.: Characterization of submicron aerosols at a rural site in Pearl River Delta of China using an Aerodyne High-Resolution Aerosol Mass Spectrometer, Atmos. Chem. Phys., 11, 1865-1877, 10.5194/acp-11-1865-2011, 2011.

Huang, X.-F., He, L.-Y., Xue, L., Sun, T.-L., Zeng, L.-W., Gong, Z.-H., Hu, M., and Zhu, T.: Highly time-resolved chemical characterization of atmospheric fine particles during 2010 Shanghai World Expo, Atmos. Chem. Phys., 12, 4897–4907, https://doi.org/10.5194/acp-12-4897-2012, 2012.

Huang, R. J., Wang, Y., Cao, J., Lin, C., Duan, J., Chen, Q., Li, Y., Gu, Y., Yan, J., Xu, W., Fröhlich, R., Canonaco, F., Bozzetti, C., Ovadnevaite, J., Ceburnis, D., Canagaratna, M. R., Jayne, J., Worsnop, D. R., El-Haddad, I., Prévôt, A. S. H., amp, apos, and Dowd, C. D.: Primary emissions versus secondary formation of fine particulate matter in the most polluted city (Shijiazhuang) in North China, Atmos. Chem. Phys., 19, 2283-2298, 10.5194/acp-19-2283-2019, 2019.

Jiang, Q., Sun, Y. L., Wang, Z., and Yin, Y.: Aerosol composition and sources during the Chinese Spring Festival: fireworks, secondary aerosol, and holiday effects, Atmos. Chem. Phys., 15, 6023–6034, https://doi.org/10.5194/acp-15-6023-2015, 2015.

Li, Y. J., Lee, B. P., Su, L., Fung, J. C. H., and Chan, C. K.: Seasonal characteristics of fine particulate matter (PM) based on high-resolution time-of-flight aerosol mass spectrometric (HR-ToF-AMS) measurements at the HKUST Supersite in Hong Kong, Atmos. Chem. Phys., 15, 37–53, https://doi.org/10.5194/acp-15-37-2015, 2015.

Li, H., Zhang, Q., Zhang, Q., Chen, C., Wang, L., Wei, Z., Zhou, S., Parworth, C., Zheng, B., Canonaco, F., Prévôt, A. S. H., Chen, P., Zhang, H., Wallington, T. J., and He, K.: Wintertime aerosol chemistry and haze evolution in an extremely polluted city of the North China Plain: significant contribution from coal and biomass combustion, Atmos. Chem. Phys., 17, 4751–4768, https://doi.org/10.5194/acp-17-4751-2017, 2017.

Qin, Y. M., Tan, H. B., Li, Y. J., Schurman, M. I., Li, F., Canonaco, F., Prévôt, A. S. H., and Chan, C. K.: Impacts of traffic emissions on atmospheric particulate nitrate and organics at a downwind site on the periphery of Guangzhou, China, Atmos. Chem. Phys., 17, 10245-10258, 10.5194/acp-17-10245-2017, 2017.

Sun, C., Lee, B. P., Huang, D., Jie Li, Y., Schurman, M. I., Louie, P. K. K., Luk, C., and Chan, C. K.: Continuous measurements at the urban roadside in an Asian megacity by Aerosol Chemical Speciation Monitor (ACSM): particulate matter characteristics during fall and winter seasons in Hong Kong, Atmos. Chem. Phys., 16, 1713-1728, 10.5194/acp-16-1713-2016, 2016.

Sun, Y. L., Wang, Z. F., Fu, P. Q., Yang, T., Jiang, Q., Dong, H. B., Li, J., and Jia, J. J.: Aerosol composition, sources and processes during wintertime in Beijing, China, Atmos. Chem. Phys., 13, 4577–4592, https://doi.org/10.5194/acp-13-4577-2013, 2013.

Sun, Y. L., Jiang, Q., Wang, Z., Fu, P., Li, J., Yang, T., and Yin, Y.: Investigation of the sources and evolution processes of severe haze pollution in Beijing in January 2013, J. Geophys. Res., 119, 4380–4398, https://doi.org/10.1002/2014JD021641, 2014.

Sun, Y., Du,W., Fu, P.,Wang, Q., Li, J., Ge, X., Zhang, Q., Zhu, C., Ren, L., Xu, W., Zhao, J., Han, T., Worsnop, D. R., and Wang, Z.: Primary and secondary aerosols in Beijing in winter: sources,

variations and processes, Atmos. Chem. Phys., 16, 8309–8329, https://doi.org/10.5194/acp-16-8309-2016, 2016.

Xu, J., Zhang, Q., Chen, M., Ge, X., Ren, J., and Qin, D.: Chemical composition, sources, and processes of urban aerosols during summertime in northwest China: insights from high-resolution aerosol mass spectrometry, Atmos. Chem. Phys., 14, 12593–12611, https://doi.org/10.5194/acp-14-12593-2014, 2014.

Xu, J., Shi, J., Zhang, Q., Ge, X., Canonaco, F., Prévôt, A. S. H., Vonwiller, M., Szidat, S., Ge, J., Ma, J., An, Y., Kang, S., and Qin, D.: Wintertime organic and inorganic aerosols in Lanzhou, China: sources, processes, and comparison with the results during summer, Atmos. Chem. Phys., 16, 14937-14957, 10.5194/acp-16-14937-2016, 2016.

Wang, Q., Sun, Y., Jiang, Q., Du,W., Sun, C., Fu, P., andWang, Z.: Chemical composition of aerosol particles and light extinction apportionment before and during the heating season in Beijing, China, J. Geophys. Res.-Atmos., 120, 12708–12722, 2015.

Zhang, Y. J., Tang, L. L., Wang, Z., Yu, H. X., Sun, Y. L., Liu, D., Qin, W., Canonaco, F., Prévôt, A. S. H., Zhang, H. L., and Zhou, H. C.: Insights into characteristics, sources, and evolution of submicron aerosols during harvest seasons in the Yangtze River delta region, China, Atmos. Chem. Phys., 15, 1331–1349, https://doi.org/10.5194/acp-15-1331-2015, 2015.

Zhang, Y., Tang, L., Croteau, P. L., Favez, O., Sun, Y., Canagaratna, M. R., Wang, Z., Couvidat, F., Albinet, A., Zhang, H., Sciare, J., Prévôt, A. S. H., Jayne, J. T., and Worsnop, D. R.: Field characterization of the $PM_{2.5}$ Aerosol Chemical Speciation Monitor: insights into the composition, sources, and processes of fine particles in eastern China, Atmos. Chem. Phys., 17, 14501-14517, 10.5194/acp-17-14501-2017, 2017.

Characterization of submicron particles by Time-of-Flight Aerosol Chemical Speciation Monitor (ToF-ACSM) during wintertime: aerosol composition, sources and chemical processes in Guangzhou, China

Junchen Guo[1], Shengzhen Zhou[1,8], Minfu Cai[1], Jun Zhao[1,8], Wei Song[2], Weixiong Zhao[3], Weiwei Hu[2], Yele Sun[4], Yao He[4], Chengqiang Yang[3], Xuezhe Xu[3], Zhisheng Zhang[5], Peng Cheng[6], Qi Fan[1], Jian Hang[1], Shaojia Fan[1], Xinming Wang[2], Xuemei Wang[7]

[1]School of Atmospheric Sciences, Guangdong Province Key Laboratory for Climate Change and Natural Disaster Studies, and Institute of Earth Climate and Environment System, Sun Yat-sen University, Guangzhou, 510275, P. R. China

[2]State Key Laboratory of Organic Geochemistry, Guangzhou Institute of Geochemistry, Chinese Academy of Sciences, Guangzhou, 510640, P. R. China

[3]Laboratory of Atmospheric Physico-Chemistry, Anhui Institute of Optics and Fine Mechanics, Chinese Academy of Sciences, Hefei, 230031, P. R. China

[4]State Key Laboratory of Atmospheric Boundary Layer Physics and Atmospheric Chemistry, Institute of Atmospheric Physics, Chinese Academy of Sciences, Beijing 100029, P. R. China

[5]South China Institute of Environmental Sciences, Ministry of Ecology and Environment, Guangzhou, 510655, China

[6] Institute of Technology on Atmospheric Environmental Safety and Pollution Control, Jinan University, Guangzhou, 510632, P. R. China

[7]Institute for Environmental and Climate Research, Jinan University, Guangzhou, 511443, P. R. China

[8]Southern Marine Science and Engineering Guangdong Laboratory (Zhuhai), Zhuhai, 519082, P. R. China

Correspondence to: Shengzhen Zhou (zhoushzh3@mail.sysu.edu.cn); Jun Zhao (zhaojun23@mail.sysu.edu.cn)

Abstract. Particulate matter (PM) pollution in China is an emerging environmental issue which policy makers and public have increasingly paid attention to. In order to investigate the characteristics, sources, and chemical processes of PM pollution in Guangzhou, a field measurement was conducted from 20 November 2017 to 5 January 2018, with a Time-of-Flight Aerosol Chemical Speciation Monitor (ToF-ACSM) and other collocated instruments. Mass concentrations of non-refractory submicron particulate

matters (NR-PM_1) measured by the ToF-ACSM were correlated well with those of $PM_{2.5}$ or $PM_{1.1}$ measured by filter-based methods. The organic mass fraction increased from 45% to 53% when the air switched from non-pollution periods to pollution episodes, indicating significant roles of organic aerosols (OA) during the whole study. Based on the mass spectra measured by the TOF-ACSM, Positive Matrix Factorization (PMF) with multilinear engine (ME-2) algorithm was performed to deconvolve OA into four factors, including hydrocarbon-like OA (HOA, 12%), cooking OA (COA, 18%), semi-volatile oxygenated OA (SVOOA, 30%), and low-volatility oxygenated OA (LVOOA, 40%). Furthermore, we found that SVOOA and nitrate were significantly contributed from local traffic emissions while sulfate and LVOOA were mostly attributed to regional pollutants. Comparisons between this work and other previous studies in China show that SOA fraction in total OA increases spatially across China from the North to the South.

Two distinctly opposite trends for NR-PM_1 formation were observed during non-pollution period and pollution EPs. The ratio of secondary PM (SPM = SVOOA + LVOOA + sulfate + nitrate + ammonium) to primary PM (PPM = HOA + COA + chloride), together with peroxy radicals RO_2* and ozone, increased with increasing NR-PM_1 concentration during non-pollution period, while an opposite trend of these three quantities was observed during pollution EPs. Furthermore, oxidation degrees of both OA and SOA were investigated using the f_{44}/f_{43} space and the results show that at least two OOA factors are needed to cover a large range of f_{44} and f_{43} in Guangzhou. Comparisons between our results and other laboratory studies imply that volatile organic compounds (VOCs) from traffic emissions in particular from diesel combustion and aromatic compounds are most possible SOA precursors in Guangzhou. Peroxy radical RO_2* was used as a tracer for SOA formed through gas phase oxidation. For non-pollution period, SOA concentration was reasonably correlated with RO_2* concentration during both daytime and nighttime, suggesting that gas phase oxidation was primarily responsible for SOA formation. However, there was no correlation between SOA and RO_2* in pollution EPs, suggesting dramatically changed mechanism for SOA formation. This conclusion can also be supported by different features of SOA in Van Krevelen diagram between non-pollution period and pollution EPs. Furthermore, for pollution EPs, when NR-PM_1 mass concentration was divided into six segments, in each segment except for the lowest one, SOA concentration was correlated moderately with RO_2* concentration, suggesting that gas phase oxidation still plays important roles in SOA formation. The intercepts of the above linear regressions, which likely correspond to the extent of other mechanisms (i.e., heterogeneous and multiphase reactions), increased with increasing NR-PM_1 mass concentration. Our results suggest that while gas phase oxidation

contributes predominantly to SOA formation during non-pollution periods, other mechanisms such as heterogeneous and multiphase reactions play more important roles in SOA formation during pollution EPs than gas phase oxidation.

1 Introduction

With rapid development of human civilization, more attention is paid to air quality by public, government, and scientists, especially in developing countries like China. In recent years, particulate matter (PM) pollution has become one of the most concerned environmental issues because of its significant effects on both climate change (IPCC 2013) and human health (Pope III et al., 2006). Atmospheric aerosols exert radiative forcing directly through scattering or absorbing solar radiation or indirectly through cloud formation. In addition, previous studies in the last decade have shown that respiratory and cardiovascular diseases are highly related to fine particles, revealing significant deleterious effects of ambient aerosols on human health (Kreyling et al., 2006). Thus, knowledge of chemical composition, formation mechanisms, and potential sources of fine particles is essential for both academic community and the public, since it is still currently very limited even through decades of investigation. In last decades, most studies focused on $PM_{2.5}$ and made significant progresses while less attention was paid to submicron particles (i.e., PM_1). For instance, although China National Ambient Air Quality Standard (CNAAQS) for $PM_{2.5}$ was established in 2012, the corresponding national standard for submicron particles such as PM_1 has not yet been set up. In fact, it has been shown that PM_1 particles may cause much more damage to human health than $PM_{2.5}$ due to their smaller sizes which make them more easily access to human bodies (Ibald-Mulli et al., 2002; Kreyling et al., 2006). Therefore, more extensive and in-depth studies should be conducted for submicron particles besides $PM_{2.5}$ to obtain a comprehensive understanding on health and climate impacts of fine particles.

Field measurements of aerosol chemical composition mainly employ filter-based offline and mass spectrometric online technologies. Although traditional filter-based methods which are still widely used contribute substantially to understanding of bulk aerosol chemical composition, its obvious shortcomings which include low time resolution from hours to days and evaporative loss limit the capacity of this technology in aerosol measurements. In comparison, mass spectrometric online methods have higher time resolutions varying from seconds to hours, therefore proven to be an efficient way for measurements of aerosol mass concentration and chemical composition (Aiken et al., 2009; Zhang et al., 2011; Sun et al., 2013; Crippa et al., 2013; Sun et al., 2014; Lee et al., 2015; Hu et al., 2017). For example, aerosol mass

spectrometer (AMS) is one such instrument that is widely employed in aerosol chemical composition measurements for its reliable data quality and relatively high mass resolution. However, the full version of AMS tends to be costly and time-consuming in terms of its operation and maintenance. As a simplified version of AMS, Aerosol Chemical Speciation Monitor (ACSM) has been widely adopted in recent years among research institutions and environmental monitoring stations for its relatively simple operation, robustness, low cost and sufficient time resolution for field observations spanning months or longer (Allan et al., 2010; Ng et al., 2011; Sun et al., 2013; Fröhlich et al., 2013; Sun et al., 2014; Sun et al., 2016). Certainly, this simplified design is inevitable to bring a few disadvantages for ACSM. Compared with all types of AMS, ACSM gives up the ability of measuring particle size distribution, which makes users lose a robust tool to characterize ambient particulate matters and identify potential sources (Frank et al., 2005; Ge et al., 2012; Lee et al., 2017). Besides, limited by relatively poorer resolution, mass spectra collected by ACSM cannot execute high-resolution peak fitting (Timonen et al., 2016). This incapability prevents users from obtaining some further information such as elemental ratio in particulate matters, which is essential to our knowledge about climate effects or toxicity of aerosols (Aiken et al., 2007; Chhabra et al., 2011; Canagaratna et al., 2015). The simplification of fragmentation table for ACSM, based on ambient AMS data, also likely leads to some small deviations and makes this instrument unsuitable for laboratory studies requiring high precision (Jimenez et al., 2003; Allen et al., 2004; De Haan et al., 2009).

Numerous studies were conducted to investigate chemical composition, sources and secondary processes of PM pollution through AMS or ACSM. It has been shown that organics generally account for a large proportion of PM (Zhang et al., 2007; Aiken et al., 2009; Allan et al., 2010; DeCarlo et al., 2010; Sun et al., 2013; Lee et al., 2015; Bressi et al., 2016; Li et al. 2017). In previous studies, mass spectral signals were input into the Positive Matrix Factorization (PMF) to explore source information of organic aerosols (Zhang et al., 2011). Generally, OA can be deconvolved into primary organic aerosols (POA) which can be further classified according to different markers of primary emissions (e.g., HOA, COA and BBOA), and oxygenated organic aerosols (OOA) which can be further resolved based on oxidation degree (e.g., SVOOA and LVOOA). However, detailed source features are diverse at different regions. For example, Aiken et al. (2009) identified industry-induced local nitrogen-containing OA (LOA), which was barely reported in other cities such as Beijing (Sun et al., 2018), London (Allan et al., 2010) or Paris (Crippa et al., 2013). Similarly, biomass burning OA (BBOA) which was clearly identified at some sites such as those in Hebei (Huang et al., 2019), Mexico (Aiken et al., 2009) or Fresno (Ge et al., 2012), was missing in other locations (during same seasons) such as Hong Kong (Sun et al., 2016), or Beijing (Sun

et al., 2013). Although OA sources have obvious spatial distinction, Jimenez et al. (2009) found a common trend that the fraction of OOA (especially LVOOA) increases from urban to rural areas.

Physical/chemical characteristics and secondary processes of PM were investigated in previous studies (Liggio et al., 2006; Shilling et al., 2009; Marais et al., 2016). Photochemistry which highly depends on daytime solar radiation is commonly believed to play a dominant role in formation of secondary PM (SPM = ammonium + nitrate + sulfate + OOA); However, recent studies showed that the contribution from aqueous reactions or heterogeneous reactions cannot be ignored. For instances, it has been found that the heterogeneous hydrolysis of N_2O_5 on the surface of deliquescent aerosols is a significant pathway for nitrate formation during nighttime (Wang et al., 2018; Wen et al., 2018). Sun et al. (2013) proposed that the mass concentration of sulfate substantially increased through fog processes. Besides, numerous studies have suggested that the amount of SOA from reactive uptake of water-soluble VOCs is comparable to that from gas phase oxidation (Ervens et al., 2011; McNeill, 2015; Herrmann et al., 2015; Marais et al., 2016).

Meanwhile, secondary organic aerosols, the most significant OA composition in China, have not been sufficiently researched, especially in field measurements. In general, the odd oxygen ($O_x = O_3 + NO_2$) was proven to be a robust indicator of photochemical intensity and was therefore adopted in previous measurements to discuss SOA formation (Herndon et al., 2008; Zhou et al., 2014). However, these studies employing O_x only focused on daytime SOA formation while the nocturnal SOA formation was generally ignored due to the limitation of O_x. Meanwhile, interference form directly emitted NO_2 will also lead to some uncertainties.

According to the traditional theory, oxidation of atmospheric VOCs, a significant path for SOA growth, is initiated by important oxidants (e.g., OH, O_3 or NO_3) to form alkyl radicals ($R^{\bullet}$) which are subsequently oxidized to form peroxy organic radicals ($RO_2^{\bullet}$) and alkoxy radicals ($RO^{\bullet}$) (Kroll et al., 2008; Ziemann et al., 2012). The simplest RO_2*, HO_2, is formed in the atmosphere via three pathways: (1) from reactions of OH radicals with ozone or CO; (2) from oxidation of VOCs; (3) from photolysis of formaldehyde (Levy et al., 1971; Ziemann et al., 2012; Sheehy et al., 2010; Stone et al., 2012; Griffith et al., 2013; Wang et al., 2014). During daytime, RO_2* radicals are mainly photochemical products since their formation depends highly on solar radiation or OH radical (Sheehy et al., 2010; Stone et al., 2012; Griffith et al., 2013; Wang et al., 2014). During nighttime, however, nighttime oxidation of VOCs initiated by ozone or nitrate radicals dominates formation of RO_2* radicals especially in urban area, which

has been proven in Volkamer et al. (2010) and Stone et al. (2014). It is hence that RO_2* can served as a tracer for photochemical induced SOA formation during daytime and SOA formation induced by nocturnal gas phase oxidation of VOCs during nighttime.

Results from previous studies suggested that primary emissions, secondary chemical processes, meteorological conditions and regional transport are possible major factors that determine local PM concentration but significantly vary with seasons and locations (Sun et al., 2013; Lee et al., 2015; Sun et al., 2016; Bressi et al., 2016; Gani et al., 2019). Therefore, it is essential to conduct continuous field measurements at various locations to investigate the PM formation mechanisms, as well as the temporal and spatial evolution. Guangzhou, a highly developed city in the Pearl River Delta (PRD) region, is considered to be one of the most densely populated cities in China. However, previous studies on local PM characteristics in Guangzhou were mainly conducted by filter-based methods with low time resolutions (Tan et al., 2009; Zhang et al., 2010; Tao et al., 2012) and therefore knowledge of detailed PM characteristics is still lacking. It is hence urged to perform field measurements with high-time resolutions in the city.

In this study, we employed Time-of-Flight Aerosol Chemical Speciation Monitor (ToF-ACSM) to measure chemical composition and mass concentrations of submicron particles at an urban site in Guangzhou which locates at Guangzhou Institute of Geochemistry, Chinese Academy of Sciences. The following sections present measurement techniques for gases and aerosols, followed by the methodology for data analyses. In the results and discussion section, temporal variations of chemical composition and mass concentration for NR-PM_1 are illustrated, followed by the source apportionment for OA and the diurnal profiles for NR-PM_1. Possible mechanisms for wintertime SOA formation were explored through introducing RO_2* as a proxy for gas-phase oxidation capacity during both daytime and nighttime.

2 Experimental

2.1 Measurement site and techniques

Chemical compositions of NR-PM_1 consisting of Cl^-, SO_4^{2-}, NO_3^-, NH_4^+, and organics were measured from 20 November 2017 to 5 January 2018 by a ToF-ACSM at an urban air quality monitoring site locating at Guangzhou Institute of Geochemistry, Chinese Academy of Sciences (GIG). Detailed descriptions of ToF-ACSM can be found elsewhere (Fröhlich et al., 2013) and the methodology for data analysis is presented in the next section. The site is surrounded by three major traffic roads including Guangyuan road, Huanan road and Keyun road. Several university campuses are located to north and

west of the site while commercial buildings, restaurants, and residential areas are next to its east and south. In addition to aerosol measurements by the ToF-ACSM, ambient gas species such as NO_x and O_3 were measured at the same site by various gas analyzers (Thermo Scientific, USA) while filter samples were collected by an Anderson nine-stage sampler. Meteorological data (wind speed and direction, relative humidity, temperature and pressure) and $PM_{2.5}$ concentrations were measured about 2 and 4 kilometers away from sample site by South China Institute of Environmental Science and Guangzhou Environmental Monitoring Center respectively. The concentrations of the total peroxy radicals ($RO_2^* = \Sigma RO_2^{\cdot} + HO_2$) were measured with a dual-channel PERCA (Peroxy Radical Chemical Amplification) instrument (Yang et al., 2018; Yang et al., 2019). In this instrument, ambient mixing ratios of RO_2^* radicals were converted to a larger amount of NO_2 by reacting with NO and CO. The amplified NO_2 concentrations were then measured with a portable broadband cavity enhanced spectrometer (BBCES) with a precision of 40 pptv (1σ, with 21 s data acquisition time) (Fang, et al., 2017). The total uncertainty of the PERCA instrument was about 10% with a precision of about 0.4 pptv (1σ, 21 s).

2.2 ACSM data analysis

The final mass concentrations and mass spectra were processed from the raw ToF-ACSM data by a standard ACSM data analysis software (Tofware, version 2.5.13) based on Igor pro (version 6.37), with the widely applied procedures described in Ng et al. (2011b) and Sun et al. (2012). Based on the on-site calibrations, a relative ionization efficiency (RIE) value of 1.2 and 3.3 was obtained for sulfate and ammonium respectively. A RIE value of 1.1, 1.3 and 1.4 was respectively adopted for nitrate, chloride and organics according to literature (Takegawa et al., 2005; Canagaratna et al., 2007). Collection efficiency (CE), compensating for losses of the particles during their collection, is considered to be another extremely important parameter for quantification of the ACSM data. This quantity varies with acidity, chemical composition, and water content of the particles (Matthew et al., 2008). Here we consider the effects of acidity and water content to be negligible based on the facts that the RH in the sample line kept below 30% through a Nafion dryer and the aerosols were approximately neutralized in Guangzhou ($NH_4^+/NH_4^+_{predict} = 0.87$). Thus, only chemical composition was considered to affect CE in this work and we adopted a composition-dependent CE formulated by Middlebrook et al. (2012) (i.e., CE = max (0.45, 0.0833 + 0.9167 × ANMF), where ANMF is the mass fraction of ammonium nitrate in NR-PM_1) instead of a widely used empirical value of 0.5. The results showed that only about 1% of samples (78 of 6623)

had CE values larger than 0.45 (others are 0.45), with the largest value being 0.578. Hence the influence induced by fluctuation of the CE values is negligible and we chose a CE value of 0.45 for the ACSM measurements in this study.

3 Results and discussion

3.1 Mass concentrations and chemical composition

Figure 1 shows the time series of meteorological conditions (relative humidity, temperature, pressure, wind speed and direction), NR-PM_1 and $PM_{2.5}$ mass concentrations, and NR-PM_1 composition (SO_4^{2-}, NO_3^-, NH_4^+, Cl^-, and organics) from 20 November 2017 to 5 January 2018. Overall, the 10-minute averaged mass concentration of NR-PM_1 ranged from 2.4 to 130 μg m^{-3}. The averaged concentration during the measurement period was 35.3 ± 22.3 μg m^{-3}, among which about half (17.5 μg m^{-3}) was organics, followed by sulfate (7.0 μg m^{-3}), nitrate (6.0 μg m^{-3}), ammonium (4.6 μg m^{-3}), and chloride (0.5 μg m^{-3}). The NR-PM_1 concentration (from the ToF-ACSM) was correlated well with concentrations of both $PM_{2.5}$ (Pearson Correlation Coefficient (R_p) = 0.83, from BAM-1020) and $PM_{1.1}$ (R_p = 0.86, from Anderson nine-stage sampler). Comparisons between ToF-ACSM and other instruments are detailed in Fig. S1. Overall, high NR-PM_1 mass concentration was observed after 22 December 2017 when the air was more stagnant according to the wind speed (Fig. 1).

Moderate to severe pollution events were observed during the measurement period and we classified five pollution episodes (EP1~EP5) alongside with other periods defined as non-pollution based upon the NR-PM_1 mass concentrations in order to better understand the intrinsic mechanisms on the PM evolution. Each pollution episode was defined as a period that the NR-PM_1 mass concentration continually increased from less than 20 μg m^{-3} (10^{th} percentile) to greater than 75 μg m^{-3} (90^{th} percentile) and then fell below 20 μg m^{-3} again (Fig. 1d). For the entire study, organics and sulfate (Fig. 2) dominated NR-PM_1 mass concentration, consistent with previous studies conducted in the PRD region during autumn and winter (He et al., 2011; Huang et al., 2011; Qin et al., 2017). Fractions of 20% and 49% respectively for sulfate and organics were similar to those in Panyu (25% and 50% for sulfate and organics respectively) and Shenzhen (28% and 46% for sulfate and organics respectively) but quite differed from those in Kaiping (both 36%). This comparison reflects that the sulfate fraction increased and the organic fraction simultaneously decreased from urban to rural areas (Table S1), which could be likely attributed to different sources and chemical aging processes between urban and rural areas in the PRD region. The obvious facts are that heavy industry sections, such as power plants and oil refineries which emit a

tremendous amount of sulfur dioxide, the primary precursor of sulfate, are mainly located in non-urban areas. Similar urban-to-rural evolution of PM chemical composition was reported in previous studies (Jimenez et al., 2009; Zhang et al., 2011; Li et al., 2017), providing further rationales for performing field measurements under different source environments to investigate the chemical evolution of PM.

Figure 3 shows a comparison of NR-PM_1 characteristics among our work in the PRD region and previous wintertime studies conducted in several other Chinese megacities (Beijing, Nanjing, Shijiazhuang, Lanzhou, Hong Kong) beyond PRD region. Compared to other locations, the averaged mass concentration of NR-PM_1 in Guangzhou was much lower (35.5 μg m^{-3}), indicating that the air of PRD region was relatively clean in terms of fine PM. The concentrations of NR-PM_1 in the abovementioned cities were all composed of a large fraction of OA, with a substantial variation (37%~58%), indicating the significant contribution of OA to fine particle mass loading over China. In addition, a remarkable distinction on the fraction of secondary OA (SOA) in OA between southern and northern China was found, that is, SOA dominated OA in southern China (A SOA to OA ratio of 0.66 in Nanjing, 0.58 in Hong Kong, and 0.7 in Guangzhou), compared to a lower ratio of SOA to OA in northern China (0.43 in Beijing, 0.37 in Lanzhou, and 0.22 in Shijiazhuang). The increasing ratio of SOA to OA from the North to the South is probably due to more favorable meteorological conditions such as solar radiation and temperature for secondary chemical processes in southern China and more significant contribution of coal combustion in northern China during wintertime (Sun et al., 2013; Sun et al., 2014; Sun et al., 2018). Furthermore, Table 1 shows that the SOA fraction is generally enhanced from winter to summer for a specific site in China. In addition, Table 1 also revealed that SOA formation is significantly influenced under different underlying surfaces (urban, suburban, and country).

3.2 OA apportionment

Positive matrix factorization with ME-2 engine algorithm was employed to deconvolve OA into four factors, including two primary OA components (HOA and COA) and two OOA components (SVOOA and LVOOA) which are usually treated as SOA. The mass spectra and corresponding time series are depicted in Fig. 4.

3.2.1 Hydrocarbon-like OA (HOA)

A widely referred standard mass spectrum of HOA (Sun et al., 2013; Sun et al., 2016; Huang et al., 2019) derived by Ng et al. (2011) was introduced as an external constraint in this work, with an a-value of 0.3 being chosen to derive the final solution. Detailed selection of a-value can be found in

supplementary (method section). The final mass spectrum of HOA was identified by the ion series representing $C_nH^+_{2n-1}$ (*m/z* = 27, 41, 55, 69, 83, 97, typical tracers of cycloalkanes or unsaturated hydrocarbon) and $C_nH^+_{2n+1}$ (*m/z* = 29, 43, 57, 71, 85, 99, typical tracers of alkanes). As shown in Fig. 4b, the concentration of HOA was well correlated with that of NO_x during the measurement period when both concentrations were available, indicating considerable influences of traffic emissions on the HOA mass loading. Diurnal variations of HOA concentration for both pollution EPs and non-pollution period are depicted in Fig. 5. The variations for both mass concentrations of HOA and NO_x were pronounced for pollution EPs (much higher concentrations at night), which can be attributed to human activities (e.g., traffic emission during rush hours). The averaged HOA concentration for pollution EPs ranged diurnally from 2.8 to 5.2 μg m^{-3} with the maximum value (about 16% of total OA) found around midnight and the minimum value (12% of total OA) at noon (13:00). Meanwhile, the HOA concentration in pollution EPs increased rapidly from 3.1 μg m^{-3} at ~17:00 to 5.2 μg m^{-3} at around midnight and remained high afterward. Nocturnal rush hours corresponded to HOA concentration peak around 20:00 but could not account for the continuously high HOA concentration afterward. These consistent high concentrations were likably attributed to emissions of heavy-duty vehicles (HDV) which are only allowed to drive through the city after 22:00 until 6:00 the next day according to the traffic regulation enforced in Guangzhou. The pronounced impact of HDV on the concentrations of both HOA and NO_x agrees with the previous study conducted in Panyu district, Guangzhou (Qin et al., 2017). Other possible reasons for high nocturnal HOA mass loading included lower boundary layer and frequent thermal inversion layer formed at night during winter. Besides, effects of emissions from heavy duty vehicles and the rapidly rising boundary layer after 7:00 would also account for the insignificant peak of HOA during morning rush hour. In comparison, the HOA concentration showed almost no variations during non-pollution period (even during rush hours), which likely arose from its extremely low value (< 1 μg m^{-3} which was close to an estimated detection limit of 0.7 μg m^{-3} for OA with the ToF-ACSM).

3.2.2 Cooking OA (COA)

Through factorization using PMF or ME-2 engine, COA was frequently deconvolved as a common OA component in urban areas (Sun et al., 2013; Lee et al., 2015; Sun et al., 2016; Qin et al., 2017). The mass spectrum of COA deconvolved in this work was very similar to that of HOA except a higher *m/z* 55 to 57 ratio of 2.1 which is very close to the range of 2.2-2.8 reported from real cooking source measurements (Mohr et al., 2012). The concentration of COA was correlated reasonably well (R_p= 0.86) with m/z 55. As shown in Fig. 5, the diurnal profile of COA for non-pollution period showed a typical

bimodal pattern with a noon peak concentration of 1.6 μg m^{-3} (16% of OA) at 13:00 during lunch time and a night peak concentration of 4.3 μg m^{-3} (33% of OA) at 19:00 during dinner time. A similar bimodal pattern of COA diurnal profile for pollution EPs was found, with a much higher ratio of night concentration peak (12.2 μg m^{-3}) to noon concentration peak (2.5 μg m^{-3}) than that for non-pollution period (5 vs 2.7). In addition, compared to non-pollution period, the remarkably enhanced night concentration peak of COA for pollution EPs was delayed from 19:00 to 21:00. Here three reasons are attributed to the much higher peak concentration at night than at noon for COA: (1) more intensive cooking activities at night than at noon in the Chinese cooking routine; (2) more adverse diffusion conditions caused by a lower boundary layer and a frequent thermal inversion layer at night; (3) the lower temperature at night which facilitates semi-volatile compounds from cooking emissions to partition into particles. Furthermore, pollution EPs with remarkably enhanced and delayed night COA concentration peaks corresponded to several important holidays such as Winter solstice festival (EP3), Christmas (EP4), and New Year's Day (EP5), implying that festival-induced emissions have significant impacts on local air pollution.

3.2.3 Oxygenated OA (OOA)

OOA, the generally accepted surrogate of SOA (Jimenez et al., 2009), characterized by a high peak at *m/z* 44 (CO_2^+) in the mass spectra, was almost exclusively contributed from electron ionization of ketones, aldehydes, esters and carboxylic acids. Furthermore, OOA could be further deconvolved into two subcomponents, SVOOA and LVOOA, based on different degrees of oxidation. SVOOA was distinguished from LVOOA by a higher ratio of f_{43} to f_{44} (0.7 for SVOOA and 0.18 for LVOOA).

A high similarity between SVOOA and secondary inorganic aerosols (nitrate and sulfate) was observed for the entire study (Fig. 4). It was found that Pearson correlation coefficient (R_p) between SVOOA and nitrate (0.76) was higher than that between SVOOA and sulfate (0.61), consistent with the trend reported by previous studies which attributed it to analogous semi-volatility and gas-particle partitioning between SVOOA and nitrate (Aiken et al., 2009; DeCarlo et al., 2010; Zhang et al., 2011). Interestingly, we found that the correlation between SVOOA and nitrate was much better for pollution EPs than for non-pollution period (R_p = 0.64 vs 0.34, Fig. 6d), which cannot be simply attributed to similar volatility and photochemistry. Meanwhile, concentration of neither nitrate nor SVOOA was obviously dependent on temperature in this study. Furthermore, we found that the air during all pollution EPs was much more stagnant, supported by much lower wind speed than that during non-pollution period (Fig. 6f), implying that most nitrate and SVOOA were locally formed during pollution EPs, while they likably

originated from regional transport during non-pollution period. Since traffic emissions contribute largely to NO_x and VOCs, a higher correlation between SVOOA and nitrate during pollution EPs than during non-pollution period likely stemmed from shared sources of precursors for the two aerosol components and implies that traffic emissions could significantly influence SVOOA and nitrate mass loading under stagnant meteorological conditions. These are further confirmed by the fact that in general much higher correlations between SVOOA (or nitrate) and the traffic trace species (CO, HOA and NO_x) were found during pollution EPs than during non-pollution period (Table 2). As mentioned above, non-pollution period was always associated with high wind speeds which would induce strong air advection and make local emissions hardly accumulate, leading to a large fraction of PM_1 contributed from regional transport. These regionally transported nitrate and SVOOA were usually less correlated with traffic tracers because of more complicated sources for SVOOA and nitrate outside urban Guangzhou, and different influences of secondary processes on these species through transport. A previous laboratory study suggested that photooxidation of traffic related emissions leads to substantial amounts of SOA (Weitkamp et al., 2007) which in our case are likely locally formed SVOOA. The diurnal profiles of SVOOA for non-pollution period and pollution EPs showed explicit distinctions. During pollution EPs, the concentration of SVOOA showed a pronounced diurnal variation which in general formed a flat trough around noon and reached the maximum value around midnight. In comparison, diurnal profile of SVOOA concentration for non-pollution period, however, was much flatter, with two weak peaks likably reflecting photochemical oxidation and local anthropogenic emissions respectively. These two different diurnal patterns of SVOOA concentration suggest accumulation of local anthropogenic emissions under stagnant air condition during pollution EPs could largely influence mass loading of SVOOA.

In contrast to SVOOA, the concentration of LVOOA showed a better correlation with that of sulfate (R_p = 0.85) than with nitrate (R_p = 0.77), which is likably attributed to similarly low volatility of both LVOOA and sulfate. Diurnal profile of LVOOA concentration showed roughly no variation with slightly elevated values during afternoon for both pollution EPs and non-pollution period, demonstrating that LVOOA was not significantly influenced by local emissions but by aging processes in particular photochemistry. Prolonged aging of SOA leads to the high oxidation degree of LVOOA which should be considered as a kind of regional pollutant or background aerosol (Li et al., 2013; Li et al., 2015; Sun et al., 2016; Qin et al., 2017), while freshly formed SOA from local emissions remains a lower oxidation state which more readily becomes the SVOOA component as is discussed in this section.

3. 3 Diurnal profiles

In the previous section, we have discussed diurnal variations of the four deconvolved OA components and here important variations of other species and meteorological conditions are detailed to better understand evolution of NR-PM_1 species and pollution characteristics in Guangzhou (Fig. 5). Similar to SVOOA, remarkably different diurnal profiles of nitrate concentration between pollution EPs and non-pollution period were observed. For non-pollution period, diurnal nitrate concentration varied little with slight maximum occurring at 13:00, implying the influence of photochemistry on nitrate formation. For pollution EPs, however, nitrate concentration showed a much more pronounced diurnal variation, that is, nitrate mass loading kept low around noon to afternoon and then increased steadily during the night until it reached the maximum at 9:00 in the next day. Note that nitrate concentration increased from dusk to early morning with similarly increasing RH and oppositely decreasing temperature. Meanwhile, the nocturnal NO_x concentration was 67% more than that during daytime (Table 3). Thus, higher RH, more abundant NO_x, and lower temperature during nighttime facilitate aqueous reactions and gas-to-particle partitioning between gas phase nitric acid and ammonium nitrate, which played important roles in nocturnal nitrate formation during pollution EPs, consistent with the previous study (Xue et al., 2014). In addition, the morning nitrate peak at 9:00 can be attributed to a synergy of high NO_x emissions during rush hours and most favorable conditions for ammonium nitrate formation during 8:00~9:00 am (i.e., low temperature, high RH). Our results strongly demonstrate importance of local anthropogenic emissions and aqueous reactions in nitrate accumulation under stagnant air condition during pollution EPs.

The diurnal concentration of sulfate showed very slight variation for both pollution EPs and non-pollution period, with the averaged daytime concentration being almost the same as that at night. This indicates that the sulfate concentration was always less influenced by local anthropogenic emissions due to the fact that power plants, the most important source of sulfur dioxide (SO_2), are rarely located in urban Guangzhou (Bian et al., 2019). Thus, the sulfate concentration in this study should be largely determined by regional transport during both pollution EPs and non-pollution period, which can also be supported by similar diurnal profiles of SO_2 (Fig. S2). Interestingly, the diurnal variations of O_3 and RO_2* ($\Sigma RO_2^{\bullet}$ +HO_2) for pollution EPs and non-pollution period showed a distinct daytime-to-nighttime pattern. The daytime concentrations of the two species during pollution EPs were higher than those during non-pollution period while the nighttime concentrations during pollution EPs were lower than those during

non-pollution period. This variation pattern differed from all other NR-PM_1 species which always showed higher concentrations during pollution EPs than those during the non-pollution period within a day. The lower nighttime concentrations of O_3 and RO_2* during pollution EPs were probably attributed to the enhanced consumption of O_3 and RO_2* due to elevated NO_x and VOCs concentrations at night. Our results suggest that O_3 and RO_2* were important nocturnal oxidants during pollution events.

3.4 Chemical evolution

Figure 7 depicts the dependence of mass concentrations and fractions of NR-PM_1 components on NR-PM_1 mass loading. The mass concentrations of all the NR-PM_1 components increased almost linearly with increase of the NR-PM_1 mass concentration. However, various trends were detected for the fractions of different NR-PM_1 components. For example, organics were the dominant component of NR-PM_1 with an increasing fraction from 44% to 57% as the NR-PM_1 mass concentration increased up to > 90 μg m^{-3} (Fig. 7b). The fractions of HOA and COA, considered as primary OA, varied in a similar way, that is, both fractions increased up to 11% for HOA and 15% for COA as NR-PM_1 mass concentration increased from ~35 μg m^{-3} to > 90 μg m^{-3}. The variations of the fractions of SOA species and SIA species with NR-PM_1 mass loading were much more complicated. To have an overall insight on chemical evolution of the aerosols, we compare dependences of the ratio of secondary particulate matters (SPM = SVOOA + LVOOA + sulfate + nitrate + ammonium) to primary particulate matters (PPM = HOA + COA + chloride) and the concentration of RO_2* and O_3 on NR-PM_1 mass concentration (Fig. 8). For the whole period, all the three quantities followed consistent and clear trends that they all initially increased with increase of NR-PM_1 mass concentration until all reached peak values at a NR-PM_1 concentration of ~35 μg m^{-3}, and subsequently decreased with increase of the NR-PM_1 mass loading. Interestingly, the trends for the three quantities during non-pollution period were consistent with the initial monotonic increase when NR-PM_1 mass concentration was below 35 μg m^{-3} (Fig. 8c), a concentration value that was rarely exceeded during this period, while only if pollution EPs were considered, the trends became monotonic decrease with NR-PM_1 mass concentration up to ~95 μg m^{-3} (Fig. 8b). During non-pollution period when strong advection induced by high wind speed facilitated dilution and diffusion of local primary pollutants, the SPM/PPM ratio increased with increasing concentrations of photochemical products (i.e., O_3 and RO_2*) and NR-PM_1, strongly suggesting that secondary processes especially photochemistry were the main drivers for NR-PM_1 accumulation during this period. Under this circumstance, interestingly, the overall increase of SPM fraction (or SPM/PPM) with increase of NR-PM_1 mass concentration was consistent with increasing

mass fractions of LVOOA and nitrate, yet opposite from decrease of SVOOA fraction (Fig. 7b and Fig. S3). The decrease of SVOOA fraction with increase of NR-PM_1 mass concentration corresponded to increase of LVOOA fraction, implying progressive conversion of SVOOA to LVOOA during the aerosol aging processes. During pollution EPs when stagnant air condition supported by low wind speeds facilitated accumulation of local primary pollutants, the SPM/PPM ratio together with concentration of O_3 and RO_2*, was observed to drop with increasing mass concentration of NR-PM_1, indicating that production of NR-PM_1 was more driven by primary emissions rather than secondary processes under this circumstance. Thus, our results indicate totally different intrinsic mechanisms responsible for NR-PM_1 accumulation between pollution EPs and non-pollution period.

3.5 Oxidation degree and peroxy radical tracer

3.5.1 Oxidation degree

Oxidation degree represents the extent to which aerosols (OA and SOA) are oxidized. Figure 9 depicts locations of both OA and SOA from this study in f_{44}/f_{43} space. The triangle area (enclosed by two black dash lines and the f_{43} axis) for ambient OOA (SOA) was defined by Ng et al. (2010) and results from several laboratory studies with or without aerosol seeds (Bahreini et al., 2005; Liggio et al., 2005; Liggio et al., 2006; Weitkamp et al., 2007) are also shown for comparison. The f_{44} and f_{43} for each SOA point were calculated through an algorithm reported in Canonaco et al. (2015). Most of OA samples in this study were located inside the triangle area, indicating that OA is mainly composed of SOA which was consistent with the finding from ME-2 analyses, that is, SOA contributes about 70% to total OA. Interestingly, SOA points in f_{44}/f_{43} space showed a strong linear trend that f_{44} increased with decreasing f_{43}, leading to a large span of f_{44} and f_{43} in SOA which then requires more than one SOA factor to explain such a large variation. This result quite differs from some other studies in northern China where usually only one SOA factor was deconvolved (Sun et al., 2012; Sun et al., 2013; Huang et al., 2019). The substantial differences on SOA factorization between Guangzhou and other cities in northern China can be likably attributed to much higher oxidative atmosphere in Guangzhou. In fact, a previous study has shown that the second highest OH concentration was observed in the PRD region around the world (Rohrer et al., 2014). In addition, the majority of SOA points were well distributed around the connection line of SVOOA and LVOOA (unimodal residual), indicating that SOA points were well captured by ME-2 engine in our study (Canonaco et al., 2015). Thus, the deconvolution of SVOOA and LVOOA in this study well represented the observed large variation of f_{44} and f_{43} for SOA in Guangzhou.

Most SOA points were located closely to the right side of the triangle, which was quite different from the OA points. Interestingly, the shape of SOA points in f_{44}/f_{43} space formed roughly a tilted triangle which means both average values and variation ranges of f_{43} remarkably decreased with increasing f_{44}.The triangle suggests that aging processes result in substantially similar OOA components regardless of their original precursors (Ng et al., 2010). The f_{44} values of SOA in this study were much higher than those of SOA generated in laboratory, which should be attributed to limited residence time in chamber or much higher mass loadings of laboratory-produced aerosols which facilitate gas-to-particle partitioning of semi-volatile organic compounds (SVOCs) and heterogeneous reactions (Liggio et al., 2006; Shilling et al., 2009; Ng et al., 2010; Ziemann et al., 2012). Figure 9 also shows that the f_{44} and f_{43} values of SOA generated from laboratory m-xylene oxidation and from aged diesel exhaust were closest to those of the SOA and modeled SVOOA from this study, implying that traffic emissions (in particular from diesel combustion) and aromatic compounds are likably precursors for SOA in Guangzhou. This result also agrees with numerous studies conducted in urban areas (Lee et al., 2015; Sun et al., 2016; Qin et al., 2017).

3.5.2 Peroxy radical tracer

Here we introduce peroxy radicals ($RO_2^* = \Sigma RO2^{\bullet} + HO_2$) as a reference tracer to discuss both daytime and nocturnal SOA formation (Figs. 10, S13 and S14). Figure 10 shows the variations of SOA concentration with RO_2^* concentration under different scenarios (non-pollution daytime period, pollution daytime EPs, non-pollution nighttime period, and pollution nighttime EPs). The SOA concentration increased with the RO_2^* concentration for both non-pollution daytime and nighttime periods with both moderate correlation coefficients ($R^2 = 0.41$), indicating that formation and growth of SOA could be attributed to photochemical oxidation during non-pollution daytime while nocturnal gas phase oxidation of VOCs led to SOA accumulation during non-pollution nighttime. Thus, it can be concluded that gas phase oxidation was responsible for SOA formation during non-pollution periods. Meanwhile, SOA oxidation degree, represented by f_{44} in SOA, increased in general with increasing SOA concentration during non-pollution periods, implying that a higher oxidative condition simultaneously led to generation of SOA and conversion of SVOOA to LVOOA (Fig. 7b). In contrast to the well correlations between SOA and RO_2^* concentrations during non-pollution period, such correlations were not seen during the pollution EPs for both daytime and nighttime scenarios (Fig. 10); instead, an opposite trend that f_{44} in SOA decreased with increase of SOA concentration was observed (Figs. 10c-d). These results imply that other mechanisms besides gas phase oxidation were responsible for the formation of SOA that is less

oxidized during pollution EPs. In addition, correlations between SVOOA/LVOOA and RO_2 were explored by plotting dependence of SVOOA/LVOOA concentrations on RO_2* concentration during non-pollution periods and pollution periods (Fig. S15). The results show that better correlations and larger slope for LVOOA vs RO_2* than for SVOOA vs RO_2* during non-pollution periods. In contrast, neither LVOOA nor SVOOA were correlated to RO_2* during pollution EPs.

We further investigate the distinctly different mechanisms for SOA formation between non-pollution and pollution EPs by plotting estimated H/C ratio as a function of O/C ratio in the Van Krevelen diagram (Fig.11). The O/C and H/C ratios were estimated from f_{43} and f_{44}, which were proposed by Aiken et al. (2008) and Ng et al. (2011) respectively. Similar diagrams based on ACSM unit mass resolution data were reported in previous studies (Brito et al., 2014; Reece et al., 2017; Saha et al., 2018). The area enclosed by the two red boundary lines was defined for ambient OOA components in Ng et al. (2011). Our data points were slightly outside of this area and were further shifted to the upper right corner of the plot. Similar differences from other ambient or laboratory measurements were also reported in previous studies (Budisulistiorini et al., 2018; Saha et al., 2018), which were attributed to different precursors emitted or aging processes. As shown in Fig. 11 a, the H/C ratio is linearly correlated with the O/C ratio and is confined into a narrow belt during non-pollution periods, indicating the precursors, mechanism, and chemical components of SOA are likely similar (Ng et al. 2010, 2011). Although the H/C ratio follows similar trends with O/C ratio during pollution periods, the shape is much broader with respect to the H/C ratio especially in the middle portion of the O/C ratio, strongly indicating that more diverse components in SOA are present surrounding the measurement site in Guangzhou. A wider range of H/C ratio during pollution EPs imply more diverse precursor sources and (or) different mechanisms which lead to formation of SOA components with highly variable H/C ratios (Ng et al. 2010, 2011). Although we cannot totally rule out the possibility of dramatic changes in the emission sources, it is unlikely for those changes to occur within a month of the measurement period. Hence it is more likely that the formation mechanisms during non-pollution and pollution periods are distinctly different. Here we propose two most possible different mechanisms of SOA formation during pollution EPs: (1) gas-phase oxidation under enhanced NOx concentration which leads to dramatically different SOA components from these under lower NOx concentration (Ziemann et al., 2012); (2) other mechanisms such as additional heterogeneous/multiphase reactions from dramatic increases of PM mass loading and hence more available particle surfaces or volumes for reactions. We replot estimated H/C ratio vs estimated O/C ratio in the Van Krevelen diagram with an overlapped NOx concentration range during the two periods to remove the enhanced NOx effects

(Fig. 11b). Similar patterns were obtained, highlighting the possibility of significant heterogeneous/multiphase reactions in the pollution EPs.

To further explore mechanisms that can explain SOA formation during pollution EPs, a plot of SOA concentration as a function of RO_2* concentration for segmental NR-PM_1 mass concentrations is shown in Fig. 12. A total of six segments of concentrations were set, with concentrations smaller than 30 and larger than 70 up to about 110 μg m^{-3} being the lowest and highest segments respectively, and with an interval of 10 μg m^{-3} between 30 and 70 μg m^{-3} (Fig. 12a). For comparison, dependence of SOA concentration on RO_2* concentration during non-pollution period is also included in Fig. 12. As is discussed above, the overall correlation between SOA and RO_2* concentrations was poor without a clear trend between the two quantities (Figs. 10c-d). However, they were reasonably correlated and showed reasonable trend that SOA concentration increased with increasing RO_2* concentration in all segments except for the lowest one, suggesting that gas phase oxidation still played important roles in SOA formation. Poor correlation between SOA and RO_2* concentrations in the lowest segment might be due in part to substantial scattering of the data. Under a same RO_2* concentration, interestingly, more SOA was formed with increasing NR-PM_1 concentration. Here, for simplicity, we define that the slope and intercept of linear regression between SOA and RO_2* concentrations in each segment when NR-PM_1 ranged from 30-40 to > 70 μg m^{-3} represented respectively SOA formed due to RO_2* and SOA contributed from other pathways. It is found that substantial intercept values were obtained from the linear regressions during pollution EPs, while they approached almost zero during non-pollution period. Meanwhile, these intercepts increased from 7.5 to 16.2 μg m^{-3} when NR-PM_1 mass loading increased from 30-40 to >70 μg m^{-3}. Thus, although the exact pathways implied by these significant intercepts could not be identified from this study due to obviously insufficient measurement data. They are most likably attributed to heterogeneous or/and multiphase reactions on particle surfaces or inside particles.

4 Conclusions

A field campaign employing ToF-ACSM for measurements of NR-PM_1 chemical composition was conducted from 20 November 2017 to 5 January 2018 at an urban site in Guangzhou, China. The reliability of the ToF-ACSM was confirmed by the well correlation between mass concentrations of NR-PM_1 measured by this instrument and those of $PM_{2.5}$ and $PM_{1.1}$ measured from other filter-based methods. Chemical composition of NR-PM_1 at this site was dominant by organics, followed by sulfate, nitrate, and ammonium, and only an insignificant fraction (1-2%) of chlorine was measured. We classified five

pollution episodes (EPs) according to mass concentration of NR-PM_1. Mass fraction of organics was higher during pollution EPs than during non-pollution period, corresponding to a decrease and an increase of sulfate fraction respectively for the two periods. Our results together with other previous studies show increasing SOA/OA mass concentration ratio across China from the North to the South.

Positive Matrix Factorization (PMF) with multilinear engine (ME-2) algorithm was employed to deconvolve OA into four factors including hydrocarbon-like OA (HOA, 12%), cooking OA (COA, 18%), semi-volatile oxygenated OA (SVOOA, 30%), and low-volatility oxygenated OA (LVOOA, 40%) according to the mass spectra acquired by the ToF-ACSM during the study. One primary OA, HOA, was found to originate from heavy-duty vehicles (HDV) emissions after midnight during which those vehicles are allowed to enter urban Guangzhou according to the traffic regulation. Another primary OA, COA, was found to be significantly contributed by nocturnal cooking activities during pollution EPs. Those activities were extended during festival celebrations, leading to an obviously delayed peak concentration for COA. Both cooking and traffic emissions contributed significantly to nocturnal PM accumulation because they emitted not only primary aerosols (COA and HOA) but also substantial amounts of precursors for SOA or nitrate. Concentrations of SVOOA and nitrate were correlated well with traffic tracers (i.e., CO, HOA and NO_x) during the pollution EPs, suggesting that SVOOA and nitrate were significantly contributed from local traffic emissions under stagnant meteorological conditions and that they originated from shared precursor sources.

Concentrations of HOA, COA, nitrate, and SVOOA showed much more pronounced diurnal variations during pollution EPs since all four species were largely influenced by local anthropogenic emission under stagnant conditions. For comparison, both sulfate and LVOOA showed little diurnal variations during both non-pollution period and pollution EPs as they were contributed form regional pollutants and were barely influenced by local anthropogenic emissions. In addition, nocturnal concentrations of both O_3 and RO_2* during pollution EPs were lower than those during non-pollution period, implying that both O_3 and RO_2* could serve as important nocturnal oxidants during pollution EPs. Chemical evolution of NR-PM_1 suggests that different intrinsic mechanisms were responsible for NR-PM_1 accumulation between pollution EPs and non-pollution period. During non-pollution period, the SPM/PPM ratio increased with increasing concentrations of photochemical products (i.e., O_3 and RO_2*) and NR-PM_1 concentration, strongly suggesting that secondary processes especially photochemistry were the main mechanism for NR-PM_1 accumulation. During pollution EPs, the SPM/PPM ratio, together with concentration of O_3 and RO_2*, was observed to drop with increasing NR-PM_1 mass concentration,

indicating that production of NR-PM_1 was more driven by primary emissions rather than secondary processes. The f_{44}/f_{43} space, proposed by Ng. et al. (2010), was employed to investigate oxidation degree of OA and SOA and the results suggested that two OOA factors were needed to cover a wide range of f_{44} and f_{43} in SOA in Guangzhou. Furthermore, we conclude that traffic-emitted VOCs and aromatic compounds were most likably SOA precursors in Guangzhou by comparing SOA from our measurements with those from other laboratory studies.

Peroxy radicals RO_2* were measured in this study and were used as a tracer for gas phase oxidation to explore SOA formation during both daytime and nighttime, advantaging over O_x which can only be used as an indicator of daytime photochemistry in addition to significant interference by directly emitted NO_2 especially in urban area. During non-pollution periods, SOA concentration increased with RO_2* concentration for both daytime and nighttime and we conclude that formation and growth of SOA could be attributed to photochemical oxidation during daytime while nocturnal gas phase oxidation of VOCs led to SOA accumulation during nighttime. We also found that SOA oxidation degree increased in general with increasing SOA concentrations, implying that a higher oxidation condition simultaneously led to generation of SOA and conversion of SVOOA to LVOOA. During pollution EPs, however, an overall opposite trend was observed, that is, f_{44} in SOA decreased with increase of SOA concentration. In addition, the overall correlations between SOA and RO_2* concentrations were poor for both daytime and nighttime. The reasons for the above poor correlations are attributed to other mechanisms besides gas phase oxidation which are responsible for SOA formation during pollution EPs. Possible mechanisms were explored by dividing PM_1 mass loadings into six segments and linear regression in each segment was made between SOA and RO_2* concentrations. The results showed that individual correlations were reasonably good except for the lowest segment due to data scattering, indicating that gas phase oxidation still play important roles. Values of slopes from linear regressions of those reasonable correlations were then found to increase with increasing NR-PM_1 mass loading, suggesting that more gas phase oxidation products of VOCs were partitioned into particles under high PM mass loading. Furthermore, substantial intercept values were found from the above linear regressions in contrast to almost zero intercept for non-pollution period, strongly suggesting that other mechanisms besides gas phase oxidation contributed significantly to SOA formation. We speculate that those other mechanisms are most likably heterogeneous or/and multiphase reactions.

Acknowledgement

This work was funded by the National Key Research and Development Program of China (2016YFC0202205, 2017YFC0210104), the National Natural Science Foundation of China (41875152, 91644225, 21577177), Science and Technology Program of Guangdong Province (Science and Technology Innovation Platform Category, No. 2019B121201002), and the National Natural Science Foundation as a key project (41530641, 41630422). J.Z. acknowledges funding support from the "111 plan" Project of China (Grant B17049), Scientific and Technological Innovation Team Project of Guangzhou Joint Research Center of Atmospheric Sciences, China Meteorological Administration (Grant No. 201704). The authors thank Prof. Xinhui Bi and Jingjing Feng for their support in the field study.

Author contributions. SZ and XW designed this study. SZ, JG, MC, WZ, CY, XX and WS conducted the experiments. JG, SZ and JZ wrote the paper. YS, WH, YH, ZZ, PC, QF, JH, SF, XW were involved in the data analysis and scientific discussions to the paper.

Data availability. All the data presented are available from the corresponding author upon reasonable request.

Competing interests. The authors declare no competing financial interests.

Table 1. Summary of published NR-PM_1 measurements in China.

Location	Time	Area	NR-PM_1 (μg m^{-3})	OA (%)	SOA/OA (%)	Ref.
Guangzhou	Winter, 2017	Pearl River Delta region	35.3	49	70	This study
Panyu	Winter, 2014	Pearl River Delta region	55.4	50.5	61	Qin et al., 2017
Shenzhen	Winter, 2009	Pearl River Delta region	44.5	46.2	46.6	He et al., 2011
Kaiping	Winter, 2008	Pearl River Delta region	33.1	36.3	75.4	Huang et al. 2011
Nanjing	Winter, 2015	Yangtze River Delta region	32.5	36	66	Zhang et al., 2017
Nanjing	Summer, 2013	Yangtze River Delta region	36.8	42	72	Zhang et al., 2015
Shanghai	Summer, 2010	Yangtze River Delta region	27	31	78	Huang et al., 2012
Beijing[1]	Winter	Beijing-Tianjin-Hebei region	70	52	43	**[1]**
Beijing	Summer, 2011	Beijing-Tianjin-Hebei region	80	32	65	Hu et al., 2016a
Shijiazhuang	Winter, 2014	Beijing-Tianjin-Hebei region	178	50	22	Huang et al. 2019
Handan	Winter, 2015	Beijing-Tianjin-Hebei region	178	47	17	Li et al., 2017
Lanzhou	Winter, 2014	Northwest of China	57.3	55	37	Xu et al., 2016
Lanzhou	Summer, 2012	Northwest of China	24	53	59	Xu et al., 2014
Hong Kong	Winter	South of China	20.7	45.5	69	Sun et al., 2016
Hong Kong	Summer, 2011	South of China	15.6	26	82	Li et al., 2015
Ziyang	Winter, 2012	Southwest of China	60	40	71.2	Hu et al., 2016

[1]: the three quantities for winter Beijing are the averages of 6 researches (Sun et al., 2013; Sun et al., 2014; Jiang et al., 2015; Wang et al., 2015; Hu et al., 2016a; Sun et al., 2016).

Table 2. Pearson correlation for traffic tracers (CO, HOA and NO_x) with SVOOA (nitrate and sulfate) during different periods.

Species	Period	CO	HOA	NO_x
SVOOA	Pollution EPs	0.64	0.70	0.81
	Non-pollution	0.37	0.55[a]	0.63
	Entire study	0.72	0.82	0.82
NO_3^-	Pollution EPs	0.53	0.61	0.52
	Non-pollution	0.09	0.45[a]	0.22
	Entire study	0.57	0.75	0.59
SO_4^{2-}	Pollution Eps	0.35	0.39	0.00
	Non-pollution	0.28	0.45[a]	0.12
	Entire study	0.47	0.59	0.28

[a] Pearson correlations involving HOA for non-pollution period may have nonnegligible uncertainty since HOA concentration in non-pollution period is near method detection limit (MDL) of ToF-ACSM for OA.

Table 3. Overview of meteorological conditions, trace gases, peroxy radical, and NR-PM_1 components during day and night.

	Non-pollution		Pollution		Entire study	
	Day	Night	Day	Night	Day	Night
Gas&radical(ppb)						
O_3	20.3	10.4	27.5	7.2	22.6	9.7
NO_x	28.6	34.2	43.1	72.7	31.4	41.5
RO_2*	0.15	0.12	0.17	0.11	0.16	0.11
Meteorological condition						
T(°C)	16.6	15.4	19.1	17.6	17.5	16.2
RH (%)	48.3	52.9	41.0	45.6	45.6	50.1
WS(m s^{-1})	3.1	3.2	1.6	1.4	2.5	2.5
NR-PM1(μg m^{-3})						
Org	9.0	10.0	23.8	32.0	15.0	19.0
SO_4^{2-}	4.6	4.9	9.9	10.2	6.8	7.1
NO_3^-	3.5	3.2	9.6	9.7	6.0	5.9
NH_4^+	3.1	3.1	6.5	6.6	4.5	4.5
Cl^-	0.2	0.3	0.6	0.9	0.4	0.5
HOA	0.7	0.8	3.4	4.7	1.8	2.4
COA	1.3	2.0	2.0	7.2	1.6	4.1
SVOOA	2.5	3.0	7.3	9.6	4.4	5.7
LVOOA	4.5	4.3	10.7	10.0	7.1	6.6

Figure captions

Figure 1. Temporal variation of (a) relative humidity, temperature, and pressure; (b) wind speed and direction (color-contoured); (c) total NR-PM_1 & $PM_{2.5}$; and (d) speciated concentrations of NR-PM_1. EP1~EP5 are classified as pollution episodes (EP1: 6~8 December, EP2: 9~13 December, EP3: 21~23 December, EP4: 25~30 December, EP5: 31 December ~ 5 January), see text for details.

Figure 2. The average fraction of each chemical composition of (a) NR-PM_1 (OA, nitrate, sulfate, ammonium, and chloride) and (b) organic aerosols (LV-OOA, SV-OOA, HOA, and COA).

Figure 3. Comparison of submicron aerosols among several megacities in China during winter including Guangzhou (this study) and five other cities. Red bars represent the fraction of OA to NR-PM_1 and blue bars represent the fraction of SOA to OA. Green diamonds represent average concentration of NR-PM_1 in each city.

Figure 4. The mass spectra and time series of the four OA components (HOA, COA, SVOOA, and LVOOA).

Figure 5. Diurnal profiles of NR-PM_1 species, trace gases, radicals, and meteorological conditions. Dash lines and solid lines represent the averaged values during non-pollution period and pollution EPs.

Figure 6. Correlations between OOA and SIA, along with correlation between nitrate and sulfate, and the wind speed during pollution EPs and non-pollution period. (a) LVOOA vs. NO_3^-; (b) LVOOA vs. SO_4^{2-}; (c) NO_3^- vs. SO_4^{2-}; (d) SVOOA vs. NO_3^-; (e) SVOOA vs. SO_4^{2-}. Blue circles represent pollution EPs while gray crosses represent non-pollution period. (f) Box plot of wind speed in non-pollution period and pollution EPs. Whiskers are 10th and 90th percentile; the top, median and bottom lines of box represent 75th, 50th and 25th percentile respectively. Red dots are the averaged wind speed for each scenario.

Figure 7. Dependences of (a) mass concentration and (b) mass fraction of NR-PM_1 components on NR-PM_1 mass loading. The data are plotted in an interval of 10 μg m^{-3} of NR-PM_1. The error bars are standard deviations of each NR-PM_1 species.

Figure 8. Dependences of SPM/PPM ratio, concentrations of the atmospheric oxidants (O_3 and RO_2*) on NR-PM_1 mass loading for (a) entire study, (b) non-pollution period and (c) pollution EPs. The binned data are also presented as solid circles with an interval of 10 μg m^{-3} NR-PM_1. The error bars are standard deviations.

Figure 9. Plot of f_{44} vs f_{43} for this study, along with several laboratory studies ([a] Bahreini et al., 2005; [b]Liggio et al., 2005; [c]Weitkamp et al., 2007). SOA are color-coded by OA mass concentration and the size of a circle is proportional to corresponding NR-PM_1 mass concentration. The triangle area (enclosed by two black dash lines and the f_{43} axis) for ambient OOA (SOA) was defined by Ng et al. (2010).

Figure 10. SOA concentration as a function of RO_2* concentration during different scenarios (non-pollution daytime period, pollution daytime EPs, non-pollution nighttime period, and pollution nighttime EPs). SOA concentrations are color-coded by f_{44} in SOA. All the regressions are orthogonally linear.

Figure 11. Plot of estimated H/C ratio as a function of estimated O/C ratio in the Van Krevelen diagram: (a) Non-pollution vs. pollution EPs; (b) Non-pollution vs. pollution EPs with an overlaped NO_x concentration range during the two periods. The area enclosed by the two red boundary lines was defined for ambient OOA components in Ng et al. (2011).

Figure 12. (a) Scatter plots of SOA and RO_2* during pollution EPs at different NR-PM_1 mass concentration segments, and (b) Correlation coefficients, slopes, and intercepts of linear regressions between SOA and RO_2* for NR-PM_1 mass concentration segments ranging from 30-40 to > 70 μg m^{-3}. The regressions are orthogonally linear, and all correlations of the concentration segments were statistically significant (p-value < 0.01, see detailed statistical information in Table S3).

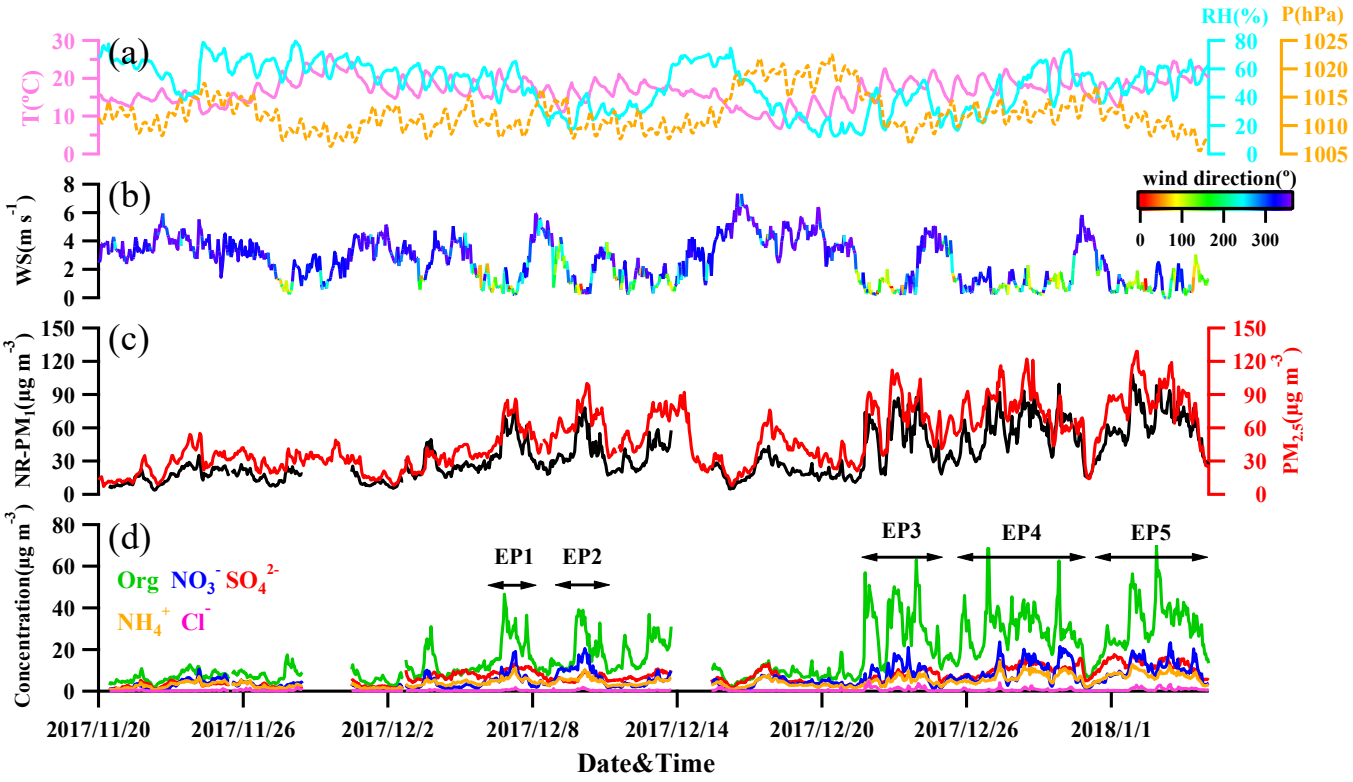
(a)
T(°C)
RH(%)
P(hPa)
(b)
WS(m s-1)
wind direction(°)
0
100
200
300
(c)
NR-PM1(μg m-3)
PM2.5(μg m-3)
(d)
Concentration(μg m-3)
Org
NO3-
SO4 2-
NH4+
Cl-
EP1
EP2
EP3
EP4
EP5
2017/11/20
2017/11/26
2017/12/2
2017/12/8
2017/12/14
2017/12/20
2017/12/26
2018/1/1
Date&Time

Fig. 1.

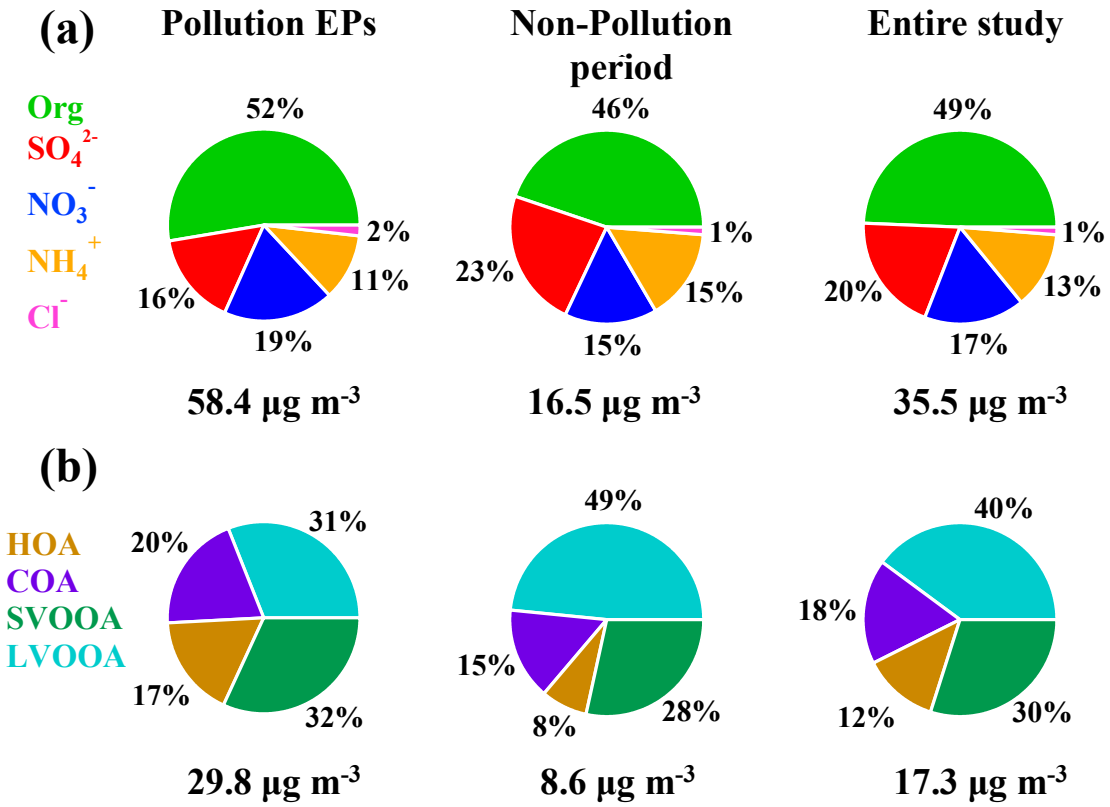
(a)
Pollution EPs
Non-Pollution period
Entire study
Org
SO4 2-
NO3 -
NH4 +
Cl-
52%
2%
11%
19%
16%
46%
1%
15%
15%
23%
49%
1%
13%
17%
20%
58.4 µg m-3
16.5 µg m-3
35.5 µg m-3
(b)
HOA
COA
SVOOA
LVOOA
20%
31%
17%
32%
49%
15%
8%
28%
40%
18%
12%
30%
29.8 µg m-3
8.6 µg m-3
17.3 µg m-3

Fig. 2.

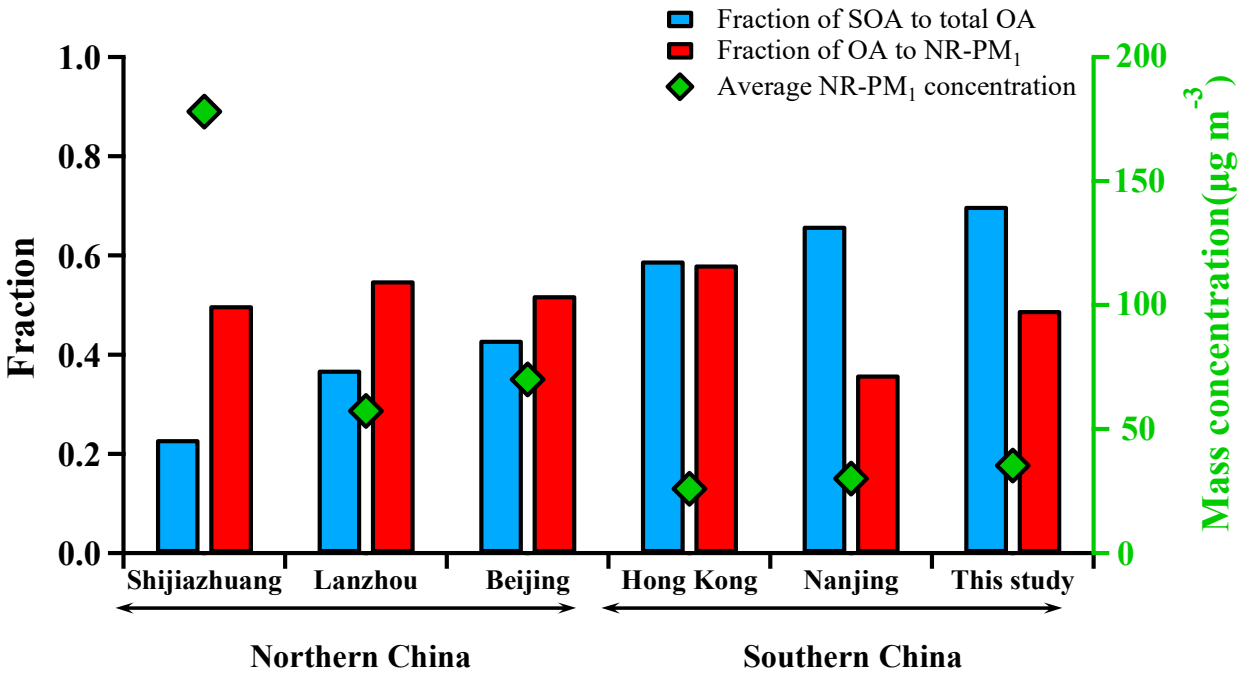
Fraction of SOA to total OA
Fraction of OA to NR-PM1
Average NR-PM1 concentration
Fraction
Mass concentration(μg m-3)
1.0
0.8
0.6
0.4
0.2
0.0
200
150
100
50
0
Shijiazhuang
Lanzhou
Beijing
Hong Kong
Nanjing
This study
Northern China
Southern China

Fig. 3.

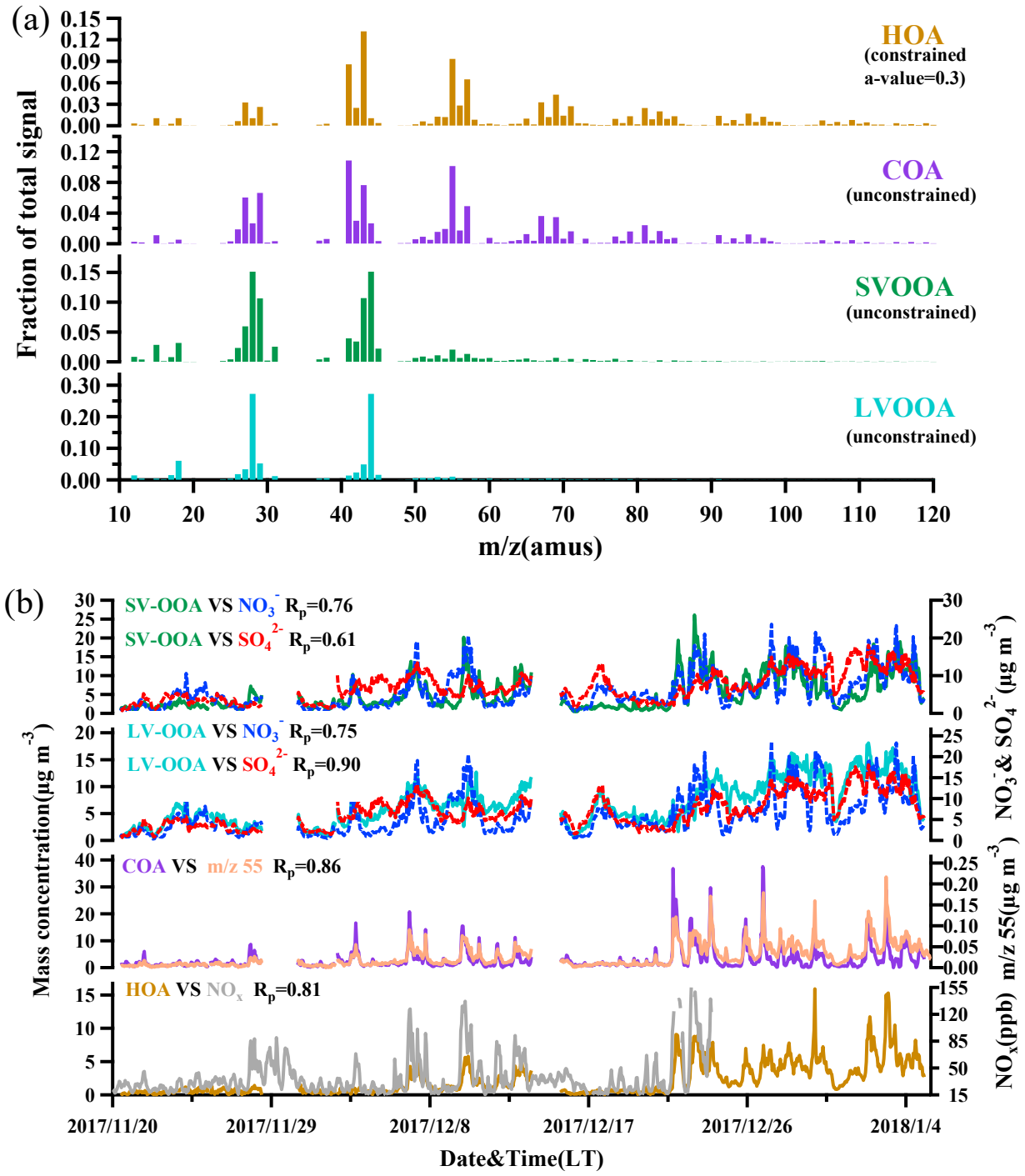
(a)
Fraction of total signal
HOA
(constrained
a-value=0.3)
COA
(unconstrained)
SVOOA
(unconstrained)
LVOOA
(unconstrained)
m/z(amus)
(b)
SV-OOA VS NO3- Rp=0.76
SV-OOA VS SO4 2- Rp=0.61
LV-OOA VS NO3- Rp=0.75
LV-OOA VS SO4 2- Rp=0.90
COA VS m/z 55 Rp=0.86
HOA VS NOx Rp=0.81
Mass concentration(μg m-3)
NO3- & SO4 2- (μg m-3)
m/z 55(μg m-3)
NOx(ppb)
2017/11/20
2017/11/29
2017/12/8
2017/12/17
2017/12/26
2018/1/4
Date&Time(LT)

Fig. 4.

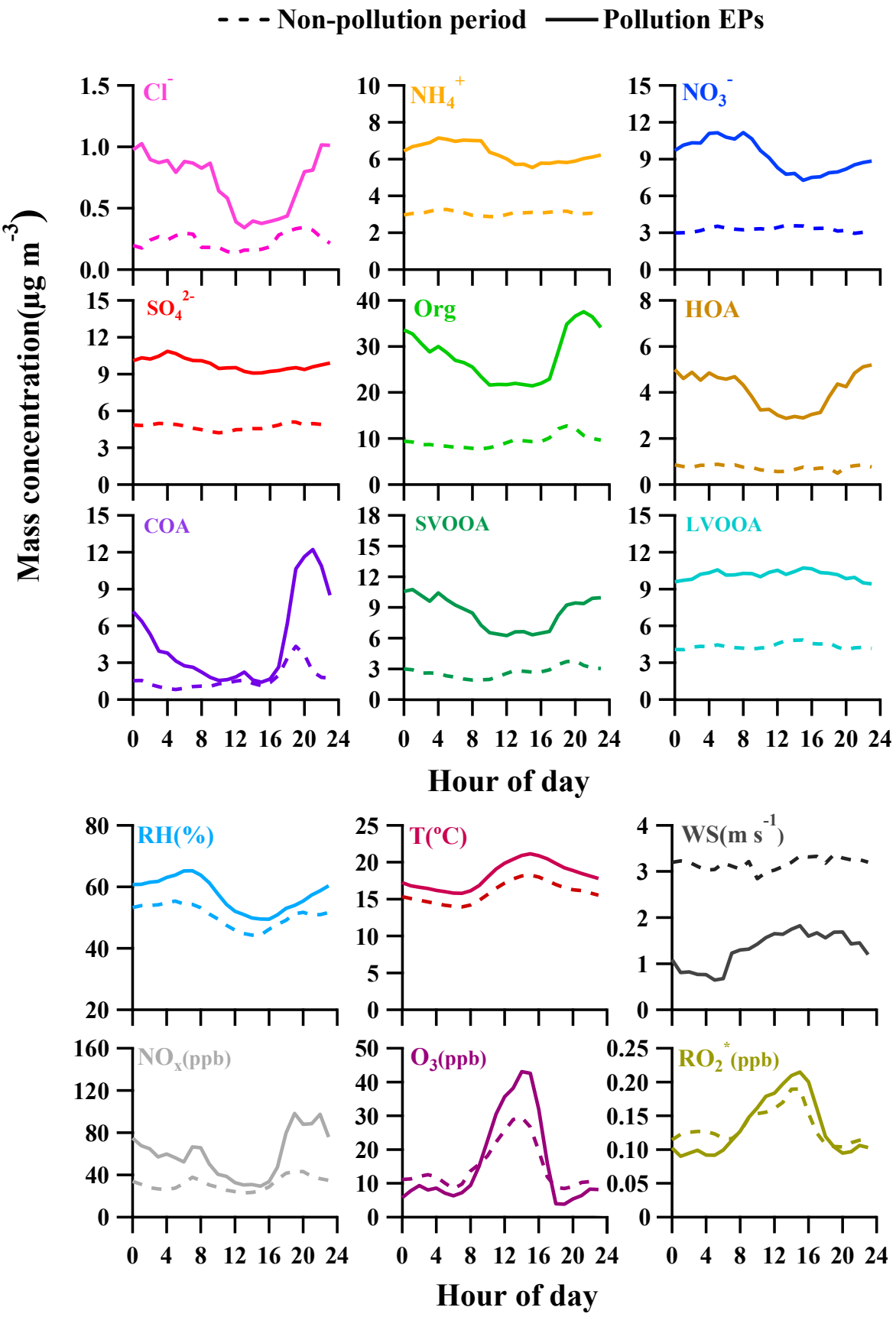
- - - Non-pollution period
—— Pollution EPs
Mass concentration(μg m-3)
Cl-
NH4+
NO3-
SO4 2-
Org
HOA
COA
SVOOA
LVOOA
Hour of day
RH(%)
T(°C)
WS(m s-1)
NOx(ppb)
O3(ppb)
RO2* (ppb)
Hour of day

Fig. 5.

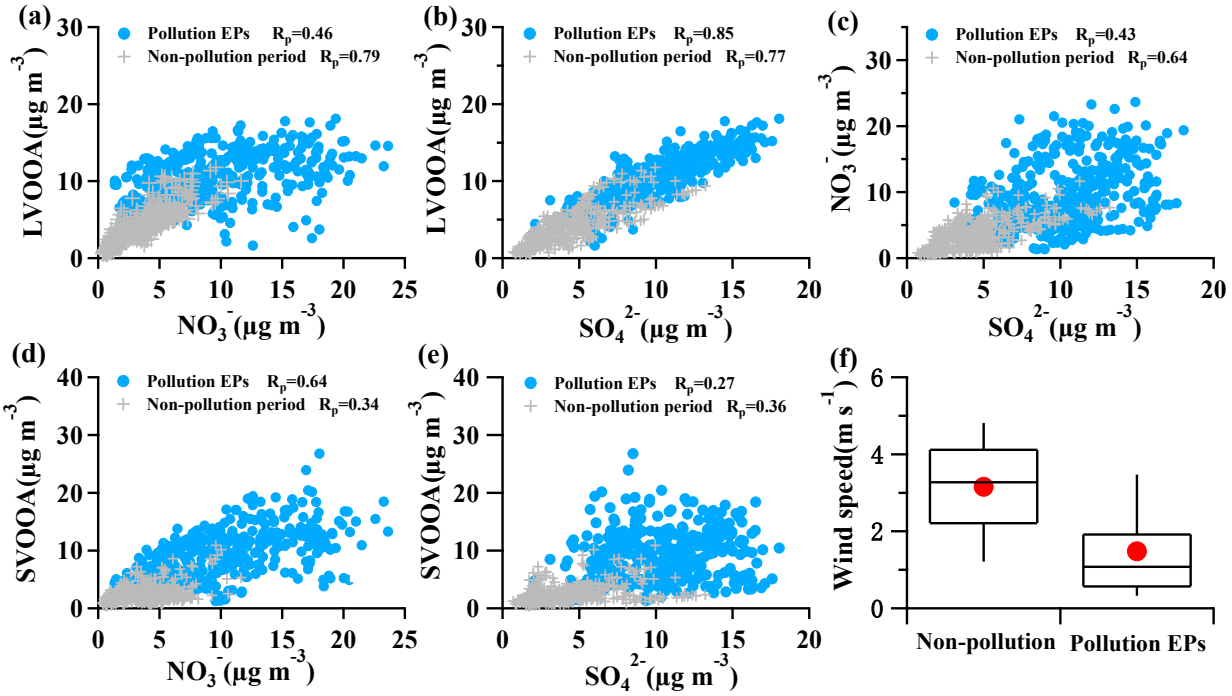
(a)
Pollution EPs Rp=0.46
Non-pollution period Rp=0.79
LVOOA(μg m-3)
NO3- (μg m-3)
(b)
Pollution EPs Rp=0.85
Non-pollution period Rp=0.77
LVOOA(μg m-3)
SO42- (μg m-3)
(c)
Pollution EPs Rp=0.43
Non-pollution period Rp=0.64
NO3- (μg m-3)
SO42- (μg m-3)
(d)
Pollution EPs Rp=0.64
Non-pollution period Rp=0.34
SVOOA(μg m-3)
NO3- (μg m-3)
(e)
Pollution EPs Rp=0.27
Non-pollution period Rp=0.36
SVOOA(μg m-3)
SO42- (μg m-3)
(f)
Wind speed(m s-1)
Non-pollution
Pollution EPs

Fig. 6.

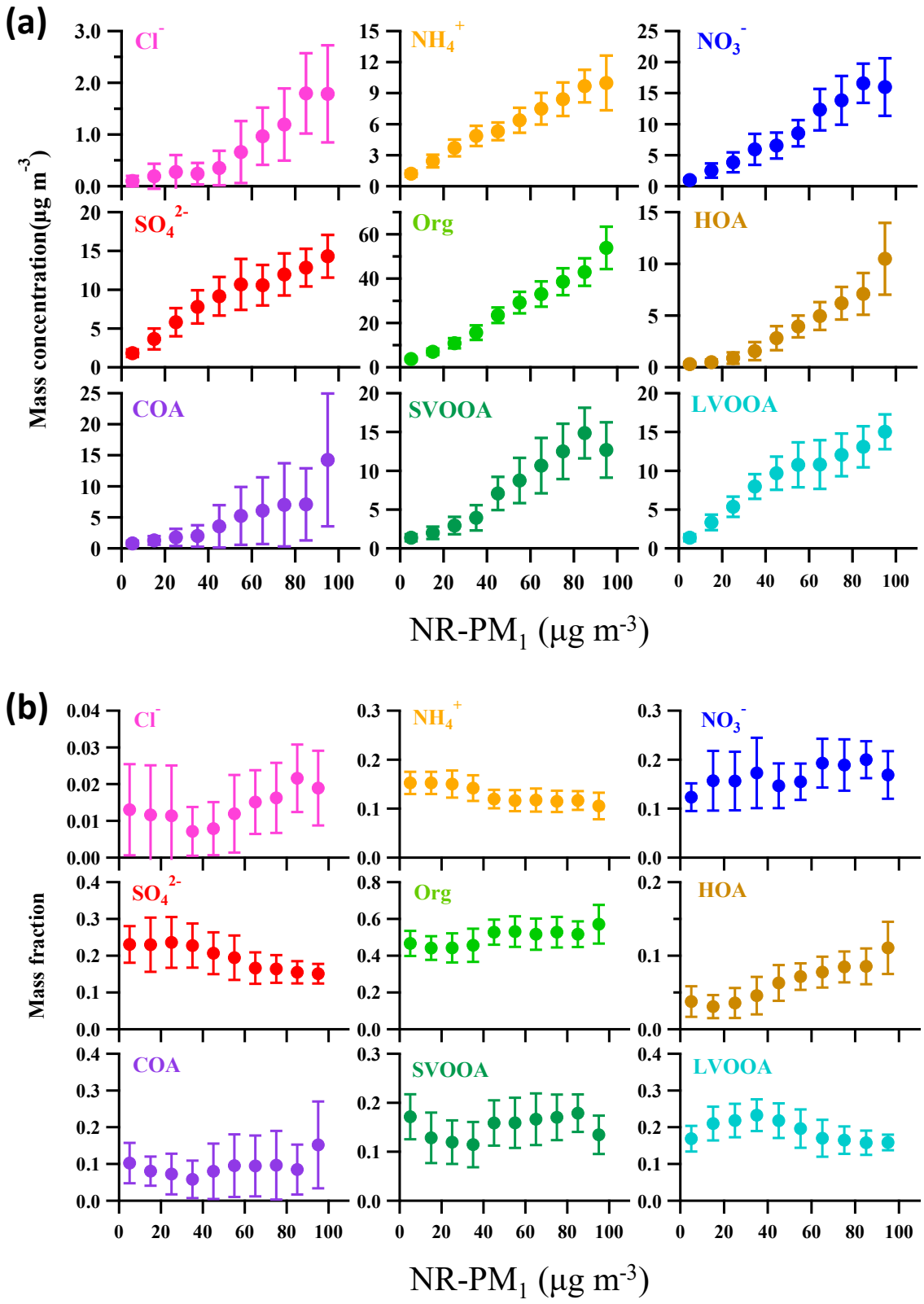
(a)
Cl-
NH4+
NO3-
SO4 2-
Org
HOA
COA
SVOOA
LVOOA
Mass concentration(μg m-3)
NR-PM1 (μg m-3)
(b)
Mass fraction
NR-PM1 (μg m-3)

Fig. 7.

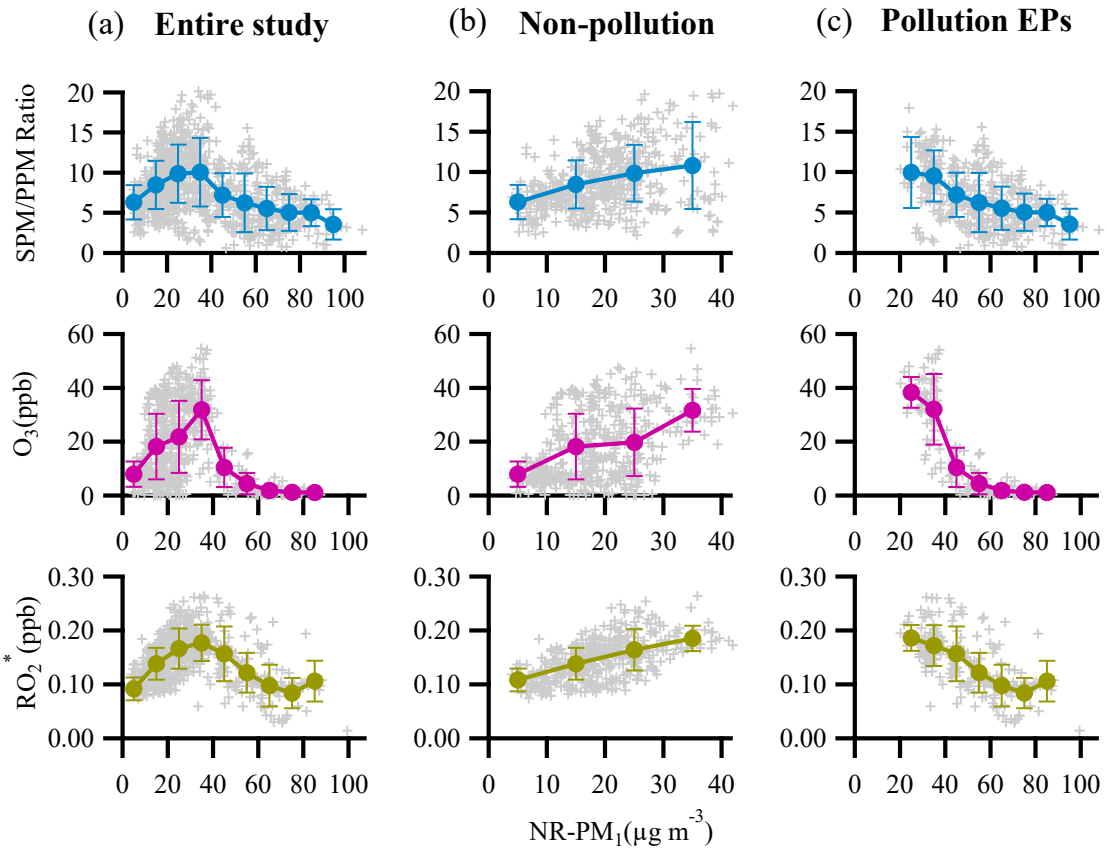
(a) Entire study
(b) Non-pollution
(c) Pollution EPs
SPM/PPM Ratio
O3(ppb)
RO2* (ppb)
NR-PM1(μg m-3)

Fig. 8.

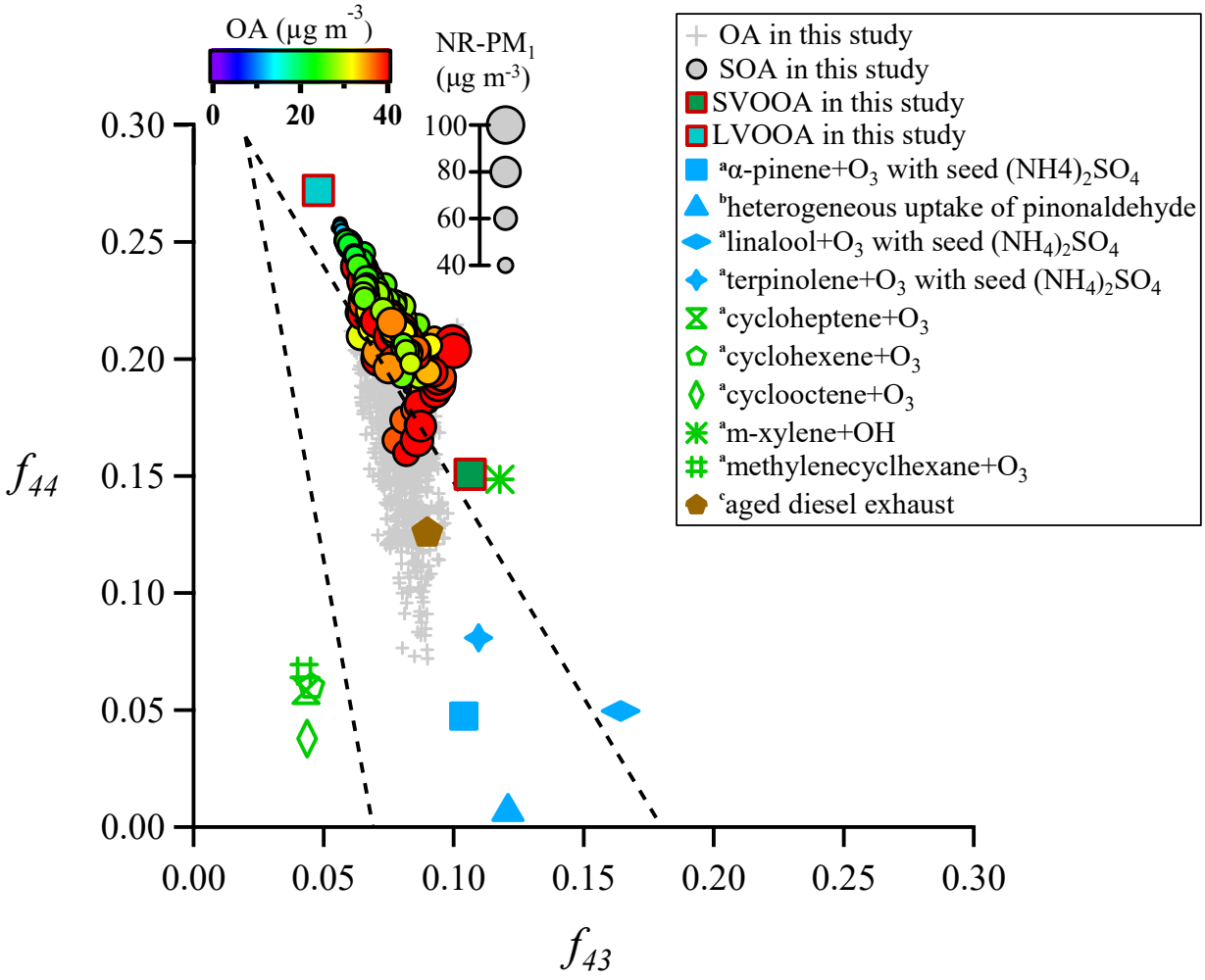
OA (μg m-3)
0
20
40
NR-PM1 (μg m-3)
100
80
60
40
OA in this study
SOA in this study
SVOOA in this study
LVOOA in this study
[a]α-pinene+O3 with seed (NH4)2SO4
[b]heterogeneous uptake of pinonaldehyde
[a]linalool+O3 with seed (NH4)2SO4
[a]terpinolene+O3 with seed (NH4)2SO4
[a]cycloheptene+O3
[a]cyclohexene+O3
[a]cyclooctene+O3
[a]m-xylene+OH
[a]methylenecyclhexane+O3
[c]aged diesel exhaust
f44
f43
0.00
0.05
0.10
0.15
0.20
0.25
0.30

Fig. 9.

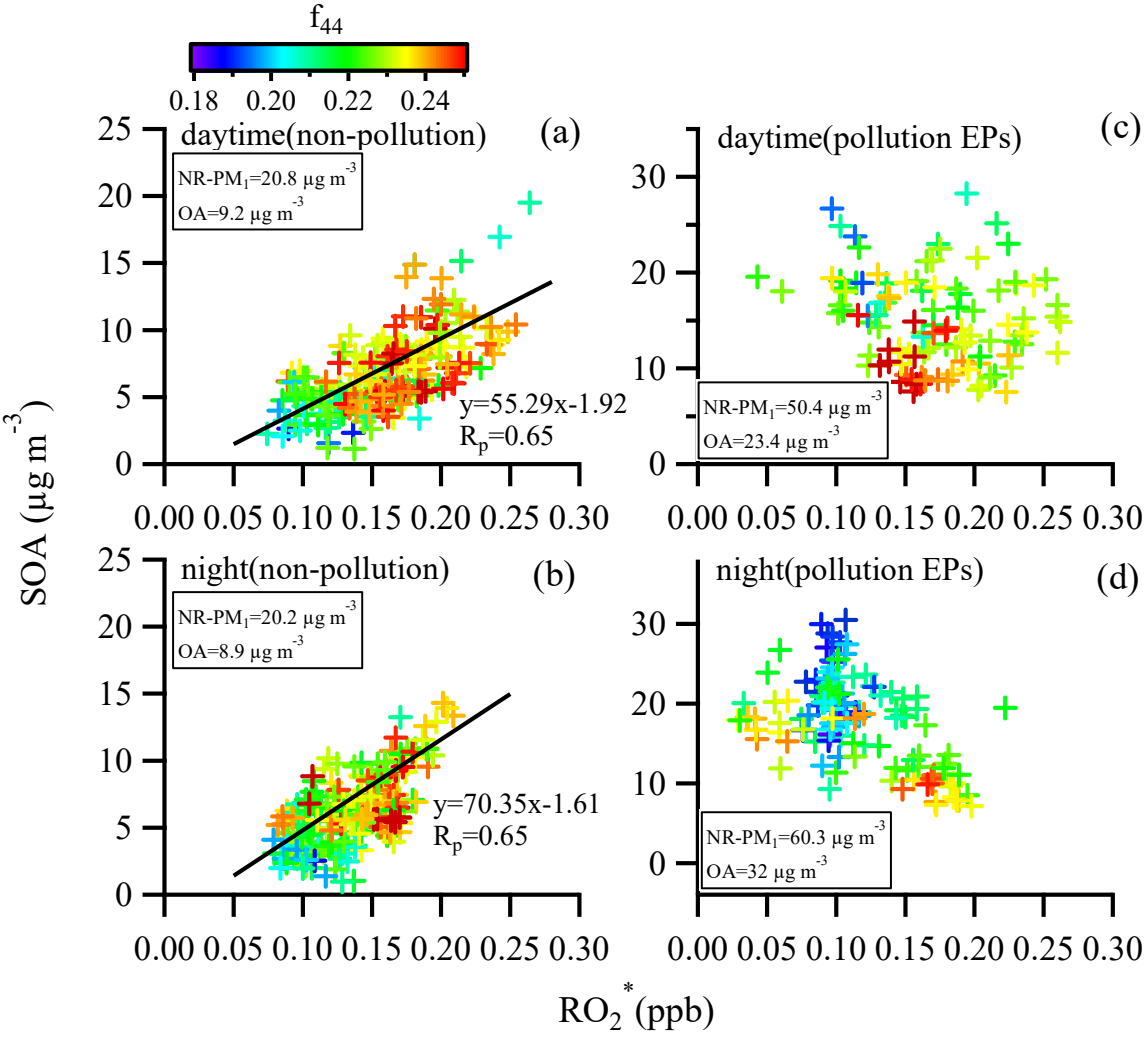
f44
0.18 0.20 0.22 0.24
daytime(non-pollution)
(a)
NR-PM1=20.8 μg m-3
OA=9.2 μg m-3
y=55.29x-1.92
Rp=0.65
daytime(pollution EPs)
(c)
NR-PM1=50.4 μg m-3
OA=23.4 μg m-3
night(non-pollution)
(b)
NR-PM1=20.2 μg m-3
OA=8.9 μg m-3
y=70.35x-1.61
Rp=0.65
night(pollution EPs)
(d)
NR-PM1=60.3 μg m-3
OA=32 μg m-3
SOA (μg m-3)
RO2* (ppb)

Fig. 10.

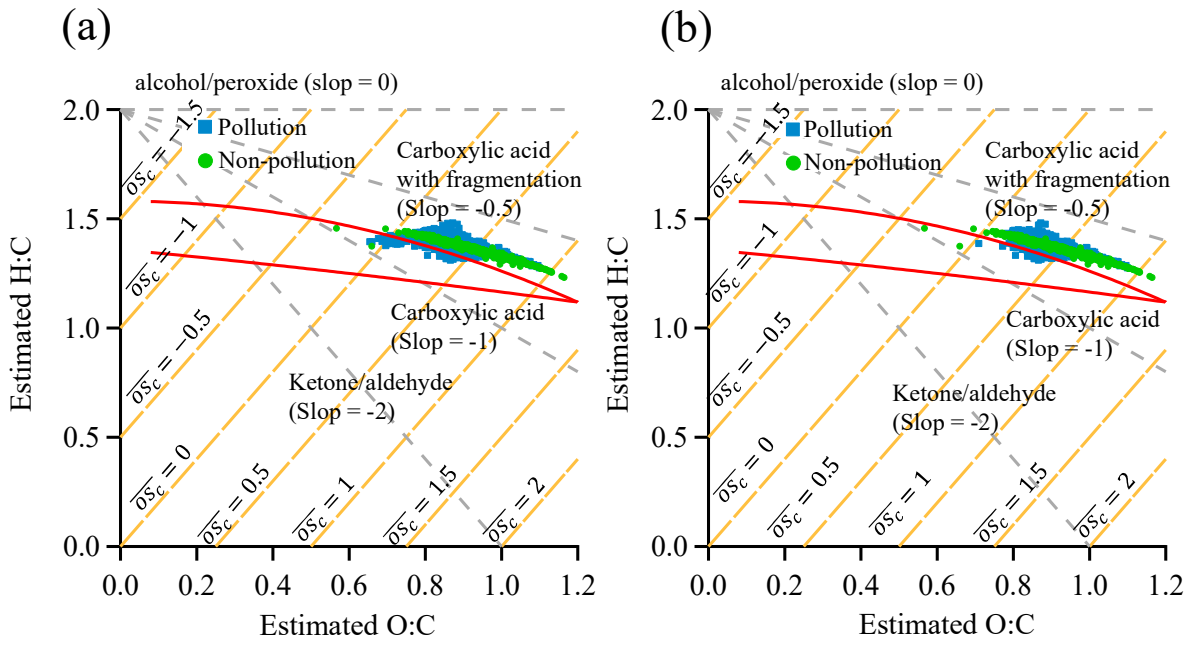
(a)
alcohol/peroxide (slop = 0)
Pollution
Non-pollution
Carboxylic acid
with fragmentation
(Slop = -0.5)
Carboxylic acid
(Slop = -1)
Ketone/aldehyde
(Slop = -2)
Estimated H:C
Estimated O:C
(b)
alcohol/peroxide (slop = 0)
Pollution
Non-pollution
Carboxylic acid
with fragmentation
(Slop = -0.5)
Carboxylic acid
(Slop = -1)
Ketone/aldehyde
(Slop = -2)
Estimated H:C
Estimated O:C

Fig. 11.

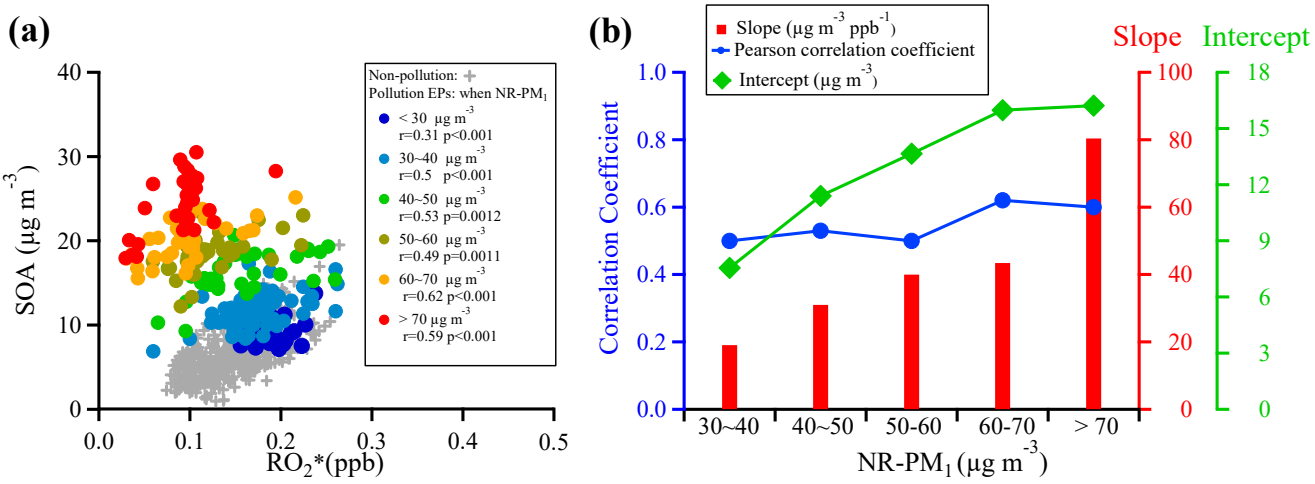
(a)
SOA (μg m-3)
RO2*(ppb)
Non-pollution:
Pollution EPs: when NR-PM1
< 30 μg m-3 r=0.31 p<0.001
30~40 μg m-3 r=0.5 p<0.001
40~50 μg m-3 r=0.53 p=0.0012
50~60 μg m-3 r=0.49 p=0.0011
60~70 μg m-3 r=0.62 p<0.001
> 70 μg m-3 r=0.59 p<0.001
(b)
Slope (μg m-3 ppb-1)
Pearson correlation coefficient
Intercept (μg m-3)
Slope
Intercept
Correlation Coefficient
NR-PM1 (μg m-3)
30~40
40~50
50-60
60-70
> 70

Fig. 12.

References

Aiken, A. C., DeCarlo, P. F., and Jimenez, J. L.: Elemental Analysis of Organic Species with Electron Ionization High-Resolution Mass Spectrometry, Anal. Chem., 79, 8350-8358, 10.1021/ac071150w, 2007.

Aiken, A. C., DeCarlo, P. F., Kroll, J. H., Worsnop, D. R., Huffman, J. A., Docherty, K. S., Ulbrich, I. M., Mohr, C., Kimmel, J. R., Sueper, D., Sun, Y., Zhang, Q., Trimborn, A., Northway, M., Ziemann, P. J., Canagaratna, M. R., Onasch, T. B., Alfarra, M. R., Prevot, A. S. H., Dommen, J., Duplissy, J., Metzger, A., Baltensperger, U., and Jimenez, J. L.: O/C and OM/OC ratios of primary, secondary, and ambient organic aerosols with high-resolution time-of-flight aerosol mass spectrometry, Environ. Sci. Technol., 42, 4478–4485, 2008.

Aiken, A. C., Salcedo, D., Cubison, M. J., Huffman, J. A., DeCarlo, P. F., Ulbrich, I. M., Docherty, K. S., Sueper, D., Kimmel, J. R., and Worsnop, D. R.: Mexico City aerosol analysis during MILAGRO using high resolution aerosol mass spectrometry at the urban supersite (T0)–Part 1: Fine particle composition and organic source apportionment, Atmos. Chem. Phys., 9, 6633-6653, 2009.

Allan, J. D., Delia, A. E., Coe, H., Bower, K. N., Alfarra, M. R., Jimenez, J. L., Middlebrook, A. M., Drewnick, F., Onasch, T. B., Canagaratna, M. R., Jayne, J. T., and Worsnop, D. R.: A generalised method for the extraction of chemically resolved mass spectra from Aerodyne aerosol mass spectrometer data, J. Aerosol. Sci., 35, 909-922, 10.1016/j.jaerosci.2004.02.007, 2004.

Allan, J. D., Williams, P. I., Morgan, W. T., Martin, C. L., Flynn, M. J., Lee, J., Nemitz, E., Phillips, G. J., Gallagher, M. W., and Coe, H.: Contributions from transport, solid fuel burning and cooking to primary organic aerosols in two UK cities, Atmos. Chem. Phys., 10, 647-668, 10.5194/acp-10-647-2010, 2010.

Bahreini, R., Keywood, M. D., Ng, N. L., Varutbangkul, V., Gao, S., Flagan, R. C., Seinfeld, J. H., Worsnop, D. R., and Jimenez, J. L.: Measurements of Secondary Organic Aerosol from Oxidation of Cycloalkenes, Terpenes, and m-Xylene Using an Aerodyne Aerosol Mass Spectrometer, Environ. Sci. Technol., 39, 5674-5688, 10.1021/es048061a, 2005.

Bian, Y., Huang, Z., Ou, J., Zhong, Z., Xu, Y., Zhang, Z., Xiao, X., Ye, X., Wu, Y., Yin, X., Li, C., Chen, L., Shao, M., and Zheng, J.: Evolution of anthropogenic air pollutant emissions in Guangdong Province, China, from 2006 to 2015, Atmos. Chem. Phys., 19, 11701-11719, 10.5194/acp-19-11701-2019, 2019

Bressi, M., Cavalli, F., Belis, C. A., Putaud, J.-P., Fröhlich, R., Martins dos Santos, S., Petralia, E., Prévôt, A. S. H., Berico, M., Malaguti, A., and Canonaco, F.: Variations in the chemical composition of the submicron aerosol and in the sources of the organic fraction at a regional background site of the Po Valley (Italy), Atmos. Chem. Phys., 16, 12875-12896, 10.5194/acp-16-12875-2016, 2016.

Canagaratna, M. R., Jayne, J. T., Jimenez, J. L., Allan, J. D., Alfarra, M. R., Zhang, Q., Onasch, T. B.,

Drewnick, F., Coe, H., Middlebrook, A., Delia, A., Williams, L. R., Trimborn, A. M., Northway, M. J., DeCarlo, P. F., Kolb, C. E., Davidovits, P., and Worsnop, D. R.: Chemical and microphysical characterization of ambient aerosols with the aerodyne aerosol mass spectrometer, Mass Spectrom. Rev., 26, 185-222, 10.1002/mas.20115, 2007.

Canagaratna, M. R., Jimenez, J. L., Kroll, J. H., Chen, Q., Kessler, S. H., Massoli, P., Hildebrandt Ruiz, L., Fortner, E., Williams, L. R., and Wilson, K. R.: Elemental ration measurements of organic compounds using aerosol mass spectrometry: characterization, improved calibration, and implications, Atmos. Chem. Phys, 15, 253-272, 2015.

Canonaco, F., Slowik, J. G., Baltensperger, U., and Prévôt, A. S. H.: Seasonal differences in oxygenated organic aerosol composition: implications for emissions sources and factor analysis, Atmos. Chem. Phys., 15, 6993-7002, 10.5194/acp-15-6993-2015, 2015.

Chhabra, P. S., Ng, N. L., Canagaratna, M. R., Corrigan, A. L., Russell, L. M., Worsnop, D. R., Flagan, R. C., and Seinfeld, J. H.: Elemental composition and oxidation of chamber organic aerosol, Atmos. Chem. Phys., 11, 8827, 2011.

Crippa, M., DeCarlo, P. F., Slowik, J. G., Mohr, C., Heringa, M. F., Chirico, R., Poulain, L., Freutel, F., Sciare, J., Cozic, J., Di Marco, C. F., Elsasser, M., Nicolas, J. B., Marchand, N., Abidi, E., Wiedensohler, A., Drewnick, F., Schneider, J., Borrmann, S., Nemitz, E., Zimmermann, R., Jaffrezo, J. L., Prévôt, A. S. H., and Baltensperger, U.: Wintertime aerosol chemical composition and source apportionment of the organic fraction in the metropolitan area of Paris, Atmos. Chem. Phys., 13, 961-981, 10.5194/acp-13-961-2013, 2013.

DeCarlo, P. F., Ulbrich, I. M., Crounse, J., de Foy, B., Dunlea, E. J., Aiken, A. C., Knapp, D., Weinheimer, A. J., Campos, T., Wennberg, P. O., and Jimenez, J. L.: Investigation of the sources and processing of organic aerosol over the Central Mexican Plateau from aircraft measurements during MILAGRO, Atmos. Chem. Phys., 10, 5257-5280, 10.5194/acp-10-5257-2010, 2010.

De Haan, D. O., Corrigan, A. L., Tolbert, M. A., Jimenez, J. L., Wood, S. E., and Turley, J. J.: Secondary organic aerosol formation by self-reactions of methylglyoxal and glyoxal in evaporating droplets, Environ. Sci. Technol., 43, 8184-8190, 2009.

Ervens, B., Turpin, B. J., and Weber, R. J.: Secondary organic aerosol formation in cloud droplets and aqueous particles (aqSOA): a review of laboratory, field and model studies, Atmos. Chem. Phys., 11, 11069-11102, 10.5194/acp-11-11069-2011, 2011.

Fang, B., Zhao, W.X., Xu, X.Z., Zhou, J.C., Ma, X., Wang, S., Zhang, W.J., Dean S. Venables and Chen, W.D. (2017). Portable broadband cavity-enhanced spectrometer utilizing Kalman filtering: application to real-time, in situ monitoring of glyoxal and nitrogen dioxide. Optics Express 25(22): 26910-26922, https://doi.org/10.1364/OE.25.026910, 2017.

Frank Drewnick, Silke S. Hings, Peter DeCarlo, John T. Jayne, Marc Gonin, Katrin Fuhrer, Silke Weimer,

Jose L. Jimenez, Kenneth L. Demerjian, Stephan Borrmann & Douglas R. Worsnop (2005) A New Time-of-Flight Aerosol Mass Spectrometer (TOF-AMS)—Instrument Description and First Field Deployment, Aerosol. Sci. Tech., 39:7, 637-658, DOI: 10.1080/02786820500182040

Fröhlich, R., Cubison, M. J., Slowik, J. G., Bukowiecki, N., Prévôt, A. S. H., Baltensperger, U., Schneider, J., Kimmel, J. R., Gonin, M., Rohner, U., Worsnop, D. R., and Jayne, J. T.: The ToF-ACSM: a portable aerosol chemical speciation monitor with TOFMS detection, Atmos. Meas. Tech., 6, 3225-3241, 10.5194/amt-6-3225-2013, 2013.

Gani, S., Bhandari, S., Seraj, S., Wang, D. S., Patel, K., Soni, P., Arub, Z., Habib, G., Hildebrandt Ruiz, L., and Apte, J. S.: Submicron aerosol composition in the world's most polluted megacity: the Delhi Aerosol Supersite study, Atmos. Chem. Phys., 19, 6843-6859, 10.5194/acp-19-6843-2019, 2019.

Ge, X., Setyan, A., Sun, Y., and Zhang, Q.: Primary and secondary organic aerosols in Fresno, California during wintertime: Results from high resolution aerosol mass spectrometry, J. Geophys. Res., 117, n/a-n/a, 10.1029/2012jd018026, 2012.

Griffith, S. M., Hansen, R. F., Dusanter, S., Stevens, P. S., Alaghmand, M., Bertman, S. B., Carroll, M. A., Erickson, M., Galloway, M., Grossberg, N., Hottle, J., Hou, J., Jobson, B. T., Kammrath, A., Keutsch, F. N., Lefer, B. L., Mielke, L. H., amp, apos, Brien, A., Shepson, P. B., Thurlow, M., Wallace, W., Zhang, N., and Zhou, X. L.: OH and HO2 radical chemistry during PROPHET 2008 and CABINEX 2009-Part 1: Measurements and model comparison, Atmos. Chem. Phys., 13, 5403-5423, 10.5194/acp-13-5403-2013, 2013.

He, L. Y., Huang, X. F., Xue, L., Hu, M., Lin, Y., Zheng, J., Zhang, R., and Zhang, Y. H.: Submicron aerosol analysis and organic source apportionment in an urban atmosphere in Pearl River Delta of China using high-resolution aerosol mass spectrometry, J. Geophys. Res., 116, 10.1029/2010jd014566, 2011.

Herndon, S. C., Onasch, T. B., Wood, E. C., Kroll, J. H., Canagaratna, M. R., Jayne, J. T., Zavala, M. A., Knighton, W. B., Mazzoleni, C., Dubey, M. K., Ulbrich, I. M., Jimenez, J. L., Seila, R., de Gouw, J. A., de Foy, B., Fast, J., Molina, L. T., Kolb, C. E., and Worsnop, D. R.: Correlation of secondary organic aerosol with odd oxygen in Mexico City, Geophys. Res. Lett., 35, 10.1029/2008gl034058, 2008.

Herrmann, H., Schaefer, T., Tilgner, A., Styler, S. A., Weller, C., Teich, M., and Otto, T.: Tropospheric aqueous-phase chemistry: kinetics, mechanisms, and its coupling to a changing gas phase, Chem. Rev., 115, 4259-4334, 10.1021/cr500447k, 2015.

Hu, W., Hu, M., Hu, W.-W., Niu, H., Zheng, J., Wu, Y., Chen, W., Chen, C., Li, L., Shao, M., Xie, S., and Zhang, Y.: Characterization of submicron aerosols influenced by biomass burning at a site in the Sichuan Basin, southwestern China, Atmos. Chem. Phys., 16, 13213–13230, https://doi.org/10.5194/acp-16-13213-2016, 2016.

Hu, W., Hu, M., Hu, W., Jimenez, J. L., Yuan, B., Chen, W., Wang, M., Wu, Y., Chen, C., Wang, Z., Peng, J., Zeng, L., and Shao, M.: Chemical composition, sources and aging process of submicron aerosols in Beijing: contrast between summer and winter, J. Geophys. Res., 121, 1955–1977, https://doi.org/10.1002/2015JD024020, 2016a.

Hu, W., Campuzano-Jost, P., Day, D. A., Croteau, P., Canagaratna, M. R., Jayne, J. T., Worsnop, D. R., and Jimenez, J. L.: Evaluation of the new capture vaporizer for aerosol mass spectrometers (AMS) through field studies of inorganic species, Aerosol Sci. Tech., 51, 735-754, 10.1080/02786826.2017.1296104, 2017.

Huang, X.F., He, L.Y., Xue, L., Sun, T.-L., Zeng, L.W., Gong, Z.H., Hu, M., and Zhu, T.: Highly time-resolved chemical characterization of atmospheric fine particles during 2010 Shanghai World Expo, Atmos. Chem. Phys., 12, 4897–4907, https://doi.org/10.5194/acp-12-4897-2012, 2012.

Huang, R. J., Wang, Y., Cao, J., Lin, C., Duan, J., Chen, Q., Li, Y., Gu, Y., Yan, J., Xu, W., Fröhlich, R., Canonaco, F., Bozzetti, C., Ovadnevaite, J., Ceburnis, D., Canagaratna, M. R., Jayne, J., Worsnop, D. R., El-Haddad, I., Prévôt, A. S. H., amp, apos, and Dowd, C. D.: Primary emissions versus secondary formation of fine particulate matter in the most polluted city (Shijiazhuang) in North China, Atmos. Chem. Phys., 19, 2283-2298, 10.5194/acp-19-2283-2019, 2019.

Huang, X. F., He, L. Y., Hu, M., Canagaratna, M. R., Kroll, J. H., Ng, N. L., Zhang, Y. H., Lin, Y., Xue, L., Sun, T. L., Liu, X. G., Shao, M., Jayne, J. T., and Worsnop, D. R.: Characterization of submicron aerosols at a rural site in Pearl River Delta of China using an Aerodyne High-Resolution Aerosol Mass Spectrometer, Atmos. Chem. Phys., 11, 1865-1877, 10.5194/acp-11-1865-2011, 2011.

Ibald-Mulli, A., Wichmann, H. E., Kreyling, W., and Peters, A.: Epidemiological evidence on health effects of ultrafine particles, J. Aerosol Med., 15, 189-201, 2002.

IPCC: Climate Change 2013 – The Physical Science Basis. Working Group I Contribution to the Fifth Assessment Report of the IPCC, Cambridge University Press, Cambridge, UK, 2013.

Jiang, Q., Sun, Y. L., Wang, Z., and Yin, Y.: Aerosol composition and sources during the Chinese Spring Festival: fireworks, secondary aerosol, and holiday effects, Atmos. Chem. Phys., 15, 6023–6034, https://doi.org/10.5194/acp-15-6023-2015, 2015.

Jimenez, J. L., Jayne, J. T., Shi, Q., Kolb, C. E., Worsnop, D. R., Yourshaw, I., Seinfeld, J. H., Flagan, R. C., Zhang, X., and Smith, K. A.: Ambient aerosol sampling using the aerodyne aerosol mass spectrometer, J. Geophys. Res.-Atmos., 108, 2003.

Jimenez, J. L., Canagaratna, M. R., Donahue, N. M., Prevot, A. S. H., Zhang, Q., Kroll, J. H., DeCarlo, P. F., Allan, J. D., Coe, H., Ng, N. L., Aiken, A. C., Docherty, K. S., Ulbrich, I. M., Grieshop, A. P., Robinson, A. L., Duplissy, J., Smith, J. D., Wilson, K. R., Lanz, V. A., Hueglin, C., Sun, Y. L., Tian, J., Laaksonen, A., Raatikainen, T., Rautiainen, J., Vaattovaara, P., Ehn, M., Kulmala, M., Tomlinson, J. M., Collins, D. R., Cubison, M. J., Dunlea, J., Huffman, J. A., Onasch, T. B., Alfarra, M. R.,

Williams, P. I., Bower, K., Kondo, Y., Schneider, J., Drewnick, F., Borrmann, S., Weimer, S., Demerjian, K., Salcedo, D., Cottrell, L., Griffin, R., Takami, A., Miyoshi, T., Hatakeyama, S., Shimono, A., Sun, J. Y., Zhang, Y. M., Dzepina, K., Kimmel, J. R., Sueper, D., Jayne, J. T., Herndon, S. C., Trimborn, A. M., Williams, L. R., Wood, E. C., Middlebrook, A. M., Kolb, C. E., Baltensperger, U., and Worsnop, D. R.: Evolution of Organic Aerosols in the Atmosphere, Science, 326, 1525, 10.1126/science.1180353, 2009.

Kreyling, W. G., Semmler-Behnke, M., and Möller, W.: Ultrafine particle–lung interactions: does size matter?, J. Aerosol Med., 19, 74-83, 2006.

Kroll, J. H., and Seinfeld, J. H.: Chemistry of secondary organic aerosol: Formation and evolution of low-volatility organics in the atmosphere, Atmos. Environ., 42, 3593-3624, 10.1016/j.atmosenv.2008.01.003, 2008.

Lee, B. P., Li, Y. J., Yu, J. Z., Louie, P. K. K., and Chan, C. K.: Characteristics of submicron particulate matter at the urban roadside in downtown Hong Kong-Overview of 4 months of continuous high-resolution aerosol mass spectrometer measurements, J. Geophys. Res., 120, 7040-7058, 10.1002/2015jd023311, 2015.

Lee, B. P., Wang, H., and Chan, C. K.: Diurnal and day-to-day characteristics of ambient particle mass size distributions from HR-ToF-AMS measurements at an urban site and a suburban site in Hong Kong, Atmos. Chem. Phys., 17, 13605-13624, 10.5194/acp-17-13605-2017, 2017.

Levy, H.: Normal Atmosphere: Large Radical and Formaldehyde Concentrations Predicted, Science, 173, 141, 10.1126/science.173.3992.141, 1971.

Li, Y. J., Lee, B. Y. L., Yu, J. Z., Ng, N. L., and Chan, C. K.: Evaluating the degree of oxygenation of organic aerosol during foggy and hazy days in Hong Kong using high-resolution time-of-flight aerosol mass spectrometry (HR-ToF-AMS), Atmos. Chem. Phys., 13, 8739-8753, 10.5194/acp-13-8739-2013, 2013.

Li, Y. J., Lee, B. P., Su, L., Fung, J. C. H., and Chan, C. K.: Seasonal characteristics of fine particulate matter (PM) based on high-resolution time-of-flight aerosol mass spectrometric (HR-ToF-AMS) measurements at the HKUST Supersite in Hong Kong, Atmos. Chem. Phys., 15, 37-53, 10.5194/acp-15-37-2015, 2015.

Li, H., Zhang, Q., Zhang, Q., Chen, C., Wang, L., Wei, Z., Zhou, S., Parworth, C., Zheng, B., Canonaco, F., Prévôt, A. S. H., Chen, P., Zhang, H., Wallington, T. J., and He, K.: Wintertime aerosol chemistry and haze evolution in an extremely polluted city of the North China Plain: significant contribution from coal and biomass combustion, Atmos. Chem. Phys., 17, 4751–4768, https://doi.org/10.5194/acp-17-4751-2017, 2017.

Li, Y. J., Sun, Y., Zhang, Q., Li, X., Li, M., Zhou, Z., and Chan, C. K.: Real-time chemical characterization of atmospheric particulate matter in China: A review, Atmos. Environ., 158, 270-

304, 10.1016/j.atmosenv.2017.02.027, 2017.

Liggio, J., Li, S.-M., and McLaren, R.: Heterogeneous Reactions of Glyoxal on Particulate Matter: Identification of Acetals and Sulfate Esters, Environ. Sci. Technol., 39, 1532-1541, 10.1021/es048375y, 2005.

Liggio, J., and Li, S.-M.: Organosulfate formation during the uptake of pinonaldehyde on acidic sulfate aerosols, Geophys. Res. Lett., 33, 10.1029/2006gl026079, 2006.

Marais, E. A., Jacob, D. J., Jimenez, J. L., Campuzano-Jost, P., Day, D. A., Hu, W., Krechmer, J., Zhu, L., Kim, P. S., Miller, C. C., Fisher, J. A., Travis, K., Yu, K., Hanisco, T. F., Wolfe, G. M., Arkinson, H. L., Pye, H. O. T., Froyd, K. D., Liao, J., and McNeill, V. F.: Aqueous-phase mechanism for secondary organic aerosol formation from isoprene: application to the southeast United States and co-benefit of SO_2 emission controls, Atmos. Chem. Phys., 16, 1603-1618, 10.5194/acp-16-1603-2016, 2016.

Matthew, B. M., Middlebrook, A. M., and Onasch, T. B.: Collection Efficiencies in an Aerodyne Aerosol Mass Spectrometer as a Function of Particle Phase for Laboratory Generated Aerosols, Aerosol Sci. Tech., 42, 884-898, 10.1080/02786820802356797, 2008.

McNeill, V. F.: Aqueous organic chemistry in the atmosphere: sources and chemical processing of organic aerosols, Environ. Sci. Technol, 49, 1237-1244, 10.1021/es5043707, 2015.

Middlebrook, A. M., Bahreini, R., Jimenez, J. L., and Canagaratna, M. R.: Evaluation of Composition-Dependent Collection Efficiencies for the Aerodyne Aerosol Mass Spectrometer using Field Data, Aerosol Sci. Technol., 46, 258-271, 10.1080/02786826.2011.620041, 2012.

Mohr, C., DeCarlo, P. F., Heringa, M. F., Chirico, R., Slowik, J. G., Richter, R., Reche, C., Alastuey, A., Querol, X., Seco, R., Peñuelas, J., Jiménez, J. L., Crippa, M., Zimmermann, R., Baltensperger, U., and Prévôt, A. S. H.: Identification and quantification of organic aerosol from cooking and other sources in Barcelona using aerosol mass spectrometer data, Atmos Chem. Phys., 12, 1649-1665, 10.5194/acp-12-1649-2012, 2012.

Ng, N. L., Canagaratna, M. R., Zhang, Q., Jimenez, J. L., Tian, J., Ulbrich, I. M., Kroll, J. H., Docherty, K. S., Chhabra, P. S., Bahreini, R., Murphy, S. M., Seinfeld, J. H., Hildebrandt, L., Donahue, N. M., DeCarlo, P. F., Lanz, V. A., Prévôt, A. S. H., Dinar, E., Rudich, Y., and Worsnop, D. R.: Organic aerosol components observed in Northern Hemispheric datasets from Aerosol Mass Spectrometry, Atmos. Chem. Phys., 10, 4625-4641, 10.5194/acp-10-4625-2010, 2010.

Ng, N. L., Canagaratna, M. R., Jimenez, J. L., Chhabra, P. S., Seinfeld, J. H., and Worsnop, D. R.: Changes in organic aerosol composition with aging inferred from aerosol mass spectra, Atmos. Chem. Phys., 11, 6465-6474, 10.5194/acp-11-6465-2011, 2011.

Ng, N. L., Herndon, S. C., Trimborn, A., Canagaratna, M. R., Croteau, P. L., Onasch, T. B., Sueper, D., Worsnop, D. R., Zhang, Q., Sun, Y. L., and Jayne, J. T.: An Aerosol Chemical Speciation Monitor

(ACSM) for Routine Monitoring of the Composition and Mass Concentrations of Ambient Aerosol, Aerosol Sci. Tech., 45, 780-794, 10.1080/02786826.2011.560211, 2011.

Pope III, C. A., and Dockery, D. W.: Health effects of fine particulate air pollution: lines that connect, J. Air & Waste Manage., 56, 709-742, 2006.

Qin, Y. M., Tan, H. B., Li, Y. J., Schurman, M. I., Li, F., Canonaco, F., Prévôt, A. S. H., and Chan, C. K.: Impacts of traffic emissions on atmospheric particulate nitrate and organics at a downwind site on the periphery of Guangzhou, China, Atmos. Chem. Phys., 17, 10245-10258, 10.5194/acp-17-10245-2017, 2017.

Rohrer, F., Lu, K., Hofzumahaus, A., Bohn, B., Brauers, T., Chang, C.-C., Fuchs, H., Häseler, R., Holland, F., Hu, M., Kita, K., Kondo, Y., Li, X., Lou, S., Oebel, A., Shao, M., Zeng, L., Zhu, T., Zhang, Y., and Wahner, A.: Maximum efficiency in the hydroxyl-radical-based self-cleansing of the troposphere, Nature Geosci., 7, 559-563, 10.1038/ngeo2199, 2014.

Sheehy, P. M., Volkamer, R., Molina, L. T., and Molina, M. J.: Oxidative capacity of the Mexico City atmosphere – Part 2: A RO_x radical cycling perspective, Atmos. Chem. Phys., 10, 6993-7008, 10.5194/acp-10-6993-2010, 2010.

Shilling, J. E., Chen, Q., King, S. M., Rosenoern, T., Kroll, J. H., Worsnop, D. R., DeCarlo, P. F., Aiken, A. C., Sueper, D., Jimenez, J. L., and Martin, S. T.: Loading-dependent elemental composition of α-pinene SOA particles, Atmos. Chem. Phys., 9, 771-782, 10.5194/acp-9-771-2009, 2009.

Stone, D., Whalley, L. K., and Heard, D. E.: Tropospheric OH and HO2 radicals: field measurements and model comparisons, Chem. Soc. Rev., 41, 6348-6404, 10.1039/c2cs35140d, 2012.

Stone, D., Evans, M. J., Walker, H., Ingham, T., Vaughan, S., Ouyang, B., Kennedy, O. J., McLeod, M. W., Jones, R. L., Hopkins, J., Punjabi, S., Lidster, R., Hamilton, J. F., Lee, J. D., Lewis, A. C., Carpenter, L. J., Forster, G., Oram, D. E., Reeves, C. E., Bauguitte, S., Morgan, W., Coe, H., Aruffo, E., Dari-Salisburgo, C., Giammaria, F., Di Carlo, P., and Heard, D. E.: Radical chemistry at night: comparisons between observed and modelled HO_x, NO_3 and N_2O_5 during the RONOCO project, Atmos. Chem. Phys., 14, 1299-1321, 10.5194/acp-14-1299-2014, 2014.

Sun, C., Lee, B. P., Huang, D., Jie Li, Y., Schurman, M. I., Louie, P. K. K., Luk, C., and Chan, C. K.: Continuous measurements at the urban roadside in an Asian megacity by Aerosol Chemical Speciation Monitor (ACSM): particulate matter characteristics during fall and winter seasons in Hong Kong, Atmos. Chem. Phys., 16, 1713-1728, 10.5194/acp-16-1713-2016, 2016.

Sun, Y., Wang, Z., Dong, H., Yang, T., Li, J., Pan, X., Chen, P., and Jayne, J. T.: Characterization of summer organic and inorganic aerosols in Beijing, China with an Aerosol Chemical Speciation Monitor, Atmos. Environ., 51, 250-259, 10.1016/j.atmosenv.2012.01.013, 2012.

Sun, Y. L., Wang, Z. F., Fu, P. Q., Yang, T., Jiang, Q., Dong, H. B., Li, J., and Jia, J. J.: Aerosol composition, sources and processes during wintertime in Beijing, China, Atmos. Chem. Phys., 13,

4577–4592, https://doi.org/10.5194/acp-13-4577-2013, 2013.

Sun, Y. L., Jiang, Q., Wang, Z., Fu, P., Li, J., Yang, T., and Yin, Y.: Investigation of the sources and evolution processes of severe haze pollution in Beijing in January 2013, J. Geophys. Res., 119, 4380-4398, 10.1002/2014JD021641, 2014.

Sun, Y., Du,W., Fu, P.,Wang, Q., Li, J., Ge, X., Zhang, Q., Zhu, C., Ren, L., Xu, W., Zhao, J., Han, T., Worsnop, D. R., and Wang, Z.: Primary and secondary aerosols in Beijing in winter: sources, variations and processes, Atmos. Chem. Phys., 16, 8309–8329, https://doi.org/10.5194/acp-16-8309-2016, 2016.

Sun, Y. L., Xu, W., Zhang, Q., Jiang, Q., Canonaco, F., Prévôt, A. S. H., Fu, P., Li, J., Jayne, J., Worsnop, D. R., and Wang, Z.: Source apportionment of organic aerosol from 2-year highly time-resolved measurements by an aerosol chemical speciation monitor in Beijing, China, Atmos. Chem. Phys., 18, 8469-8489, 10.5194/acp-18-8469-2018, 2018.

Sun, Y. L., Wang, Z. F., Fu, P. Q., Yang, T., Jiang, Q., Dong, H. B., Li, J., and Jia, J. J.: Aerosol composition, sources and processes during wintertime in Beijing, China, Atmos. Chem. Phys., 13, 4577-4592, 10.5194/acp-13-4577-2013, 2013.

Tan, J. H., Duan, J. C., Chen, D. H., Wang, X. H., Guo, S. J., Bi, X. H., Sheng, G. Y., He, K. B., and Fu, J. M.: Chemical characteristics of haze during summer and winter in Guangzhou, Atmos. Res., 94, 238-245, 10.1016/j.atmosres.2009.05.016, 2009.

Takegawa, N., Miyazaki, Y., Kondo, Y., Komazaki, Y., Miyakawa, T., Jimenez, J. L., Jayne, J. T., Worsnop, D. R., Allan, J. D., and Weber, R. J.: Characterization of an Aerodyne Aerosol Mass Spectrometer (AMS): Intercomparison with Other Aerosol Instruments, Aerosol Sci. Techno., 39, 760-770, 10.1080/02786820500243404, 2005.

Tao, J., Shen, Z., Zhu, C., Yue, J., Cao, J., Liu, S., Zhu, L., and Zhang, R.: Seasonal variations and chemical characteristics of sub-micrometer particles (PM1) in Guangzhou, China, Atmos. Res., 118, 222-231, 10.1016/j.atmosres.2012.06.025, 2012.

Timonen, H. , Cubinson, M. , Aurela, M. , Brus, D. ,Lihavainen, H. , Hillamo, R. , Canagaratna, M. ,Nekat, B. , Weller, R. , Worsnop, D. and Saarikoski, S. (2016): Applications and limitations of constrained high-resolution peak fitting on low resolving power mass spectra from the ToF-ACSM , Atmos. Meas. Tech., 9 , pp. 3263-3281 . doi: 10.5194/amt-9-3263-2016

Volkamer, R., Sheehy, P., Molina, L. T., and Molina, M. J.: Oxidative capacity of the Mexico City atmosphere – Part 1: A radical source perspective, Atmos. Chem. Phys., 10, 6969-6991, 10.5194/acp-10-6969-2010, 2010.

Wang, F., An, J., Li, Y., Tang, Y., Lin, J., Qu, Y., Chen, Y., Zhang, B., and Zhai, J.: Impacts of uncertainty in AVOC emissions on the summer ROx budget and ozone production rate in the three most rapidly-developing economic growth regions of China, Advances in Atmospheric Sciences, 31, 1331-1342,

10.1007/s00376-014-3251-z, 2014

Wang, H., Lu, K., Chen, X., Zhu, Q., Wu, Z., Wu, Y., and Sun, K.: Fast particulate nitrate formation via N_2O_5 uptake aloft in winter in Beijing, Atmos. Chem. Phys., 18, 10483-10495, 10.5194/acp-18-10483-2018, 2018.

Wang, Q., Sun, Y., Jiang, Q., Du,W., Sun, C., Fu, P., andWang, Z.: Chemical composition of aerosol particles and light extinction apportionment before and during the heating season in Beijing, China, J. Geophys. Res.-Atmos., 120, 12708–12722, 2015.

Weitkamp, E. A., Sage, A. M., Pierce, J. R., Donahue, N. M., and Robinson, A. L.: Organic Aerosol Formation from Photochemical Oxidation of Diesel Exhaust in a Smog Chamber, Environ. Sci. Technol., 41, 6969-6975, 10.1021/es070193r, 2007.

Wen, L., Xue, L., Wang, X., Xu, C., Chen, T., Yang, L., Wang, T., Zhang, Q., and Wang, W.: Summertime fine particulate nitrate pollution in the North China Plain: increasing trends, formation mechanisms and implications for control policy, Atmos. Chem. Phys., 18, 11261-11275, 10.5194/acp-18-11261-2018, 2018.

Xu, J., Zhang, Q., Chen, M., Ge, X., Ren, J., and Qin, D.: Chemical composition, sources, and processes of urban aerosols during summertime in northwest China: insights from high-resolution aerosol mass spectrometry, Atmos. Chem. Phys., 14, 12593–12611, https://doi.org/10.5194/acp-14-12593-2014, 2014

Xu, J., Shi, J., Zhang, Q., Ge, X., Canonaco, F., Prévôt, A. S. H., Vonwiller, M., Szidat, S., Ge, J., Ma, J., An, Y., Kang, S., and Qin, D.: Wintertime organic and inorganic aerosols in Lanzhou, China: sources, processes, and comparison with the results during summer, Atmos. Chem. Phys., 16, 14937-14957, 10.5194/acp-16-14937-2016, 2016.

Xue, J., Yuan, Z., Lau, A. K. H., and Yu, J. Z.: Insights into factors affecting nitrate in PM2.5 in a polluted high NO_x environment through hourly observations and size distribution measurements, J. Geophys. Res., 119, 4888-4902, 10.1002/2013JD021108, 2014.

Yang, C., Zhao, W., Fang, B., Xu, X., Zhang, Y., Gai, Y., Zhang, W., Venables, D. S., and Chen, W.: Removing Water Vapor Interference in Peroxy Radical Chemical Amplification with a Large Diameter Nafion Dryer, Anal. Chem., 90, 3307-3312, 10.1021/acs.analchem.7b04830, 2018.

Yang, C., Zhao, W., Fang, B., Yu, H., Xu, X., Zhang, Y., Gai, Y., Zhang, W., Chen, W., and Fittschen, C.: Improved Chemical Amplification Instrument by Using a Nafion Dryer as an Amplification Reactor for Quantifying Atmospheric Peroxy Radicals under Ambient Conditions, Anal. Chem., 91, 776-779, 10.1021/acs.analchem.8b04907, 2019.

Zhang, Q., Jimenez, J. L., Canagaratna, M. R., Allan, J. D., Coe, H., Ulbrich, I., Alfarra, M. R., Takami, A., Middlebrook, A. M., Sun, Y. L., Dzepina, K., Dunlea, E., Docherty, K., DeCarlo, P. F., Salcedo, D., Onasch, T., Jayne, J. T., Miyoshi, T., Shimono, A., Hatakeyama, S., Takegawa, N., Kondo, Y.,

Schneider, J., Drewnick, F., Borrmann, S., Weimer, S., Demerjian, K., Williams, P., Bower, K., Bahreini, R., Cottrell, L., Griffin, R. J., Rautiainen, J., Sun, J. Y., Zhang, Y. M., and Worsnop, D. R.: Ubiquity and dominance of oxygenated species in organic aerosols in anthropogenically-influenced Northern Hemisphere midlatitudes, Geophys. Res. Lett., 34, n/a-n/a, 10.1029/2007gl029979, 2007.

Zhang, Q., Jimenez, J. L., Canagaratna, M. R., Ulbrich, I. M., Ng, N. L., Worsnop, D. R., and Sun, Y.: Understanding atmospheric organic aerosols via factor analysis of aerosol mass spectrometry: a review, Anal. Bioanal. Chem., 401, 3045-3067, 10.1007/s00216-011-5355-y, 2011.

Zhang, Y. J., Tang, L. L., Wang, Z., Yu, H. X., Sun, Y. L., Liu, D., Qin, W., Canonaco, F., Prévôt, A. S. H., Zhang, H. L., and Zhou, H. C.: Insights into characteristics, sources, and evolution of submicron aerosols during harvest seasons in the Yangtze River delta region, China, Atmos. Chem. Phys., 15, 1331–1349, https://doi.org/10.5194/acp-15-1331-2015, 2015.

Zhang, Y., Tang, L., Croteau, P. L., Favez, O., Sun, Y., Canagaratna, M. R., Wang, Z., Couvidat, F., Albinet, A., Zhang, H., Sciare, J., Prévôt, A. S. H., Jayne, J. T., and Worsnop, D. R.: Field characterization of the $PM_{2.5}$ Aerosol Chemical Speciation Monitor: insights into the composition, sources, and processes of fine particles in eastern China, Atmos. Chem. Phys., 17, 14501-14517, 10.5194/acp-17-14501-2017, 2017.

Zhang, Z., Engling, G., Lin, C.-Y., Chou, C. C. K., Lung, S.-C. C., Chang, S.-Y., Fan, S., Chan, C.-Y., and Zhang, Y.-H.: Chemical speciation, transport and contribution of biomass burning smoke to ambient aerosol in Guangzhou, a mega city of China, Atmos. Environ., 44, 3187-3195, 10.1016/j.atmosenv.2010.05.024, 2010.

Zhou, S.Z., Wang, T., Wang, Z., Li, W., Xu, Z., Wang, X., Yuan, C., Poon, C. N., Louie, P. K. K., Luk, C. W. Y., and Wang, W.: Photochemical evolution of organic aerosols observed in urban plumes from Hong Kong and the Pearl River Delta of China, Atmos. Environ., 88, 219-229, 10.1016/j.atmosenv.2014.01.032, 2014.

Ziemann, P. J., and Atkinson, R.: Kinetics, products, and mechanisms of secondary organic aerosol formation, Chem. Soc. Rev., 41, 6582-6605, 10.1039/c2cs35122f, 2012.